

hep-ph/9607414
 (accepted Phys. Rev. D)
 July 1996

Low energy supersymmetry with a neutralino LSP and the CDF $ee\gamma\gamma + \cancel{E}_T$ event

S. Ambrosanio^{*,1}, G. L. Kane², Graham D. Kribs³, Stephen P. Martin⁴

*Randall Physics Laboratory, University of Michigan,
 Ann Arbor, MI 48109-1120*

S. Mrenna⁵

*High Energy Physics Division, Argonne National Laboratory,
 Argonne, IL 60439*

Abstract

We present a refined and expanded analysis of the CDF $ee\gamma\gamma + \cancel{E}_T$ event as superpartner production, assuming the lightest neutralino is the lightest supersymmetric particle. A general low-energy Lagrangian is constrained by a minimum cross section times branching ratio into two electrons and two photons, kinematics consistent with the event, and LEP1-LEP130 data. We examine how the supersymmetric parameters depend on the kinematics, branching ratios and experimental predictions with a selectron interpretation of the event, and discuss to what extent these are modified by other interpretations. Predictions for imminent CERN LEP upgrades and the present and future Fermilab Tevatron are presented. Finally, we briefly discuss the possible connection to other phenomena including a light stop, the neutralino relic density, the shift in R_b and the associated shift in α_s , and implications for the form of the theory.

^{*}Supported mainly by a INFN postdoctoral fellowship, Italy.

¹ambros@umich.edu

²gkane@umich.edu

³kribs@umich.edu

⁴spmartin@umich.edu

⁵mrenna@hep.anl.gov

1 Introduction

Minimal low energy supersymmetry provides the most promising framework to extend the Standard Model (SM). Such extensions take the form of complete models that encompass the gauge group structure and particle content of the SM, along with the supersymmetrized interactions and superpartners. General low energy theories of supersymmetry have over 100 parameters in addition to the SM parameters; such parameters can certainly be constrained by direct collider searches, but in general one needs more information or more assumptions to do calculations that examine many parts of the remaining parameter space. In many cases only one or a few parameters enter the calculation of a given observable, so useful predictions can often be made from a small subset of the supersymmetric parameters without loss of generality. The two obvious approaches to reduce the parameter space are to use theoretical assumptions, and (direct and indirect) experimental constraints.

In Ref. [1] we showed that the CDF $ee\gamma\gamma + \cancel{E}_T$ event [2] at the Fermilab Tevatron could be interpreted in low energy supersymmetry with roughly the expected rate and kinematics. If we assume this interpretation is correct and the event *is* due to supersymmetry, then we can reduce the parameter space by searching for sets of parameters that satisfy the event's constraints. We use the term ‘model’ to describe a distinct set of parameters, but of course all of our ‘models’ parameterize only one basic supersymmetric low energy Lagrangian. The primary difficulty in deriving precise parameter constraints (hence predictions) is the somewhat arbitrary notion of interpreting one event in terms of a cross section times branching ratio. Instead of advocating a particular lower (or upper) threshold value, we vary the value in a reasonable range and show the effect on parameter space and predictions. In this way we attempt to give an appreciation for the robustness or confidence of particular constraints or predictions.

We work within a general low energy (\equiv electroweak scale) supersymmetric theory without assuming common scalar or gaugino masses at the unification scale [3]. To determine branching ratios and scalar interaction contributions to cross sections, we do assume squark mass degeneracy except possibly for the light stop \tilde{t}_1 , and a mass degeneracy among sleptons with the same electroweak quantum numbers. Such assumptions are not crucial to our analysis, and could be removed if necessary. We assume R-parity is exactly conserved, so the lightest supersymmetric particle (LSP) is stable (consistent with the $ee\gamma\gamma + \cancel{E}_T$ event where the two LSPs escape the CDF detector). Finally, throughout this paper we assume the LSP is the lightest neutralino \tilde{N}_1 , and not the gravitino. Analyses of the $ee\gamma\gamma + \cancel{E}_T$ event assuming the LSP is a light gravitino have been presented by us [1, 4] and in other Refs. [5, 6]. One cannot distinguish these scenarios based solely on the $ee\gamma\gamma + \cancel{E}_T$ event, although it is likely that associated phenomenology can distinguish the scenarios. In this paper we assume that \tilde{N}_1 is the LSP, or is at least long-lived enough to escape the detector. If \tilde{N}_1 is identified as a stable LSP, then it is a possible cold dark matter particle [7].

In minimal low energy supersymmetry the possibility of one-loop radiative decay of neutralinos [8, 9, 10, 11] leads to signals with hard isolated photons plus missing energy in the final state, a signal predicted many years prior to the $ee\gamma\gamma + \cancel{E}_T$ event. This is by no means the only mechanism to produce photons plus missing energy, but it does allow the interpretation of the $ee\gamma\gamma + \cancel{E}_T$ event as selectron production $p\bar{p} \rightarrow \tilde{e}^+\tilde{e}^- (+X)$, with the selectron \tilde{e} decaying mainly into the next-to-lightest neutralino \tilde{N}_2 and an electron, followed by $\tilde{N}_2 \rightarrow \tilde{N}_1\gamma$. It is also possible to imagine other interpretations that involve the radiative decay of \tilde{N}_2 , but for which the initial superpartner production is different. The two possibilities in this class that we consider below are chargino pair production and neutralino pair production.

The plan of the paper is as follows. In Sec. 2 we discuss the kinematics of the $ee\gamma\gamma + \cancel{E}_T$ event in the selectron interpretation, the chargino interpretation, the neutralino interpretation, and other interpretations. Using superpartner mass constraints established from the $ee\gamma\gamma + \cancel{E}_T$ event kinematics, we discuss low energy supersymmetric model building in Sec. 3. Here we present a discussion of the radiative neutralino branching ratio, slepton decay and constraints from LEP. In Sec. 4 we discuss the results obtained from a numerical scan of the parameter space, using the structure built up from Sec. 3. The bulk of our results are contained in Sec. 4, where we discuss the model building results, the chargino/neutralino/slepton branching ratios, and predictions for LEP and Tevatron. In Sec. 5 we discuss the possibility of explaining the $ee\gamma\gamma + \cancel{E}_T$ event with the further assumption of a light stop \tilde{t}_1 . Finally, in Sec. 6, we present our concluding remarks, including a summary of such questions as distinguishing left- and right-selectrons, and the main channels that can confirm the $ee\gamma\gamma + \cancel{E}_T$ event is due to supersymmetry with an $\text{LSP} = \tilde{N}_1$. In Appendix A we discuss the viability of the chargino interpretation, and the results of attempts at model building. In Appendix B we give four sample models in the selectron interpretation.

Note added: As we were completing this paper, three other papers appeared which discuss the CDF $ee\gamma\gamma + \cancel{E}_T$ event in various contexts [31, 32, 33].

2 Kinematics of the $ee\gamma\gamma + \cancel{E}_T$ event

The kinematical requirements on the intermediate particles involved in the $ee\gamma\gamma + \cancel{E}_T$ event are stringent, and for completeness we present a refined analysis based on the procedure outlined in Ref. [1]. There are three basic possibilities for intermediate (s)particles; we will present these in terms of $\text{LSP} = \tilde{N}_1$ interpretations, but the analysis is generic and could be applied to any set of intermediate particles that satisfy the criteria below. All decays are assumed to occur close to the apparent vertex, which would be true of any $\text{LSP} = \tilde{N}_1$ interpretation. The procedure we use to find kinematical constraints is to begin with the information on the observed particles [2], assume two- or three- body decays as appropriate, randomly select unconstrained momentum components of the unobserved particles on both sides of the decay chain, and then reconstruct

the intermediate particle masses based on all possible pairings of electrons and photons. The masses of identical particles on both sides of the decay chain are required to be within 2.5 GeV to ‘pass’ the kinematic cut. The net transverse momentum in the event from adding both the observed particles and the LSPs is assumed to be $|p_T| \lesssim 20$ GeV.

2.1 Selectron interpretation

The first possibility is selectron production $p\bar{p} \rightarrow \tilde{e}^+\tilde{e}^- (+X)$ and decay via the 2-body mode $\tilde{e} \rightarrow e\tilde{N}_2$ followed by $\tilde{N}_2 \rightarrow \tilde{N}_1\gamma$. All sparticles are assumed to be on mass shell. The general result is summarized in Fig. 1, where the allowed regions in the $m_{\tilde{e}}-m_{\tilde{N}_2}$ plane are given for a series of maximum values of $m_{\tilde{N}_1}$. The choice to cut off the graph at $m_{\tilde{e}} = 140$ GeV is motivated by a rough lower limit on the selectron cross section, which will be made precise in Sec. 4.2. Since the electron and photon momenta have experimental uncertainties, the kinematic results that we derive from the event will have associated uncertainties. Analytic forms of the constraints have been extracted and are presented in Table 1; a few observations are in order that will be useful in model building:

1. $m_{\tilde{N}_1} \lesssim (50, 74)$ GeV, for $m_{\tilde{e}} < (115, 137)$ GeV.
2. $m_{\tilde{N}_2} - m_{\tilde{N}_1} > 21$ GeV, this value increasing to 30 GeV as $m_{\tilde{N}_1} \rightarrow 0$ GeV.
3. $m_{\tilde{e}} - m_{\tilde{N}_2} \gtrsim 20$ GeV, this value increasing for decreasing $m_{\tilde{e}}$.
4. Given $m_{\tilde{N}_1} \gtrsim 33$ GeV, then $m_{\tilde{e}} \gtrsim 100$ GeV.
5. Only one pairing of electron and photon gives consistent kinematics for $m_{\tilde{e}} \lesssim 125$ GeV.

The non-trivial mass differences that are required are not surprising, since all of the particles in the event have large (transverse) energy. We incorporate the mass difference constraints as well as the constraints on the ranges of $m_{\tilde{N}_1}$, $m_{\tilde{N}_2}$, and $m_{\tilde{e}}$ in our model building efforts.

2.2 Chargino interpretation

The second possibility is chargino production $p\bar{p} \rightarrow \tilde{C}_i\tilde{C}_j$ ($i, j = 1, 2$), with three possible decay chains: 3-body $\tilde{C} \rightarrow \tilde{N}_2 e \nu_e$ (through an off-shell or possibly on-shell W), 2-body $\tilde{C} \rightarrow \tilde{e} \nu_e$ or $\tilde{C} \rightarrow \tilde{\nu}_e e$. For either 2-body decay, the on-shell slepton proceeds through another 2-body decay $\tilde{e}(\tilde{\nu}_e) \rightarrow e(\nu_e)\tilde{N}_2$, then the photons are obtained through $\tilde{N}_2 \rightarrow \tilde{N}_1\gamma$. Calculating consistent kinematics requires specifying the six unknown momenta of the two neutrinos as well as the unknown LSP momenta in the final state. This is too complicated to delineate any rigorous exclusion regions using the randomized momenta procedure as in the selectron

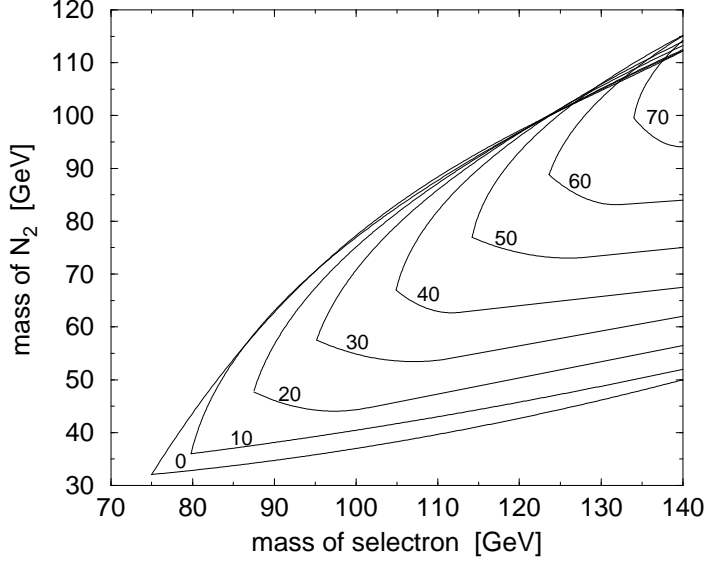


Figure 1: The kinematically allowed region of the $ee\gamma\gamma + \cancel{E}_T$ event in the $m_{\tilde{e}} - m_{\tilde{N}_2}$ plane is shown for various values of $m_{\tilde{N}_1}$ in the selectron interpretation. The allowed regions for $m_{\tilde{N}_1} = 0, 10, 20, 30, 40, 50, 60, 70 GeV are to the inside and right of the indicated lines. The allowed region for any given $m_{\tilde{N}_1}$ is roughly a subset of any lower $m_{\tilde{N}_1}$, except for large values of $m_{\tilde{N}_2}$. Since the lines are derived from the momenta of the $ee\gamma\gamma + \cancel{E}_T$ event, they are only as precise as the associated measurement of momenta.$

$m_{\tilde{e}}$	$>$	75 GeV	
$m_{\tilde{N}_2}$	$<$	$-0.00722m_{\tilde{e}}^2 + 2.71m_{\tilde{e}} - 122$ GeV	$[m_{\tilde{e}} \text{ in GeV}]$
$m_{\tilde{N}_2}$	$>$	0.286 $m_{\tilde{e}}$ + 10 GeV	
$m_{\tilde{N}_2}$	$<$	0.167 $m_{\tilde{N}_1}$ + 101 GeV	
$m_{\tilde{N}_2}$	$>$	0.955 $m_{\tilde{N}_1}$ + 25 GeV	
$m_{\tilde{N}_1}$	$<$	1.06 $m_{\tilde{e}}$ - 71 GeV	

Table 1: Kinematical constraints in the selectron interpretation.

interpretation. However, we have checked that it is possible to generate consistent kinematics for $m_{\tilde{C}} > 95$ GeV, assuming the 2-body decay $\tilde{C} \rightarrow \tilde{l}l'$ and that all (s)particles are on-shell. The rough regions where we were able to find kinematical solutions have $m_{\tilde{l}} \gtrsim 60, 75$ for slepton = sneutrino, selectron. In addition, we found solutions with $m_{\tilde{N}_2} \gtrsim 20$ GeV, $m_{\tilde{N}_2} - m_{\tilde{N}_1} \gtrsim 10$ GeV, $m_{\tilde{C}} \gtrsim \max[2.5m_{\tilde{N}_2} - 95, 1.5m_{\tilde{N}_1} + 65, 95]$ GeV. Thus a solution in the selectron interpretation need not be a solution in the chargino interpretation, and vice versa.

2.3 Neutralino interpretation

The third possibility is neutralino production, e.g. $p\bar{p} \rightarrow \tilde{N}_2 \tilde{N}_j$, where either of the heavier neutralinos $j = 3,4$ decay as $\tilde{N}_j \rightarrow l^+l^-\tilde{N}_2$, followed by the usual $\tilde{N}_2 \rightarrow \tilde{N}_1\gamma$. This interpretation contrasts with the first two by producing both leptons from one side of the decay, however it is calculable as in the selectron scenario (since the only unknown final state momenta are the two neutralinos). The invariant mass of the electron pair can be extracted from the event $m_{e^+e^-} \sim 160$ GeV [2], which implies the mass difference between $m_{\tilde{N}_j}$ and $m_{\tilde{N}_2}$ must also be greater than 160 GeV. This is almost certainly too high for a reasonable Tevatron cross section while retaining a reasonable $m_{\tilde{N}_2}$ and proper neutralino mixing to have $\tilde{N}_2 \rightarrow \tilde{N}_1\gamma$. Further, in the particular case where the branching ratio for the decay $\tilde{N}_j \rightarrow \tilde{N}_2 Z$ is large, then a lepton pair from $Z \rightarrow l^+l^-$ will always reconstruct to an invariant mass of about m_Z . Thus, a neutralino interpretation of the $ee\gamma\gamma + \cancel{E}_T$ event seems extremely unlikely, and we will not consider it further.

2.4 Other interpretations

Other supersymmetric interpretations with a neutralino LSP are in principle possible, and are based on variants of selectron production, chargino production or neutralino production. The differences lie in the particular decay from which the electrons originate, plus possibly other invisible phenomena (neutrinos). In all cases the photon is obtained from the decay $\tilde{N}_2 \rightarrow \tilde{N}_1\gamma$, and as a consequence the photon always appears in the last step of the decay chain. One example is stau production $p\bar{p} \rightarrow \tilde{\tau}^+\tilde{\tau}^- (+X)$ with the decay $\tilde{\tau} \rightarrow \tau\tilde{N}_2$, followed by $\tau \rightarrow e (+\nu_\tau\nu_e)$. The total branching ratio is suppressed compared with selectron production by a factor $\mathcal{B}(\tau \rightarrow e\nu_\tau\nu_e)^2 \sim 0.03$, hence the rate into $ee\gamma\gamma$ is much smaller than selectron production. Another example is a variant of the selectron interpretation with a chargino \tilde{C} that is lighter than the selectron, such that the decay $\tilde{e}_L \rightarrow \nu_e \tilde{C} (\rightarrow \tilde{N}_2 e \nu_e)$ is dominant. In this case it is probably not possible to have a large decay $\tilde{e}_L \rightarrow \tilde{C} \nu_e$, with both $\tilde{e}_L \rightarrow \tilde{N}_{1,2} e$ suppressed. Further, $\tilde{C} \rightarrow \tilde{N}_1 e \nu_e$ has to be suppressed with respect to $\tilde{C} \rightarrow \tilde{N}_2 e \nu_e$, which is difficult especially in the presence of $\tilde{N}_2 \rightarrow \tilde{N}_1\gamma$. Finally, with four neutrinos carrying off invisible momentum it seems difficult to have a large probability for the high energy electrons required in the final state, since the selectrons have to be light to have a large $ee\gamma\gamma$ rate.

3 Model building

The kinematics of the event have illustrated two viable sources of $ee\gamma\gamma + \cancel{E}_T$ events: slepton production or chargino production. In either case, the essential ingredient to getting photons is through the one-loop radiative decay of neutralinos. To proceed, we first define the relevant parameters of the low-energy supersymmetric theory, including the chargino and neutralino mass matrices. This sets the stage for the discussion of the radiative neutralino branching ratio. We also discuss the treatment of the squark, slepton and Higgs sectors and the relevant mixings, as well as discussing the selectron branching ratios. Once the models have been constructed, we describe the constraints imposed on the parameters from experiment.

The main focus of this paper is on the selectron interpretation and not the chargino interpretation, since it is made clear in Appendix A that the chargino interpretation is difficult for many reasons. However, in the following we have attempted to provide a general discussion of the model building, since radiative neutralino decay is required in both interpretations.

3.1 Supersymmetric parameters

The chargino and neutralino tree-level masses and mixings are determined by specifying the gaugino soft masses M_1 and M_2 , the ratio of the Higgs vacuum expectation values $\tan\beta \equiv \langle H_2^0 \rangle / \langle H_1^0 \rangle$ and the Higgs superfield mass parameter μ . The form of the mass matrices is well known, but it will prove useful in the discussion of the radiative branching ratio to have the expressions in the particular basis as follows. Note that we assume no relation between M_1 and M_2 .

The chargino mass matrix in the $(-i\tilde{W}^\pm, \tilde{H}^\pm)$ basis is

$$\mathcal{M}_{\tilde{C}^\pm} = \begin{pmatrix} M_2 & \sqrt{2}M_W \sin\beta \\ \sqrt{2}M_W \cos\beta & \mu \end{pmatrix}, \quad (1)$$

and can be diagonalized by a biunitary transformation $U^* \mathcal{M}_{\tilde{C}^\pm} V^{-1}$ to yield the masses and mixing matrices U, V (as well as fixing the sign convention of μ , consistent with Ref. [12]). The chargino masses can be found from the analytic expression

$$\begin{aligned} m_{\tilde{C}_{1,2}}^2 &= \frac{1}{2} \left\{ M_2^2 + \mu^2 + 2M_W^2 \right. \\ &\quad \left. \mp \sqrt{(M_2^2 - \mu^2)^2 + 4M_W^4 \cos^2 2\beta + 4M_W^2(M_2^2 + \mu^2 + 2M_2\mu \sin 2\beta)} \right\}. \end{aligned} \quad (2)$$

Process	LEP	Tevatron
$\tilde{N}_i \tilde{N}_j$	$m_{\tilde{e}_L}, m_{\tilde{e}_R}$	$m_{\tilde{u}_L}, m_{\tilde{d}_L}, m_{\tilde{u}_R}, m_{\tilde{d}_R}$
$\tilde{C}_i^\pm \tilde{C}_j^\mp$	$m_{\tilde{\nu}_e}$	$m_{\tilde{u}_L}, m_{\tilde{d}_L}$
$\tilde{N}_i \tilde{C}_j^\pm$	-	$m_{\tilde{u}_L}, m_{\tilde{d}_L}$

Table 2: Chargino and neutralino cross sections at LEP and Tevatron depend on M_1 , M_2 , $\tan \beta$, μ and the particular superpartner masses as above. (The Tevatron cross sections also depend on the second family masses, but these contributions are generally suppressed by Cabibbo mixing and a small parton distribution $f_{q|p}$ in the proton.)

The neutralino mass matrix in the $(-i\tilde{\gamma}, -i\tilde{Z}, \tilde{H}_a, \tilde{H}_b)$ basis is

$$\mathcal{M}_{\tilde{N}} = \begin{pmatrix} M_1 \cos^2 \theta_W + M_2 \sin^2 \theta_W & (M_2 - M_1) \sin \theta_W \cos \theta_W & 0 & 0 \\ (M_2 - M_1) \sin \theta_W \cos \theta_W & M_1 \sin^2 \theta_W + M_2 \cos^2 \theta_W & M_Z & 0 \\ 0 & M_Z & \mu \sin 2\beta & -\mu \cos 2\beta \\ 0 & 0 & -\mu \cos 2\beta & -\mu \sin 2\beta \end{pmatrix}, \quad (3)$$

and can be diagonalized by a unitary transformation $N^* \mathcal{M}_{\tilde{N}} N^{-1}$ to yield the four neutralino mass eigenvalues $\epsilon_i m_{\tilde{N}_i}$ and the mixing matrix N that we assume to be real and orthogonal (exact expressions for the mixings and masses can be found in [13, 14]). The sign of the neutralino mass eigenvalue ϵ_i enters the supersymmetric Feynman rules, while the physical masses $m_{\tilde{N}_i}$ are always positive with the ordering $0 \leq m_{\tilde{N}_1} \leq m_{\tilde{N}_2} \leq m_{\tilde{N}_3} \leq m_{\tilde{N}_4}$. The $(\tilde{\gamma}, \tilde{Z})$ basis is related to the (\tilde{B}, \tilde{W}^3) basis through

$$\begin{pmatrix} \tilde{\gamma} \\ \tilde{Z} \end{pmatrix} = \begin{pmatrix} \cos \theta_W & \sin \theta_W \\ -\sin \theta_W & \cos \theta_W \end{pmatrix} \begin{pmatrix} \tilde{B} \\ \tilde{W}^3 \end{pmatrix}, \quad (4)$$

and the $(\tilde{H}_a, \tilde{H}_b)$ basis is related to the $(\tilde{H}_1^0, \tilde{H}_2^0)$ basis through

$$\begin{pmatrix} \tilde{H}_a \\ \tilde{H}_b \end{pmatrix} = \begin{pmatrix} \cos \beta & -\sin \beta \\ \sin \beta & \cos \beta \end{pmatrix} \begin{pmatrix} \tilde{H}_1^0 \\ \tilde{H}_2^0 \end{pmatrix}. \quad (5)$$

Our notation follows Refs. [12, 15], with \tilde{H}_1^0 and \tilde{H}_2^0 coupling to the down- and up-type fermions respectively. The production cross sections for charginos and neutralinos at LEP and at the Tevatron involve graphs with s -channel gauge boson exchange and t -channel slepton or squark exchange. In Table 2, we itemize the dependence of each chargino/neutralino cross section on the squark or slepton mass.

The gluino does not enter phenomenology directly associated with the $ee\gamma\gamma + \cancel{E}_T$ event. Its tree-level mass is given by the soft mass parameter M_3 that is unconstrained without gaugino mass unification. There need be no relation between M_1 , M_2 , and M_3 , and we do not assume

one. However, one could imagine that the non-Abelian masses M_2 , M_3 are equal at the unification scale, with the U(1) mass M_1 related to them in a more subtle way. Ref. [16] has suggested that the gluino may play a dramatic role at the Tevatron, if the lightest stop \tilde{t}_1 has a mass $\mathcal{O}(50)$ GeV. However, for the primary purposes of this paper we can focus on phenomenology that is independent of the gluino. In Sec. 5 we elaborate on the possibility of models that can generate an $ee\gamma\gamma + \cancel{E}_T$ event with the additional assumption of a light stop.

The slepton sector is defined by the masses $m_{\tilde{l}_L}$ and $m_{\tilde{l}_R}$, with $m_{\tilde{\nu}}$ related by the $SU(2)_L$ sum rule

$$m_{\tilde{\nu}}^2 = m_{\tilde{l}_L}^2 - M_W^2 |\cos 2\beta|, \quad (6)$$

for $\tan \beta > 1$, and the couplings to gauge bosons and gauginos fixed by the SM gauge group. Slepton production cross sections at the Tevatron are given in Refs. [17, 18, 1], and depend *only* on the mass of the slepton. We assume slepton mass degeneracy (motivated by the absence of lepton flavor changing decays), although it is not required by the theory nor the $ee\gamma\gamma + \cancel{E}_T$ event. Where necessary, we remark on the effect of removing this assumption on associated phenomenology. We also assume L - R mixing in the slepton sector can be neglected.

The squark sector in our model building is defined for simplicity by a common squark mass $m_{\tilde{q}}$, the stop masses $m_{\tilde{t}_1}$, $m_{\tilde{t}_2}$ and the stop mixing angle $\theta_{\tilde{t}}$. In this way we achieve a useful reduction of parameter space through $m_{\tilde{q}} = m_{\tilde{u}_L} = m_{\tilde{d}_L} = m_{\tilde{u}_R} = m_{\tilde{d}_R} = \dots$, and we further assume for simplicity $m_{\tilde{t}_2} = m_{\tilde{q}}$. These assumptions can be removed if data becomes sensitive to them. The stop mass eigenstates are defined by

$$\begin{pmatrix} \tilde{t}_1 \\ \tilde{t}_2 \end{pmatrix} = \begin{pmatrix} \cos \theta_{\tilde{t}} & \sin \theta_{\tilde{t}} \\ -\sin \theta_{\tilde{t}} & \cos \theta_{\tilde{t}} \end{pmatrix} \begin{pmatrix} \tilde{t}_L \\ \tilde{t}_R \end{pmatrix} \quad (7)$$

with the stop trilinear coupling A_t (and the soft masses $m_{\tilde{Q}}$, $m_{\tilde{t}_R}$) uniquely determined by $m_{\tilde{t}_{1,2}}$ and the mixing angle $\theta_{\tilde{t}}$, for a given μ and $\tan \beta$. We assume all other L - R squark mixing can be neglected.

The Higgs sector is determined from $\tan \beta$, the neutral CP-odd Higgs mass m_A , and higher order corrections [19, 20]. We include one-loop corrections from stops [20], and neglect all other contributions. In this framework we calculate the charged Higgs mass m_{H^\pm} , the neutral CP-even Higgs masses m_h , m_H and the mixing angle α from the above parameters. The Higgs sector enters the radiative neutralino decay through the charged Higgs boson, and the branching ratios for the heavier superpartners into one or more of h , A , H , or H^\pm (neglecting off-shell Higgs exchange in 3-body $\tilde{C}, \tilde{N} \rightarrow \tilde{C}, \tilde{N} f \bar{f}$ decays).

3.2 Radiative decay of neutralinos

The radiative decay of neutralinos has been well studied [8, 9, 10, 11], and it suffices to review the mechanism that enhances the radiative branching ratio with respect to the traditional

3-body $\tilde{N}_2 \rightarrow \tilde{N}_1 f\bar{f}$ decays, as pertaining to the $ee\gamma\gamma + \cancel{E}_T$ event. We exclusively discuss $\tilde{N}_2 \rightarrow \tilde{N}_1 \gamma$, since heavier neutralinos always have sizeable tree-level branching ratios into 2- or 3-body channels, causing the radiative branching ratio to be negligible.

There exists both a kinematical and a dynamical mechanism that can give an enhancement of the radiative neutralino decay [9, 11]. The kinematic enhancement can only occur when the mass difference $m_{\tilde{N}_2} - m_{\tilde{N}_1}$ is small $\mathcal{O}(10)$ GeV, so that other decay modes are closed or suppressed. However, the kinematics in the selectron interpretation enforce $m_{\tilde{N}_2} - m_{\tilde{N}_1} > 21$ GeV by Observation 2, and so a kinematic enhancement of the radiative branching ratio is not crucial for our purposes (although see Sec. 4.2 for exceptions).

The dynamic enhancement of the radiative decay occurs as follows. First, examine the limit when $\tan \beta \rightarrow 1$ and $(M_1 - M_2) \rightarrow 0$ [15]; the neutralino mass matrix (already written in a suggestive form in Eq. (3)) becomes particularly simple,

$$\mathcal{M}_{\tilde{N}} = \begin{pmatrix} M_2 & 0 & 0 & 0 \\ 0 & M_2 & M_Z & 0 \\ 0 & M_Z & \mu & 0 \\ 0 & 0 & 0 & -\mu \end{pmatrix} \quad \text{for} \quad \begin{cases} \tan \beta = 1 \\ M_1 = M_2 \end{cases} . \quad (8)$$

In this limit two neutralinos become pure photino ($\tilde{\gamma}$) and Higgsino (\tilde{H}_b) states, with masses M_2 and $|\mu|$ respectively. The other two neutralinos are mixtures of \tilde{Z} – \tilde{H}_a , with masses

$$m_{\tilde{Z}-\tilde{H}_a} = \frac{1}{2} \left| M_2 + \mu \pm \sqrt{(M_2 - \mu)^2 + 4M_Z^2} \right|. \quad (9)$$

For pure $\tilde{\gamma}$ and \tilde{H}_b states, the tree-level couplings $\tilde{\gamma}\tilde{H}_b Z$, $\tilde{\gamma}\tilde{H}_b h(A)$, and $\tilde{H}_b\tilde{f}\bar{f}$ (in the limit $m_f \rightarrow 0$) go to zero, leaving the one-loop ‘effective’ coupling $\tilde{\gamma}\tilde{H}_b\gamma$ dominant. Thus, by associating $\tilde{N}_{1,2}$ with $\tilde{\gamma}$, \tilde{H}_b , then the one loop decay $\tilde{N}_2 \rightarrow \tilde{N}_1 \gamma$ is dominant. One consequence of requiring the two lightest neutralinos to be either of the states $\tilde{\gamma}$ or \tilde{H}_b (hence the heavier two neutralino masses are given by Eq. (9)) is that the required mass ordering $m_{\tilde{N}_{1,2}} < m_{\tilde{N}_{3,4}}$ implies

$$M_1 (= M_2), |\mu| < \frac{1}{2} \left| M_2 + \mu \pm \sqrt{(M_2 - \mu)^2 + 4M_Z^2} \right|. \quad (10)$$

See Ref. [11] for a more comprehensive treatment of this issue. What is not determined by requiring a large radiative branching ratio by this mechanism is which one of the two lightest neutralinos is the photino or Higgsino.

The extent to which a large radiative branching ratio is possible in general (and in particular through the dynamical mechanism without the exact relations above) can be evaluated semi-analytically and numerically [11]. As an example, Fig. 2(a) shows contours of the branching ratio of $\tilde{N}_2 \rightarrow \tilde{N}_1 \gamma$ in the M_1 – M_2 plane, for $\mu = -45$ GeV, $m_{\tilde{e}_L} = m_{\tilde{e}_R} = 110$ GeV, $m_A = 400$ GeV, $\tan \beta = 1.2$, and all squarks heavy $m_{\tilde{t}_1} = m_{\tilde{q}} = 500$ GeV. The thick solid line bounding the region defined by $\langle \tilde{N}_1 | \tilde{H}_b^0 \rangle^2 \langle \tilde{N}_2 | \tilde{\gamma} \rangle^2 > 0.7$ anticipates the constraint on selectron decay from

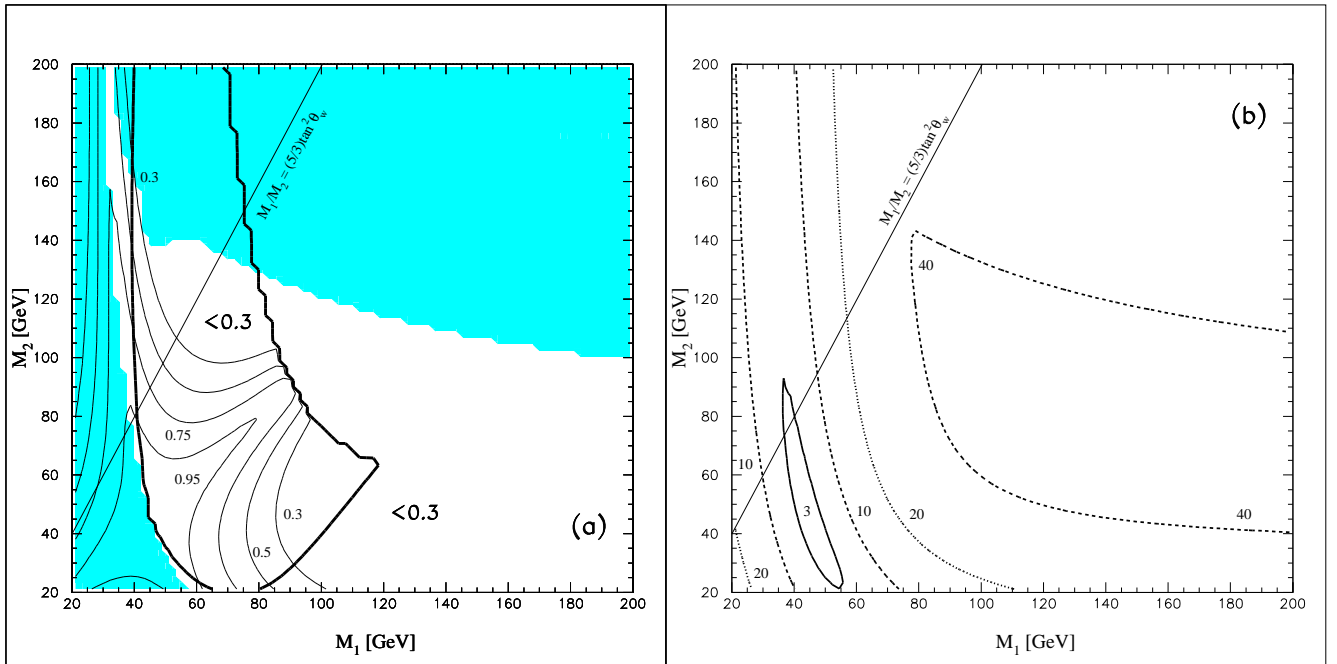


Figure 2: (a) Contour plot for the branching ratio of the radiative neutralino decay $\tilde{N}_2 \rightarrow \tilde{N}_1 \gamma$ in the M_1 - M_2 plane for the case $\tan \beta = 1.2$, $\mu = -45$ GeV, $m_{\tilde{e}_{L,R}} = 110$ GeV, $m_{\tilde{q}} = m_{\tilde{t}_{1,2}} = 500$ GeV, and $m_A = 400$ GeV. The $\mathcal{B}(\tilde{N}_2 \rightarrow \tilde{N}_1 \gamma) = 0.9, 0.75, 0.5, 0.3$ levels are shown and labeled. The LEP excluded region is shaded. The solid thick line outlines the region where $\langle \tilde{N}_1 | \tilde{H}_b^0 | \tilde{N}_2 \rangle^2 > 0.7$. (b) Contour plot in the same plane with the parameters above, showing the mass difference of the two lightest neutralinos in GeV. This figure is a result of the general radiative neutralino decay analysis of Ref. [11].

the $ee\gamma\gamma + \cancel{E}_T$ event (see Sec. 3.3 below). Contours in the mass difference $m_{\tilde{N}_2} - m_{\tilde{N}_1} > 3, 10, 20, 40$ GeV are shown in Fig. 2(b). Since the selectron interpretation requires a large mass difference $m_{\tilde{N}_2} - m_{\tilde{N}_1} > 21$ GeV, only a fairly small region of parameter space remains satisfying the constraint of a large radiative neutralino branching ratio. For example, the region bounded by $\mathcal{B}(\tilde{N}_2 \rightarrow \tilde{N}_1 \gamma) > 0.5$, $m_{\tilde{N}_2} - m_{\tilde{N}_1} > 20$ GeV, and the LEP exclusion region is characterized by roughly $0.6 < M_2/M_1 < 1.5$ for $60 < M_1 < 90$ GeV, $45 < M_2 < 90$ GeV, where the constraints on M_2/M_1 are stronger for larger values of M_1, M_2 . Of course this example only applies to the choice of $\mu, \tan \beta, m_{\tilde{e}}, m_{\tilde{q}}, m_A$ values as above, but it gives a reasonable illustration of the constraints. The region with a large radiative neutralino decay centered on the line $M_1 = M_2$ persists as $|\mu|$ is increased or decreased (the region shifts up or down the $M_1 = M_2$ line), but tends to shrink (and eventually disappear) as $\tan \beta$ is increased or the squark or slepton masses are decreased.

3.3 Slepton decay

In the selectron interpretation, the branching ratio of the selectrons $\tilde{e} \rightarrow e \tilde{N}_2$ is crucial to produce an $ee\gamma\gamma + \cancel{E}_T$ event. In general, sleptons couple to the gauginos through the usual supersymmetrized gauge interactions, and also to the Higgsinos through the Yukawa couplings. The Yukawa couplings $\lambda_{\tilde{l}} \sim m_l/M_W$ are strongly suppressed by small lepton masses, and for our purposes can be neglected. Since the radiative branching ratio $\tilde{N}_2 \rightarrow \tilde{N}_1\gamma$ requires one of $\tilde{N}_{1,2}$ to be mostly a photino and the other mostly a Higgsino, then the requirement that the selectron decays as $\tilde{e} \rightarrow e \tilde{N}_2$ implies the photino-Higgsino content of the neutralinos is unique and determined

$$\begin{aligned} \langle \tilde{N}_1 | \tilde{H}_b \rangle^2 &\approx 1 \\ \langle \tilde{N}_2 | \tilde{\gamma} \rangle^2 &\approx 1. \end{aligned} \quad (11)$$

Based on Sec. 3.2, this implies $|\mu| < M_1 (= M_2)$, in the limit of pure states.

If the $ee\gamma\gamma + \cancel{E}_T$ event is due to $\tilde{e}_L \tilde{e}_L$ production, one must also consider the branching fraction of \tilde{e}_L to charginos if kinematically accessible. In the kinematics of the selectron interpretation no such decay was considered, and naively it would seem possible to suppress this decay through a judicious choice of chargino mixings. However, it is also possible that \tilde{e}_L production occurs with the selectron decay $\tilde{e}_L \rightarrow \tilde{C}_1 \nu_e$, then the decay $\tilde{C}_1 \rightarrow e \tilde{N}_2$. In the $\tan \beta = 1$ limit (with neutralinos pure states) the masses of the charginos simplifies considerably from Eq. (2) to

$$m_{\tilde{C}_{1,2}} = \frac{1}{2} \left| M_2 + \mu \pm \sqrt{(M_2 - \mu)^2 + 4M_W^2} \right|. \quad (12)$$

This expression is the same as Eq. (9) with $M_Z \rightarrow M_W$, and shows that the chargino masses are directly correlated with the heavier two neutralino masses. It is a simple matter to show that $m_{\tilde{C}_1} > m_{\tilde{N}_2}$ is always true (in the $\tan \beta = 1$, $M_1 = M_2$ limit), while the coupling of \tilde{C}_1 to \tilde{N}_2 ($= \tilde{\gamma}$) and \tilde{N}_1 ($= \tilde{H}_b$) is dependent on the gaugino-Higgsino mixings of the chargino. The \tilde{e}_L - \tilde{C} - ν_e couplings are also proportional to the gaugino component of \tilde{C} and so a full numerical calculation is necessary to determine the relative size of the branching fractions. This will be presented in Sec. 4.4.

3.4 Constraints from LEP

Throughout our analysis, we applied the most updated limits on the supersymmetric parameters and bounds on superpartner masses coming from searches at LEP1, as well as the more recent run with $\sqrt{s} = 130.3$ and 136.3 GeV (collectively denoted ‘LEP130-136’) where integrated luminosities of about 2.8 and 2.3 pb^{-1} were accumulated [21]. We also show the combined effect of the LEP limits and kinematical constraints on the selectron and light neutralino masses in the selectron interpretation of the $ee\gamma\gamma + \cancel{E}_T$ event, and the derived ranges

of μ , M_1 and M_2 values. The somewhat conservative LEP1 bounds we imposed are [22, 23]:

$$\begin{aligned}\mathcal{B}_{\text{invisible}}(Z \rightarrow \text{SUSY}) &< 2.3 \times 10^{-3} \\ \Delta\Gamma_{\text{tot}}(Z \rightarrow \text{SUSY}) &< 23 \text{ MeV} \\ \mathcal{B}(Z \rightarrow \tilde{N}_1 \tilde{N}_2) &< 1.2 \times 10^{-5} \\ \mathcal{B}(Z \rightarrow \tilde{N}_2 \tilde{N}_2) &< 3.5 \times 10^{-5}.\end{aligned}\tag{13}$$

The evaluation of the supersymmetric contribution to the invisible Z width included not only the contribution from the direct LSP production $Z \rightarrow \tilde{N}_1 \tilde{N}_1$, but also the contribution from other channels $Z \rightarrow \tilde{N}_i (\rightarrow \tilde{N}_1 \nu \bar{\nu}) \tilde{N}_j (\rightarrow \tilde{N}_1 \nu \bar{\nu})$. These contributions were then subtracted when calculating the supersymmetric contributions to the visible Z width.

The constraints we applied at LEP130-136 are

$$\begin{aligned}\sigma(e^+e^- \rightarrow \text{visible SUSY}) &< 1.8 \text{ pb for } \sqrt{s} = 130.3 \text{ GeV} \\ \sigma(e^+e^- \rightarrow \text{visible SUSY}) &< 2.2 \text{ pb for } \sqrt{s} = 136.3 \text{ GeV}\end{aligned}\tag{14}$$

corresponding to the 5 visible event level (before detector cuts) for each of the two runs [21]. A few remarks on the calculation of the expected total visible supersymmetric cross section are in order. First, we considered only the contribution from chargino/neutralino production, since charged sleptons relevant to the $ee\gamma\gamma + \cancel{E}_T$ event need to be heavier than 75 GeV just to satisfy the kinematics (see Table 1). We require squarks to be heavier than can be produced at LEP, except possibly a light stop whose production cross section is always too small to see any events at LEP130-136 with the data sample collected. The total visible supersymmetric cross section obviously does not include processes like $e^+e^- \rightarrow \tilde{N}_1 \tilde{N}_1$, and $e^+e^- \rightarrow \tilde{N}_i \tilde{N}_j$ when both $\tilde{N}_{i,j} \rightarrow \tilde{N}_1 \nu \bar{\nu}$. This was achieved by doing a complete calculation of the branching ratios for chargino/neutralino decays for every model. To ensure the visibility of the signal, we also required large enough phase space in the decay of the produced \tilde{N}_i , \tilde{C}_i^\pm , which in practice implied the mass difference $m_{\tilde{C}_1, \tilde{N}_2} - m_{\tilde{N}_1} > 10$ GeV, in accord with [21].

The following observations are useful to understand in some detail how the LEP constraints affect our analysis in a general low energy supersymmetric framework (without assuming any relation between M_1 and M_2). Combining the bounds arising from neutralino searches at LEP with the need for a next-to-lightest neutralino $m_{\tilde{N}_2} > 30$ GeV from the $ee\gamma\gamma + \cancel{E}_T$ event kinematics (see Sec. 2), one finds the ‘‘light Higgsino-gaugino window’’ with $M_1, M_2, |\mu| \ll M_Z$ and $\tan\beta \approx 1$ [23] is excluded. This also implies $|\mu| \gtrsim 33$ GeV, at least for small $\tan\beta$. Further, given the light Higgsino-gaugino window is excluded for our purposes, only $\mu < 0$ survives LEP constraints such that a large radiative neutralino branching ratio is present [11], thus we are left with $\mu < -33$ GeV. For $\tan\beta \gtrsim 1.3$ either the LEP chargino mass bound or the direct search for neutralinos begin to exclude regions with small negative μ , irrespective of M_1 and M_2 values. Given a value of μ , one can find rough regions in the M_1 – M_2 plane that are allowed by LEP constraints, generally independent of $\tan\beta$. In our framework, the constraints we listed above exclude $M_1 \lesssim 30$ GeV and, for instance, when $\mu = -45$ GeV then

$M_1 \lesssim 55$ GeV is not allowed if $M_2 \lesssim 20$ GeV. The region in M_1 – M_2 space excluded by LEP is indicated in Fig. 2 for $\mu = -45$ GeV, etc. Notice that since the $ee\gamma\gamma + \cancel{E}_T$ event requires a suitable slepton decay, then the neutralino contents in Eq. (11) can exclude a comparable region (see Sec. 3.3, and in particular Fig. 2). In contrast, the requirement $(m_{\tilde{N}_2} - m_{\tilde{N}_1}) > 21$ GeV of Observation 2 in Sec. 2 combined with the LEP constraints effectively sets a minimum suitable value of M_1 around 52 GeV for any values of the other parameters. Only weaker bounds on M_2 can be identified in a similar way.

In addition to the constraints from chargino and neutralino production, we also imposed

$$m_h > \begin{cases} 44 \\ 58.4 \sin^2(\beta - \alpha) \end{cases} \text{ GeV}, \quad (15)$$

on our models from LEP constraints. Since the inputs to our model building to calculate the Higgs sector include m_A and $\tan\beta$, the above mass bounds impose a constraint on m_A and higher order corrections from the stop sector. This will be important for the discussion about models with a light stop in Sec. 5. Small $\tan\beta$ also suffers from possible non-perturbativity constraints, that have been discussed recently in e.g. Ref. [23] for the light Higgsino-gaugino window that requires small $\tan\beta$. However, the constraint is relatively weak ($\tan\beta \gtrsim 1.2$), since as we shall see the allowed region of $\tan\beta$ extends up to $\tan\beta \sim 2.0 \rightarrow 2.8$.

4 Numerical results – selectron interpretation

To ensure a large branching ratio for the decay $\tilde{N}_2 \rightarrow \tilde{N}_1\gamma$, pure photino and Higgsino lightest neutralinos are sufficient, but not necessary conditions. The extent of the allowable impurity determines the character of the models, but that is by no means the only degree of freedom. As we have seen, the branching ratios of the sleptons are also determined by the gaugino-Higgsino content of the neutralinos and charginos. Further, the allowed sets of masses must satisfy the $ee\gamma\gamma + \cancel{E}_T$ event kinematics, and proper experimental constraints are not trivial mass exclusions, etc. What we present here are complete low energy models constructed using the framework built up in Sec. 3 using a randomized parameter selection scheme [24], and imposing all of the above constraints.

4.1 Preliminaries

Interpreting one event as a cross section is a tenuous procedure, although some general methodology can be applied. First, we establish a minimum threshold in the Tevatron selectron cross section times branching ratio into two electrons and two photons,

$$\sigma \times \mathcal{B}^2 \equiv \sigma(p\bar{p} \rightarrow \tilde{e}^+\tilde{e}^-) \times [\mathcal{B}(\tilde{e} \rightarrow \tilde{N}_2 e) \mathcal{B}(\tilde{N}_2 \rightarrow \tilde{N}_1 \gamma)]^2 > \mathcal{A}, \quad (16)$$

where $\mathcal{A} \equiv (\sigma \times \mathcal{B}^2)|_{\min}$ is the minimum threshold value. Since the choice of the threshold \mathcal{A} is somewhat arbitrary, we show the effect of increasing the threshold from 5 to 7.5 to 10 fb to give at least some indication as to how sensitive the constraints are to the value. Imposing $\mathcal{A} = 20$ fb excludes all of our models, so there is a non-trivial importance of the precise numerical value of the threshold for phenomenology.

The quantity $\sigma \times \mathcal{B}^2$ used in the general analysis does not include detector cuts, but we have simulated particular models to get indicative efficiencies (see Sec. 4.8). For a detection efficiency of 0.2, the lowest threshold cut $\mathcal{A} = 5$ fb corresponds to assuming a cut on the effective $ee\gamma\gamma$ rate of $s = \sigma \times \mathcal{B}^2 \times \text{EFF} = 1$ fb or 1/10 of an event. Given an expected number of events s , the probability of observing exactly n events is from Poisson statistics

$$P = \frac{e^{-s} s^n}{n!}. \quad (17)$$

For $s = 0.1$ corresponding to 1 fb cross section at the Tevatron, one still has a 9% chance of seeing exactly one event.

The results are presented assuming a branching ratio into only one family, although it is straightforward to compute the total two lepton plus two photon rate including smuon and/or stau production. The effect is of course to increase our calculated rate by a factor of 2 or 3. (Our results remain unchanged if the threshold \mathcal{A} is increased by the same factor.) Note that including more than one family is of course crucially dependent on the assumption of slepton mass degeneracy.

In the selectron interpretation there is no a priori requirement of having \tilde{e}_L or \tilde{e}_R production. We consider three cases: A selectron interpretation from \tilde{e}_L production, where the kinematics of the $ee\gamma\gamma + \cancel{E}_T$ event must be satisfied for $m_{\tilde{e}_L}$, but must *not* be satisfied for $m_{\tilde{e}_R}$. In this way, $\tilde{e}_R\tilde{e}_R$ production can still give an $ee\gamma\gamma$ signal but the kinematics are not consistent with the $ee\gamma\gamma + \cancel{E}_T$ event; hence only the rate from $\tilde{e}_L\tilde{e}_L$ production ought to be considered. Second, the opposite scenario with \tilde{e}_R production where the kinematics must be satisfied for $m_{\tilde{e}_R}$ but not for $m_{\tilde{e}_L}$. Finally, we consider a set of models with the simultaneous $\tilde{e}_L\tilde{e}_L$ and $\tilde{e}_R\tilde{e}_R$ production (denoted ‘ $\tilde{e}_L + \tilde{e}_R$ models’), where the kinematics are satisfied for *both* $m_{\tilde{e}_L}$ and $m_{\tilde{e}_R}$. The threshold \mathcal{A} is applied as follows,

$$\begin{aligned} \sigma_L \times \mathcal{B}_L^2 &> \mathcal{A} \text{ for } \tilde{e}_L \text{ models} \\ \sigma_R \times \mathcal{B}_R^2 &> \mathcal{A} \text{ for } \tilde{e}_R \text{ models} \\ \sigma_L \times \mathcal{B}_L^2 + \sigma_R \times \mathcal{B}_R^2 &> \mathcal{A} \text{ for } \tilde{e}_L + \tilde{e}_R \text{ models}, \end{aligned} \quad (18)$$

where $\sigma_{L,R} \equiv \sigma(p\bar{p} \rightarrow \tilde{e}_{L,R}^+ \tilde{e}_{L,R}^-)$ and $\mathcal{B}_{L,R} \equiv \mathcal{B}(\tilde{e}_{L,R} \rightarrow \tilde{N}_2 e) \mathcal{B}(\tilde{N}_2 \rightarrow \tilde{N}_1 \gamma)$. The case of $\tilde{e}_L + \tilde{e}_R$ models assumes that the contributions to the $ee\gamma\gamma$ cross section from \tilde{e}_L and \tilde{e}_R production can be summed, hence the requirement that the kinematics of the event is satisfied for both contributions. Further, for $\tilde{e}_L + \tilde{e}_R$ models we enforce $\sigma_{L,R} > 1$ fb to avoid the difficulty of one of $\sigma_{L,R} \times \mathcal{B}_{L,R}^2$ being arbitrarily close, but below the threshold \mathcal{A} while the other contribution can

be very small. In such a case the model could still pass the cut on the sum $\sigma_L \times \mathcal{B}_L^2 + \sigma_R \times \mathcal{B}_R^2 > \mathcal{A}$, but would be on the borderline of classification as either an \tilde{e}_L , \tilde{e}_R , or $\tilde{e}_L + \tilde{e}_R$ model. We will show that this loose requirement on the cross section does not affect our results. Finally, note that since $\mathcal{B}(\tilde{N}_2 \rightarrow \tilde{N}_1 \gamma)$ depends in general on both selectron masses $m_{\tilde{e}_L}$ and $m_{\tilde{e}_R}$, then \tilde{e}_L , \tilde{e}_R and $\tilde{e}_L + \tilde{e}_R$ models can each be considered a distinct class of models.

We impose no restriction on the squared branching ratio \mathcal{B}^2 (unlike Ref. [1]), nor any restriction on associated phenomenology. In practice, the cut on $\sigma \times \mathcal{B}^2$ does provide an effective lower limit on the branching ratio based on the largest allowed cross section σ , obtained from the smallest selectron mass allowed from $ee\gamma\gamma + \cancel{E}_T$ event kinematics. This avoids generating a disproportionate number of non- $ee\gamma\gamma$ events from $\tilde{e}_L\tilde{e}_L$ production in \tilde{e}_L models, and $\tilde{e}_R\tilde{e}_R$ production in \tilde{e}_R models. However, we do not constrain possible non-standard visible phenomenology from the other selectron. The absence of knowledge of both the experimental data and the efficiency of detection of such phenomenology prevents explicitly restricting our models in this regard. As an example, slepton mass degeneracy implies the rate for two smuons or staus plus two photons is at the same rate as selectrons. But, without a fully analyzed, statistically significant sample of two lepton plus two photon events, one cannot use the lack of reported events to exclude such a scenario.

4.2 Model building results

In Table 3, we present the parameters that enter our analysis common to all selectron interpretations, and the relevant ranges. For the \tilde{e}_L and \tilde{e}_R interpretations, the allowed range of $m_{\tilde{e}}$ is determined by the lower bound from kinematics $m_{\tilde{e}} \gtrsim 100$ GeV using Observation 4 in Sec. 2 (indeed $|\mu| \sim m_{\tilde{N}_1} \gtrsim 33$ GeV, from Sec. 3.4). The upper bound is obtained from the minimum threshold in the cross section times branching ratio \mathcal{A} . For $\mathcal{A} = 5, 7.5, 10$ fb, the upper bound on the slepton mass is $m_{\tilde{e}_L} < 137, 125, 118$ GeV, and $m_{\tilde{e}_R} < 115, 105, 97$ GeV, in the \tilde{e}_L and \tilde{e}_R interpretations. Notice that \tilde{e}_R models always fail the highest threshold, since the cross section never exceeds 10 fb in the allowed mass range. The mass of the other slepton that is not the source of the $ee\gamma\gamma + \cancel{E}_T$ event (hence $ee\gamma\gamma + \cancel{E}_T$ event kinematics do not apply) is allowed to take on a much wider mass range 60–500 GeV. For the $\tilde{e}_L + \tilde{e}_R$ interpretation, both sleptons still must be greater than 100 GeV by $ee\gamma\gamma + \cancel{E}_T$ event kinematics, but the upper limits are somewhat relaxed since each individual rate $\sigma_L \times \mathcal{B}_L^2$ or $\sigma_R \times \mathcal{B}_R^2$ need not be larger than the threshold; only the sum must satisfy the $\sigma \times \mathcal{B}^2$ constraint.

We have explicitly constructed roughly 2500 models in total, with somewhat more \tilde{e}_L models than \tilde{e}_R or $\tilde{e}_L + \tilde{e}_R$. The results are shown in a series of scatter plots and bar graphs that are intended to give the general character of the models. Figures 3, 4, 5 show the distribution of all the allowed models in the M_1 – M_2 plane, with groupings of models split up into three plots. All of the models pass the $ee\gamma\gamma + \cancel{E}_T$ event kinematic cuts for one or both sleptons

Parameter	Range
$M_1, M_2, \mu, \tan \beta$	randomized throughout allowed range
$m_{\tilde{q}} = m_{\tilde{t}_2}$	250, 500, 1000 GeV
$m_{\tilde{t}_1}$	> 150 GeV, $< m_{\tilde{q}}$
$\theta_{\tilde{t}}$	$[-\pi, \pi]$
m_A	50, 100, 200, 400 GeV

Table 3: Parameter ranges common to all selectron interpretations with a heavier stop. Models with a light stop are discussed in Sec. 5.

(defined by the model type), and all models pass the minimum threshold cut $\mathcal{A} = 5$ fb. In Fig. 3, the models are grouped by the type \tilde{e}_L , \tilde{e}_R , or $\tilde{e}_L + \tilde{e}_R$ according to which slepton(s) passed the $ee\gamma\gamma + \cancel{E}_T$ event kinematic cuts. In Fig. 4, the models are grouped by the rate, $5 < \sigma \times \mathcal{B}^2 < 7.5$, $7.5 < \sigma \times \mathcal{B}^2 < 10$, and $\sigma \times \mathcal{B}^2 > 10$ fb. In Fig. 5 the models are grouped by $\tan \beta$ into the (arbitrary) ranges $1 < \tan \beta < 1.5$, $1.5 < \tan \beta < 2$, and $\tan \beta > 2$. There are perhaps four regions with distinct character, and we will discuss each of them in the following.

Region 1 defined by roughly $0.8 \lesssim M_2/M_1 \lesssim 1.2$ represents the anticipated $M_1 \sim M_2$ region. All three types of models \tilde{e}_L , \tilde{e}_R and $\tilde{e}_L + \tilde{e}_R$ fall into this range, with \tilde{e}_R models almost contained within the M_2/M_1 limits. This is the region where the dynamical enhancement of the radiative neutralino branching ratio is present, with the limiting case $(M_1 - M_2) \rightarrow 0$, $\tan \beta \rightarrow 1$ giving the largest value. Hence, the highest $\sigma \times \mathcal{B}^2$ can be found in this region, but the rate need not be high since the slepton cross section can be low independent of the branching ratio. For example, \tilde{e}_R models always have $\sigma_R \times \mathcal{B}_R^2 \lesssim 8.2$ fb with $\mathcal{B}_R^2 \lesssim 98\%$, whereas \tilde{e}_L models have $\sigma_L \times \mathcal{B}_L^2 \lesssim 16.2$ fb with $\mathcal{B}_L^2 \lesssim 88\%$. Since the decay $\tilde{e}_L \rightarrow \tilde{C}_1 \nu_e$ is always present, the maximum branching ratio \mathcal{B}_L^2 is always less than the maximum for \mathcal{B}_R^2 .

Region 2 defined by roughly $M_2/M_1 \gtrsim 1.2$ is populated with mostly \tilde{e}_L models, extending barely up to the $M_2 = 2M_1$ line near $M_1 \sim 60$ GeV. The reason for the much larger range in M_2 values for \tilde{e}_L models is a direct consequence of the higher cross section $\sigma_L \sim 2.2\sigma_R$ for a given slepton mass. With a higher cross section, the total squared branching ratio can be lower, which translates into looser restrictions on the radiative neutralino branching ratio. For \tilde{e}_L and \tilde{e}_R models, the minimum \mathcal{B}^2 is 25% and 56%, which corresponds to a minimum $\mathcal{B}(\tilde{N}_2 \rightarrow \tilde{N}_1 \gamma)$ of 50% and 75% respectively (when $\mathcal{B}(\tilde{e} \rightarrow \tilde{N}_2 e) = 100\%$). Fig. 2 already showed (for a specific set of μ , $\tan \beta$, $m_{\tilde{q}}$, m_A values) that a looser restriction on the radiative branching ratio admits a larger region in the M_1 – M_2 plane. The models observed with $M_2/M_1 \gtrsim 1.2$ lie in just this extended region which benefit from the kinematical mechanism (in addition to the dynamical mechanism) for the radiative neutralino decay enhancement. This can be deduced by examining the slepton masses for the \tilde{e}_L models in this region, where one finds $m_{\tilde{e}_R} \gg m_{\tilde{e}_L}$ by a factor of

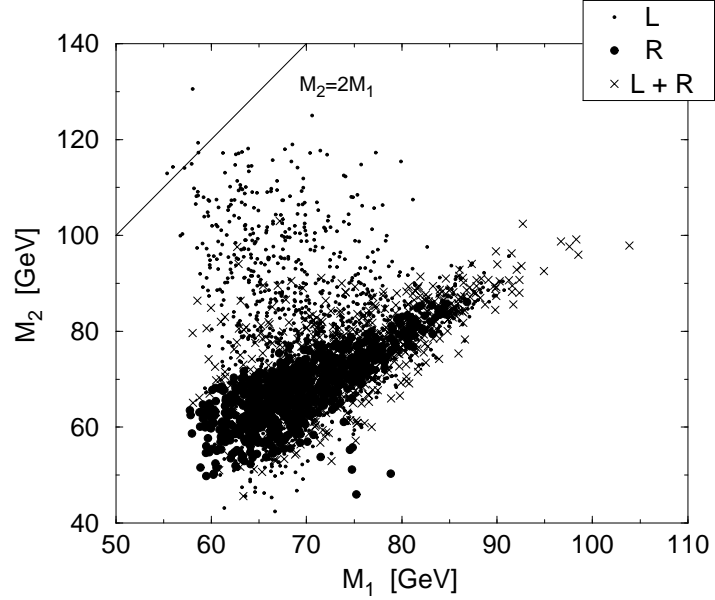


Figure 3: The models satisfying the $ee\gamma\gamma + \cancel{E}_T$ event kinematics and the minimum threshold cut $\mathcal{A} = 5$ fb are shown in the M_1 - M_2 plane. In this figure, \tilde{e}_L (L), \tilde{e}_R (R) and $\tilde{e}_L + \tilde{e}_R$ (L+R) have been separated to show the varying restrictions on either type of model.

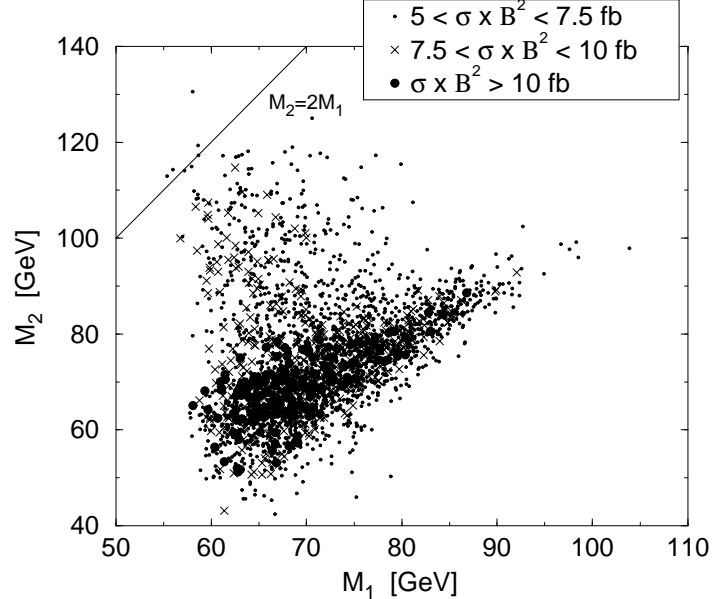


Figure 4: As in Fig. 3, except the models are distinguished by the cut on $\mathcal{A} = 5, 7.5, 10$ fb.

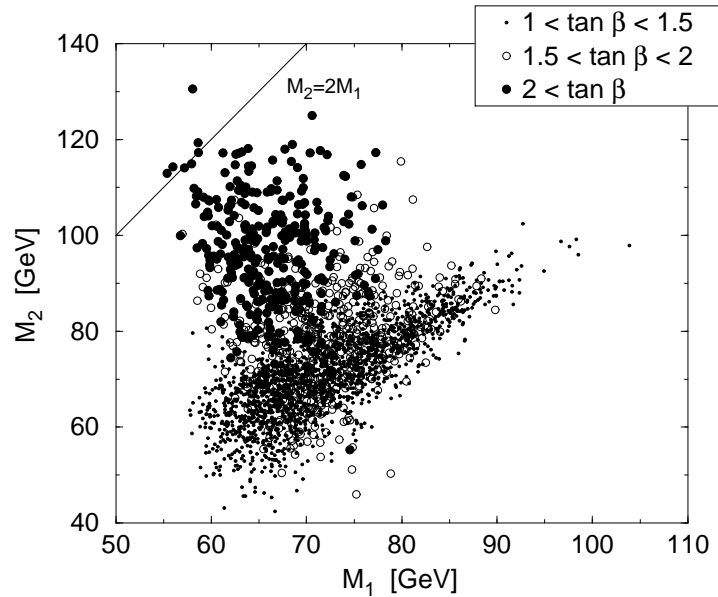


Figure 5: As in Fig. 3 except that the models are distinguished by the value of $\tan \beta$.

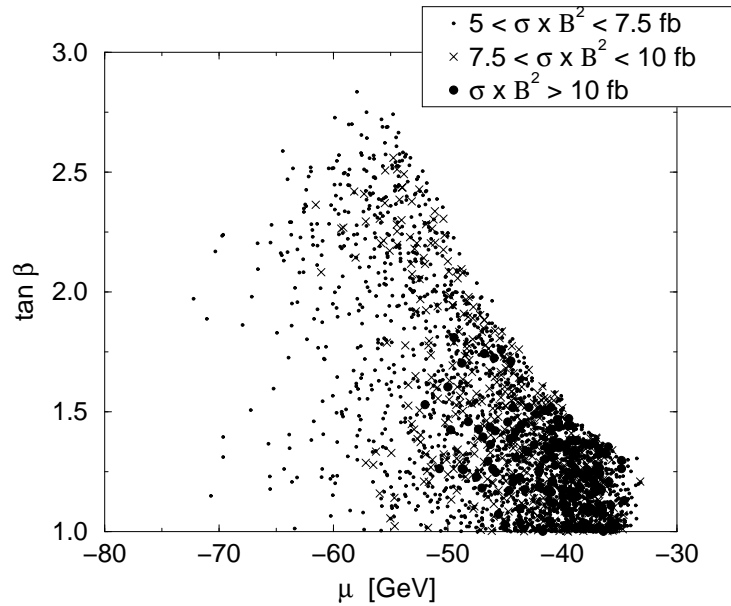


Figure 6: All of the models are shown in the μ – $\tan \beta$ plane, distinguished by the cut on $\mathcal{A} = 5, 7.5, 10 \text{ fb}$.

2 or more. This is necessary to obtain a large radiative neutralino decay, since the branching ratio for 3-body decays $\tilde{N}_2 \rightarrow \tilde{N}_1 l^+ l^-$ through sleptons cannot be reduced to zero when the kinematical mechanism for a large $\mathcal{B}(\tilde{N}_2 \rightarrow \tilde{N}_1 \gamma)$ operates [11]. In addition, the squark masses must also be heavy to prevent the analogous 3-body decays mediated by squarks, although the choice of $m_{\tilde{q}} \geq 250$ GeV in our models is sufficient. Finally, the existence of only \tilde{e}_L models in this region is due to the fact that kinematical enhancement of the radiative neutralino decay cannot be maximized simultaneously with the $m_{\tilde{N}_2} - m_{\tilde{N}_1} > 21$ GeV, and so \mathcal{B}^2 cannot be very large. Thus, one needs a large cross section to supplement a lower \mathcal{B}^2 , which can only be achieved with \tilde{e}_L models.

The character of the ‘extended’ \tilde{e}_L models in Region 2 is more clearly visible in Fig. 5, where all of the models have been plotted in the M_1 – M_2 plane distinguished only by the $\tan \beta$ value. The models with $M_2/M_1 \gtrsim 1.2$ always have $1.5 \lesssim \tan \beta \lesssim 2.8$, where the upper limit in $\tan \beta$ (and M_1, M_2) is established by the smallest allowed radiative neutralino branching ratio. Indeed, the kinematical mechanism that contributes to the enhanced radiative neutralino decay in this region does not necessarily require $\tan \beta \simeq 1$ [11]. In Fig. 4 it is clear that increasing the threshold \mathcal{A} to 7.5, 10 pb restricts $M_2/M_1 \lesssim 1.9, 1.2$, and so the existence of models with $M_2 = 2M_1$ is sensitive to the choice of the minimum threshold. Further, while $M_2 = 2M_1$ seemingly admits gaugino mass unification, we noted above that for the extended \tilde{e}_L models $m_{\tilde{e}_R} \gg m_{\tilde{e}_L}$. Hence, scalar mass unification probably cannot be achieved, at least in the slepton sector, and a completely unified scenario seems not to be compatible with the $ee\gamma\gamma + \cancel{E}_T$ event.

In Region 3 loosely defined as $M_2/M_1 \lesssim 0.8$, \tilde{e}_R models appear near $M_1 \sim 75$ GeV and $M_2 \sim 50$ GeV. These models have $\sigma_R \times \mathcal{B}_R^2 \sim 5.5$ fb and $\tan \beta \sim 2$. This is the only region where the usual mass hierarchy $|\mu| < M_2$ can be slightly violated. On closer inspection one finds the chargino mass is about ~ 68 GeV. We found no \tilde{e}_L models in this region, due to the light chargino that induces a large branching ratio for $\tilde{e}_L \rightarrow \tilde{C}\nu_e$ over $\tilde{e}_L \rightarrow \tilde{N}_2 e$. Also, the width for the 3-body decay $\tilde{N}_2 \rightarrow \tilde{N}_1 e^+ e^-$ turns out to be considerably enhanced when the \tilde{e}_L is light. Hence the radiative neutralino decay is strongly suppressed in such a case, and thus \tilde{e}_L models cannot be constructed in Region 3. As $\tan \beta$ is increased, the chargino mass becomes smaller and thus is excluded by LEP130-136 constraints. Lowering $\tan \beta$ decreases the radiative neutralino branching ratio, and so is excluded by the $\sigma \times \mathcal{B}^2$ cut. This localized region is basically due to a hybrid of the dynamical and kinematical enhancement of the radiative neutralino decay. One can use an argument analogous to that used for Region 2, to observe that $m_{\tilde{e}_L} \gg m_{\tilde{e}_R}$ in all of the models. The absence of light \tilde{e}_L is a consequence of the kinematical mechanism at least partly at work. Thus, these models sit at the edge of exclusion, between a multitude of constraints.

Finally, the voids with no models found for $M_1 \gtrsim 85$ GeV with $M_2/M_1 \lesssim 0.8$ or $M_2/M_1 \gtrsim 1.2$ are excluded by a low radiative neutralino branching ratio. This behavior can be discerned from Fig. 2, but of course the numerical result here encompasses a full range of μ and $\tan \beta$ values.

Naively one might think that $\tilde{e}_L + \tilde{e}_R$ models can always be constructed from \tilde{e}_L or \tilde{e}_R models, by simply shifting the other slepton mass such that $m_{\tilde{e}_L} \approx m_{\tilde{e}_R}$. This construction always satisfies the $ee\gamma\gamma + \cancel{E}_T$ event kinematics, which are of course invariant under $L \leftrightarrow R$. Indeed, such a construction can work in the region with a dominant dynamical enhancement of the radiative neutralino decay. However, the construction need *not* work in the region where a kinematic enhancement of the radiative neutralino decay occurs, such as in Region 2 populated by \tilde{e}_L models. As discussed above, $m_{\tilde{e}_R} \gg m_{\tilde{e}_L}$ in this region which prevented 3-body decays $\tilde{N}_2 \rightarrow \tilde{N}_1 l^+ l^-$ mediated by \tilde{l}_R to overwhelm the radiative decay $\tilde{N}_2 \rightarrow \tilde{N}_1 \gamma$.

In general, $\tilde{e}_L + \tilde{e}_R$ models tend to be constrained similar to \tilde{e}_R models, but looser bounds on M_2/M_1 are present and larger M_1 values accessible. The region with $\tilde{e}_L + \tilde{e}_R$ models that is devoid of \tilde{e}_L or \tilde{e}_R models, defined as Region 4, has the properties that the $\sigma \times \mathcal{B}^2 < 7.5$ fb and $\tan \beta \lesssim 1.5$, while simultaneously $\sigma_L \times \mathcal{B}_L^2 < 5$ fb and $\sigma_R \times \mathcal{B}_R^2 < 5$ fb. For $M_1 (\approx M_2) \gtrsim 90$ GeV, larger chargino and neutralino masses are allowed than in either \tilde{e}_L or \tilde{e}_R models. In particular, $m_{\tilde{N}_2}$ is near the upper bound from $ee\gamma\gamma + \cancel{E}_T$ event kinematics, so presumably values of M_1 higher than obtained in $\tilde{e}_L + \tilde{e}_R$ models are not accessible. As for the size of the $ee\gamma\gamma$ rate, the maximum (summed) $\sigma \times \mathcal{B}^2 \lesssim 19$ fb, so it would appear one does not gain more than a factor of about 1.2 over the maximum $ee\gamma\gamma$ rate for \tilde{e}_L models alone. Further, since $\tilde{e}_L + \tilde{e}_R$ models enlarge the allowed region of parameter space by reducing the minimum $\sigma_{L,R} \times \mathcal{B}_{L,R}^2$, one can use the results as an indication of the region resulting from relaxing the $\mathcal{A} = 5$ fb cut in \tilde{e}_L or \tilde{e}_R models separately. It is clear that $\tilde{e}_L + \tilde{e}_R$ models have a distinct character separate from \tilde{e}_L or \tilde{e}_R models.

In Fig. 6 we show the models in the μ – $\tan \beta$ plane to completely specify the parameters. Three features are worthy of explanation: First, the upper and lower limits on $|\mu|$ are approximately the upper and lower limits on $m_{\tilde{N}_1}$, since $\tilde{N}_1 \approx \tilde{H}_b$. From Observation 1 in Sec. 2, we know the upper limit on $m_{\tilde{N}_1}$ is 50, 74 GeV for \tilde{e}_R and \tilde{e}_L models, and this can be translated into rough upper limits on $|\mu|$. The lower limit on $m_{\tilde{N}_1} \sim |\mu| \gtrsim 33$ GeV, and the region devoid of models in the upper right-hand corner (larger $\tan \beta$, smaller $|\mu|$), come from a confluence of LEP1, LEP130-136 and $ee\gamma\gamma + \cancel{E}_T$ constraints as explained in Section 3.4. For example, the LEP constraints on chargino and neutralino production forbid models with $|\mu| < 40$ (50) GeV for $\tan \beta > 1.5$ (2), once very small $|\mu|$ are excluded by $ee\gamma\gamma + \cancel{E}_T$ event kinematics.

The final allowed ranges of M_1 , M_2 , μ and the ranges of masses $m_{\tilde{N}_1}$, $m_{\tilde{N}_2}$, $m_{\tilde{N}_3}$, $m_{\tilde{N}_4}$, $m_{\tilde{C}_1}$, $m_{\tilde{C}_2}$ derived from them are presented in Fig. 7. The effect of imposing a stricter cut $\mathcal{A} = 5, 7.5, 10$ fb is shown, in addition to the ranges for \tilde{e}_R models only. The latter is to give an idea of the stronger constraints that exist when a specific origin of the $ee\gamma\gamma + \cancel{E}_T$ event is assumed. Correlations between a selection of chargino/neutralino masses can be discerned from Fig. 8. Sleptons can also have correlations with chargino/neutralino masses, which are relevant for the branching ratios. We present these mass ranges in Table 4. For example, notice that the mass of the slepton satisfying the $ee\gamma\gamma + \cancel{E}_T$ event kinematics always obeys $m_{\tilde{e}} > m_{\tilde{C}_1}$.

Squarks do not play a large role in our analysis, since they are assumed to be heavier

Model Type	Mass difference	Range (in GeV)		
\tilde{e}_L	$m_{\tilde{e}_L} - m_{\tilde{N}_1}$	64	\rightarrow	87
	$m_{\tilde{e}_L} - m_{\tilde{N}_2}$	23	\rightarrow	63
	$m_{\tilde{e}_L} - m_{\tilde{N}_3}$	7	\rightarrow	35
	$m_{\tilde{e}_L} - m_{\tilde{N}_4}$	-50	\rightarrow	6
	$m_{\tilde{e}_L} - m_{\tilde{C}_1}$	18	\rightarrow	61
	$m_{\tilde{e}_L} - m_{\tilde{C}_2}$	-51	\rightarrow	14
	$m_{\tilde{e}_L} - m_{\tilde{\nu}_e}$	0	\rightarrow	26
	$m_{\tilde{\nu}_e} - m_{\tilde{N}_1}$	39	\rightarrow	79
	$m_{\tilde{\nu}_e} - m_{\tilde{N}_2}$	9	\rightarrow	55
	$m_{\tilde{\nu}_e} - m_{\tilde{N}_3}$	-17	\rightarrow	27
	$m_{\tilde{\nu}_e} - m_{\tilde{N}_4}$	-71	\rightarrow	1
	$m_{\tilde{\nu}_e} - m_{\tilde{C}_1}$	14	\rightarrow	43
	$m_{\tilde{\nu}_e} - m_{\tilde{C}_2}$	-71	\rightarrow	11
\tilde{e}_R	$m_{\tilde{e}_R} - m_{\tilde{N}_1}$	64	\rightarrow	77
	$m_{\tilde{e}_R} - m_{\tilde{N}_2}$	23	\rightarrow	53
	$m_{\tilde{e}_R} - m_{\tilde{N}_3}$	6	\rightarrow	25
	$m_{\tilde{e}_R} - m_{\tilde{N}_4}$	-27	\rightarrow	-2
	$m_{\tilde{e}_R} - m_{\tilde{C}_1}$	18	\rightarrow	44
	$m_{\tilde{e}_R} - m_{\tilde{C}_2}$	-21	\rightarrow	8

Table 4: Ranges of selected mass differences between \tilde{e}_L , $\tilde{\nu}_e$, and \tilde{e}_R and chargino/neutralinos in \tilde{e}_L and \tilde{e}_R models.

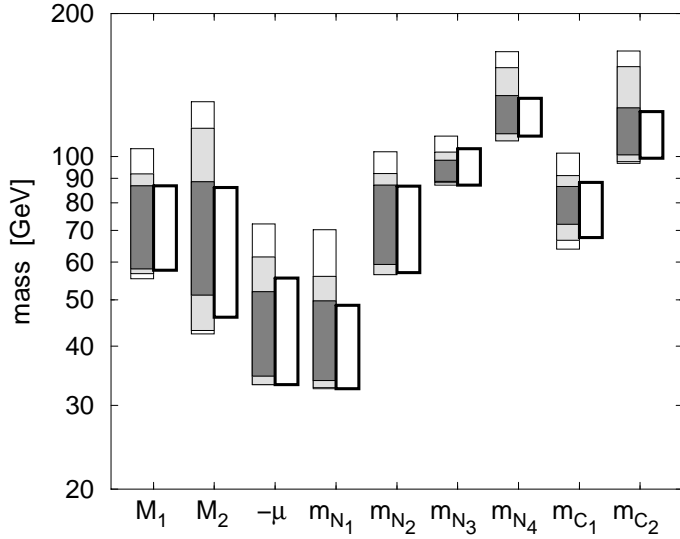


Figure 7: The allowed mass spectrum is shown for all models (shaded bands on the left) and for \tilde{e}_R models only (thick solid outline on the right). The increasingly darker shades in the left-hand column correspond to increasing stricter cuts on $\mathcal{A} = 5, 7.5, 10$ fb. As for $\tan\beta$, the allowed range in all models is $1.0 < \tan\beta < (2.8, 2.6, 1.8)$ for $\mathcal{A} = 5, 7.5, 10$ fb respectively. The allowed range of $\tan\beta$ in \tilde{e}_R models only is $1.0 < \tan\beta < 2.0$.

than charginos and neutralinos. However, two effects for a given value of the squark mass persist: First, in 3-body decays of neutralinos, the t -channel exchange of squarks can lower the branching ratio of $\tilde{N}_2 \rightarrow \tilde{N}_1\gamma$, hence the rate $\sigma \times \mathcal{B}^2$. Second, the stops enter in the loops of the one-loop radiative neutralino decay width (since the Yukawa coupling of \tilde{H}_b to \tilde{t} is significant), and also tend to slightly decrease the radiative neutralino branching ratio for lighter $m_{\tilde{t}_{1,2}}$ [11]. With $m_{\tilde{q}} = m_{\tilde{t}_2} = 250$ GeV, we found no \tilde{e}_R models satisfying the $\mathcal{A} = 5$ fb cut, and \tilde{e}_L or $\tilde{e}_L + \tilde{e}_R$ models always have $\sigma \times \mathcal{B}^2 \lesssim 8$ fb.

The effect of different neutral CP-odd Higgs masses m_A is primarily confined to the neutralino branching ratios, although H^\pm does enter the one-loop radiative neutralino decay width. We find that varying m_A from 50 to 400 GeV does not significantly change the size of the radiative neutralino branching ratio, hence the $\sigma \times \mathcal{B}^2$ for the $ee\gamma\gamma + \cancel{E}_T$ event.

4.3 Neutralino composition and branching ratios

In Fig. 9 we show the (maximum) allowed range of the neutralino composition $\langle \tilde{N}_i | \tilde{\chi} \rangle^2$ of all of the models in the $\tilde{\chi} = \tilde{\gamma}, \tilde{Z}, \tilde{H}_a, \tilde{H}_b$ basis. For a given threshold in $\sigma \times \mathcal{B}^2$ applied to all

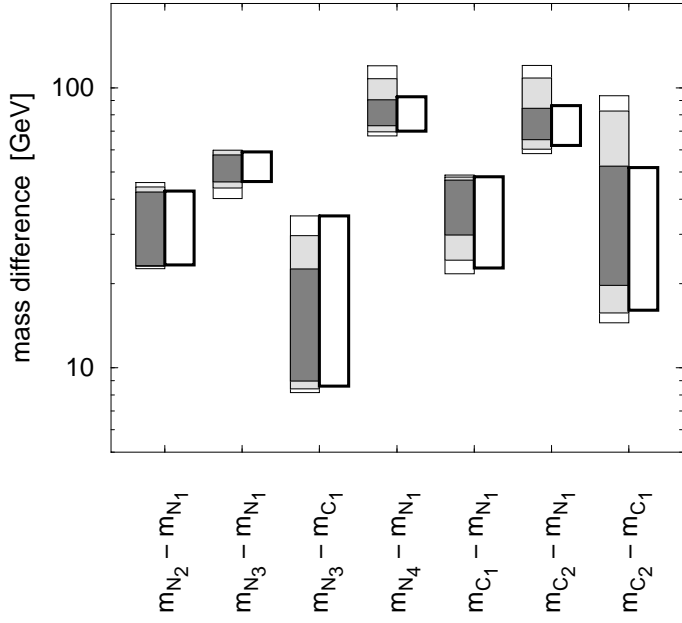


Figure 8: As in Fig. 7, except that mass differences between certain charginos and neutralinos are shown.

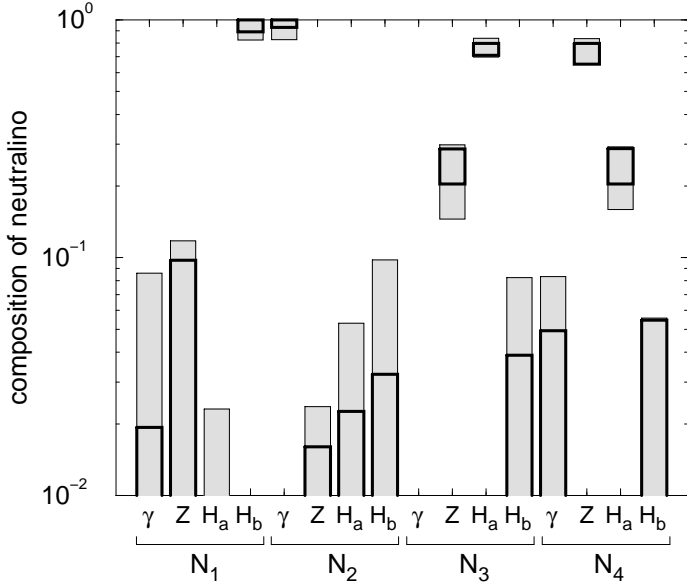


Figure 9: The allowed range of all four neutralinos' composition $\langle \tilde{N} | \tilde{\chi} \rangle^2$ in terms of the interaction eigenstates $\tilde{\chi} = \tilde{\gamma}, \tilde{Z}, \tilde{H}_a, \tilde{H}_b$ is shown for all of the models. The thick solid outline corresponds to \tilde{e}_R models only. Bars that touch the x-axis correspond to a neutralino component that can be lower than 10^{-2} ; the absence of a bar for the $\tilde{\gamma}$ component of \tilde{N}_3 implies $\langle \tilde{N}_3 | \tilde{\gamma} \rangle^2 < 10^{-2}$ for all models.

models, the minimum radiative neutralino branching ratio is always larger for \tilde{e}_R than for \tilde{e}_L models. A larger minimum radiative neutralino branching ratio implies the constraints on the neutralino composition must be similarly stronger, hence the differing notation for all models and \tilde{e}_R models in the plot. We make three observations: First, we find that

$$\tilde{N}_1 \simeq \tilde{H}_b, \quad \tilde{N}_2 \simeq \tilde{\gamma}, \quad (19)$$

so the lightest two neutralinos are composed of exactly the content expected from Eq. (11). To a lesser extent,

$$\tilde{N}_3 \sim \tilde{H}_a, \quad \tilde{N}_4 \sim \tilde{Z}, \quad (20)$$

the heavier two neutralinos turn out have a fairly specific composition as well. This will be relevant to the branching ratios and cross sections for associated phenomenology. Second, \tilde{N}_1 tends to have a much larger \tilde{Z} component than \tilde{N}_2 . Third, the required purity of the lightest neutralinos in \tilde{e}_R models is significant compared with \tilde{e}_L models, and this is perhaps most easily observed by looking at for example the photino content of \tilde{N}_1 and \tilde{N}_2 in Fig. 9.

In the following discussion of the branching ratios (and the discussion in subsequent sections), we discuss only the distinctions between \tilde{e}_L and \tilde{e}_R models, since the branching ratios in $\tilde{e}_L + \tilde{e}_R$ models are a relatively simple extension of \tilde{e}_L and \tilde{e}_R separately. The range of branching ratios of \tilde{N}_2 are shown in Table 5. In the pure state limit $\tilde{N}_2 = \tilde{\gamma}$, only the radiative channel is open for \tilde{N}_2 . However, the impurity of \tilde{N}_2 (see Fig. 9) causes other modes to have non-negligible branching fractions (\tilde{N}_2 is somewhat of a special case since the radiative decay branching ratio is required to be large). The possible decays for \tilde{N}_2 in our models are: $\tilde{N}_1\gamma$, $\tilde{N}_1\text{"}Z\text{"}$, $\tilde{C}_1\text{"}W\text{"}$, $\tilde{\nu}\nu$, \tilde{l}_Ll , \tilde{l}_Rl . We use “ Z ” and “ W ” to mean the 3-body decay mediated by an on- or off-shell Z and W , plus off-shell sleptons and squarks. The rate for the final states “ Z ” $\rightarrow l^+l^-, \nu\bar{\nu}, q\bar{q}$ and “ W ” $\rightarrow l\nu, q\bar{q}'$ are determined roughly by the corresponding SM gauge boson branching ratios. The only significant deviation from the SM gauge boson branching fractions is modes that involve sleptons, since the $ee\gamma\gamma + \cancel{E}_T$ event requires at least one slepton is light. The presence of some modes depends on the particular class of models; for example in \tilde{e}_L models, the mode $\tilde{N}_2 \rightarrow \tilde{l}_Rl$ is open if $m_{\tilde{l}_R} < m_{\tilde{N}_2}$. This never happens in \tilde{e}_R models since $\tilde{e}_R \rightarrow \tilde{N}_2e$ is required to obtain the $ee\gamma\gamma + \cancel{E}_T$ event! The 2-body mode $\tilde{N}_2 \rightarrow \tilde{\nu}\nu$ is open if $m_{\tilde{\nu}} < m_{\tilde{N}_2}$, which happens in \tilde{e}_R models and could potentially happen in \tilde{e}_L models. However, for \tilde{e}_L models one never finds decays $\tilde{N}_2 \rightarrow \tilde{\nu}\nu$ because the mass splitting between $\tilde{\nu}$ and \tilde{l}_L is never more than about 25 GeV (see Table 4). Since there always must be a large mass difference between $m_{\tilde{e}_L}$ and $m_{\tilde{N}_2}$ from $ee\gamma\gamma + \cancel{E}_T$ event kinematics, then the 2-body mode into a sneutrino is always closed.

The \tilde{N}_3 and \tilde{N}_4 branching ratio pattern is progressively more complicated than for the lighter neutralino due to possible 2-body decays into sleptons and Higgs bosons. For \tilde{N}_3 , there are several distinct classes of final states: $\tilde{N}_{1,2}\text{"}Z\text{"}$, $\tilde{C}_1\text{"}W\text{"}$, $\tilde{N}_1h(A)$, \tilde{l}_Ll , \tilde{l}_Rl , $\tilde{\nu}\nu$; all other possible channels are strongly suppressed or forbidden. For example, for the heavier chargino one has $m_{\tilde{C}_2} > m_{\tilde{N}_3}$ in all of our models, hence \tilde{N}_3 decay into \tilde{C}_2 is forbidden.

The upper limits on the mass differences $m_{\tilde{N}_3} - m_{\tilde{N}_1} < 60$ GeV and $m_{\tilde{N}_3} - m_{\tilde{C}_1} < 35$ GeV in our models are crucial to determining the allowed decays of \tilde{N}_3 . In particular, the decay $\tilde{N}_3 \rightarrow \tilde{N}_1 h$ or $\tilde{N}_3 \rightarrow \tilde{N}_1 A$ will only occur when m_h or $m_A < 60$ GeV, with constraints from LEP that exclude $m_h < 44$ GeV and the coupling $\sin^2(\beta - \alpha) \lesssim \frac{m_h}{60}$ GeV. The restriction on the mass of A from LEP that excludes $m_A < 22$ GeV is considerably weaker than the one on m_h , and so decays $\tilde{N}_3 \rightarrow \tilde{N}_1 A$ are always possible with an appropriate choice of m_A (provided this does not imply an excluded m_h value). The situation is actually considerably more subtle. We find decays into \tilde{N}_1 “Z” are not suppressed even if decays into the light Higgs h are open, with a maximum $\mathcal{B}(\tilde{N}_3 \rightarrow \tilde{N}_1 h) \sim 35\%$ while $\tilde{N}_3 \rightarrow \tilde{N}_1 A$ decay is closed. However, with low $\tan \beta$ the mass splitting between m_A and m_h tends to be small for $m_A \sim 50$ GeV, and because of the couplings, decays into A typically dominate over h if kinematically accessible. In \tilde{e}_L (\tilde{e}_R) models, the decay $\tilde{N}_3 \rightarrow \tilde{l}_L l$ ($\tilde{N}_3 \rightarrow \tilde{l}_R l$) is always kinematically forbidden. Thus, it is only when the other slepton (\tilde{l}_R in \tilde{e}_L models, \tilde{l}_L in \tilde{e}_R models) has a mass $m_{\tilde{l}} < m_{\tilde{N}_3}$ that 2-body decays into sleptons can dominate. When kinematically accessible, the branching ratio for the 2-body decay $\tilde{N}_3 \rightarrow \tilde{\nu} \nu$ can be $\sim 100\%$, and is always larger than decays into $\tilde{l}_L l$ by a factor of at least 10. This is due to the larger \tilde{Z} impurity in \tilde{N}_3 , i.e. $\langle \tilde{N}_3 | \tilde{Z} \rangle^2 \gg \langle \tilde{N}_3 | \tilde{\gamma} \rangle^2$, and Eq. (6) requiring $m_{\tilde{\nu}} < m_{\tilde{l}_L}$. The 3-body decays into the lightest chargino $\tilde{N}_3 \rightarrow \tilde{C}_1$ “W” depend on the chargino mixings, but are always smaller than the 3-body decays $\tilde{N}_3 \rightarrow \tilde{N}_1$ “Z” mainly due to phase space. The presence of decays into \tilde{C}_1 “W” can suppress the branching ratio for decays into \tilde{N}_1 “Z” by at most a factor of 2, but even then the branching ratios for \tilde{N}_3 are still larger into \tilde{N}_1 “Z”. Also, \tilde{N}_3 decays into \tilde{N}_2 are strongly suppressed, because of the particular neutralino composition in our models.

The branching ratios of \tilde{N}_4 are quite intricate, however a few features can be discerned. The main possible decays include: $\tilde{N}_{1,2,3}$ “Z”, $\tilde{C}_{1,2}$ “W”, $\tilde{N}_1 h(A)$, and possibly open 2-body modes $\tilde{l}_L l$, $\tilde{l}_R l$, $\tilde{\nu} \nu$. Since the mass difference $m_{\tilde{N}_4} - m_{\tilde{N}_1} \gtrsim 67$ GeV and can be as large as 100 (120) GeV in \tilde{e}_R (\tilde{e}_L) models, then the decay $\tilde{N}_4 \rightarrow \tilde{N}_1 h$ is a prominent possibility if kinematically allowed. We find that even if $\tilde{N}_4 \rightarrow \tilde{N}_1 A$ is also open, it is always suppressed to of order $\sim 5\%$ compared with a much larger $\tilde{N}_1 h$ mode. This is because the \tilde{N}_4 composition is roughly inverted with respect to the \tilde{N}_3 one, which feeds into the \tilde{N}_4 couplings to the Higgs sector. In \tilde{e}_R models, the 2-body slepton decay $\tilde{N}_4 \rightarrow \tilde{l}_R l$ is always open, and can be $\sim 100\%$. In \tilde{e}_L models, the decay $\tilde{N}_4 \rightarrow \tilde{\nu} \nu$ is typically open, but sometimes can be kinematically inaccessible. Note that if both $\tilde{N}_4 \rightarrow \tilde{\nu} \nu$ and $\tilde{N}_4 \rightarrow \tilde{l}_L l$ are accessible, then $\tilde{N}_4 \rightarrow \tilde{\nu} \nu$ always overwhelms $\tilde{N}_4 \rightarrow \tilde{l}_L l$ by at least a factor of 5 due to the large \tilde{Z} component of \tilde{N}_4 (see Fig. 9) and phase space. Similarly, if none of the 2-body modes are open, then the neutralino composition of \tilde{N}_4 implies \tilde{N}_1 “Z” dominates over all other 3-body decays.

4.4 Chargino composition and branching ratios

The chargino composition is determined by the mixing matrices U and V , as defined in

Final State	Kinematic Condition	Range in \tilde{e}_L models	Range in \tilde{e}_R models
\tilde{N}_1 “Z”	—	→ 47	→ 26
$\tilde{N}_1\gamma$	—	53 → 100	74 → 100
\tilde{C}_1 “W”	$m_{\tilde{N}_2} > m_{\tilde{C}_1}$	→ 10	→ 2
$\tilde{l}_L\bar{l} + \tilde{l}_L\bar{l}$	$m_{\tilde{N}_2} > m_{\tilde{l}_L}$	—	—
$\tilde{l}_R\bar{l} + \tilde{l}_R\bar{l}$	$m_{\tilde{N}_2} > m_{\tilde{l}_R}$	→ 3	—
$\tilde{\nu}\bar{\nu} + \tilde{\nu}\bar{\nu}$	$m_{\tilde{N}_2} > m_{\tilde{\nu}}$	—	→ 8

Table 5: Ranges of selected \tilde{N}_2 branching ratios (in %) in our models. The notation ‘→ X ’ denotes a range from less than 1% up to $X\%$. The kinematic condition must be satisfied for the mode to be open; no kinematic condition implies the mode always open. Note that the 2-body decays into sleptons sums over all three families, because of the assumption of slepton mass degeneracy. The final state into $\tilde{N}_1 e^+ e^-$ can be enhanced over that expected from \tilde{N}_1 “Z” because of light slepton exchange.

Final State	Kinematic Condition	Range in \tilde{e}_L models	Range in \tilde{e}_R models
\tilde{N}_1 “Z”	—	→ 99	→ 99
$\tilde{N}_1 h$	$m_{\tilde{N}_3} - m_{\tilde{N}_1} > m_h$	→ 29	→ 31
$\tilde{N}_1 A$	$m_{\tilde{N}_3} - m_{\tilde{N}_1} > m_A$	→ 66	→ 71
\tilde{C}_1 “W”	—	→ 34	→ 29
\tilde{N}_2 “Z”	—	→ 1.5	→ 1.5
$\tilde{l}_L\bar{l} + \tilde{l}_L\bar{l}$	$m_{\tilde{N}_3} > m_{\tilde{l}_L}$	—	→ 22
$\tilde{l}_R\bar{l} + \tilde{l}_R\bar{l}$	$m_{\tilde{N}_3} > m_{\tilde{l}_R}$	→ 99	—
$\tilde{\nu}\bar{\nu} + \tilde{\nu}\bar{\nu}$	$m_{\tilde{N}_3} > m_{\tilde{\nu}}$	→ 99	→ 99

Table 6: Ranges of selected \tilde{N}_3 branching ratios (in %), as in Table 5.

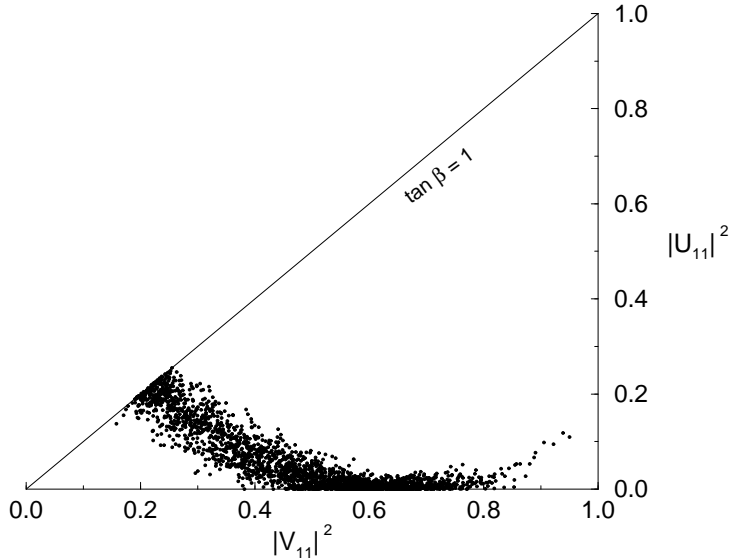


Figure 10: Scatter plot of the chargino mixing matrix elements U_{11} , V_{11} for all models. The narrow band of points indicates the presence of strong constraints in our models from the $ee\gamma\gamma + \cancel{E}_T$ event.

Sec. 3.1. U and V (real and orthogonal in our conventions) can be expressed in terms of two independent rotation angles ϕ_{\mp} (see e.g. Ref. [14]), however the Dirac nature of the chargino spinors does not allow an intuitive identification of their Wino and Higgsino components. Nevertheless, in Fig. 10 we present the elements $|V_{11}|^2 = \cos^2 \phi_+$ vs. $|U_{11}|^2 = \cos^2 \phi_-$ to give a sense of the constraints that the $ee\gamma\gamma + \cancel{E}_T$ event imposes on the chargino composition. In the limit $\tan \beta \rightarrow 1$, the chargino mass matrix is symmetric which implies $\phi_- = \phi_+$, and so $U = V$. In Fig. 10, this is the diagonal line where $|U_{11}|^2 = |V_{11}|^2$, and note that along this line our models lie in the region $0.15 \lesssim |U_{11}|^2 \lesssim 0.25$, due to the mass hierarchy $M_2 > |\mu|$. Here, one can identify \tilde{C}_1 as mostly a charged Higgsino. For larger $\tan \beta$ values, $|V_{11}|^2$ tends to increase, while $|U_{11}|^2 \lesssim 0.25$ throughout our models.

The branching ratios of \tilde{C}_1 are displayed in Table 7, that assumes $m_{\tilde{t}_1}$ is heavier than both charginos as in the discussion below. There are only a few possible channels: $\tilde{N}_{1,2}W$, $\tilde{l}_L\nu, \tilde{\nu}l$. Further, the 3-body decays into \tilde{N}_2W are always $\lesssim 5\%$ due to the photino nature of \tilde{N}_2 , the Higgsino nature of \tilde{C}_1 and phase space. Thus, the 3-body decays into \tilde{N}_1W are the typical decay pattern. In \tilde{e}_L models $\tilde{l}_L, \tilde{\nu}$ are always heavier than \tilde{C}_1 , thus it is only in \tilde{e}_R models that 2-body channels into $\tilde{l}_L\nu$ and $\tilde{\nu}l$ can possibly be open. When both are allowed, these 2-body decays can sum to a branching ratio of $\sim 100\%$ (when summed over three families).

The branching ratios of \tilde{C}_2 are displayed in Table 8. The possible decays include: $\tilde{N}_{1,2,3}W$, $\tilde{C}_1f\bar{f}$ ($f = l, \nu, q$), $\tilde{l}_L\nu, \tilde{\nu}l$, and the Higgs channels $\tilde{N}_{1,2}H^\pm, \tilde{C}_1h(A)$. When only 3-body de-

Final State	Kinematic Condition	Range in \tilde{e}_L models	Range in \tilde{e}_R models
$\tilde{N}_1 "W"$	—	95 → 100	→ 100
$\tilde{N}_2 "W"$	$m_{\tilde{C}_1} > m_{\tilde{N}_2}$	→ 5	→ 5
$\tilde{\nu}l$	$m_{\tilde{C}_1} > m_{\tilde{\nu}}$	—	→ 100
$\tilde{l}_L \nu$	$m_{\tilde{C}_1} > m_{\tilde{l}_L}$	—	→ 50

Table 7: Ranges of selected \tilde{C}_1 branching ratios (in %), as in Table 5. $m_{\tilde{t}_1} > m_{\tilde{C}_1}$ is assumed here.

Final State	Kinematic Condition	Range in \tilde{e}_L models	Range in \tilde{e}_R models
$\tilde{N}_1 "W"$	—	→ 92	→ 100
$\tilde{N}_2 "W"$	—	→ 23	→ 17
$\tilde{N}_3 "W"$	—	→ 0.7	→ 0.3
$\tilde{C}_1 f\bar{f}$	—	→ 4	→ 1
$\tilde{\nu}l$	$m_{\tilde{C}_2} > m_{\tilde{\nu}}$	→ 95	→ 69
$\tilde{l}_L \nu$	$m_{\tilde{C}_2} > m_{\tilde{l}_L}$	→ 52	→ 59

Table 8: Ranges of selected \tilde{C}_2 branching ratios (in %) assuming $m_A \gtrsim 100$ GeV, as in Table 5. $m_{\tilde{t}_1} > m_{\tilde{C}_2}$ is assumed here.

cays are open, $\tilde{N}_1 "W"$ dominates over all other decays. However, $\tilde{N}_2 l \nu_l$ is roughly 1–5%, and can be larger than the decays into $\tilde{N}_2 q \bar{q}'$ due to the possible enhancement from light slepton exchange in the 3-body decay. The 2-body decay $\tilde{C}_2 \rightarrow \tilde{\nu}l$ summed over three families can have a branching ratio up to 95%, when it is the only slepton mode open (the remainder is distributed to the 3-body decays as above). When both $\tilde{C}_2 \rightarrow \tilde{\nu}l$ and $\tilde{C}_2 \rightarrow \tilde{l}_L \nu$ are simultaneously open, the sum can be nearly 100%. Finally, the 2-body decay into $\tilde{N}_1 H^\pm$ is also possible when $m_{H^\pm} \lesssim 90$ (120) GeV, for \tilde{e}_R (\tilde{e}_L) models, which requires $m_A \lesssim 50$ (100) GeV. In addition, decays into neutral Higgs bosons are possible when $m_{\tilde{C}_2} - m_{\tilde{C}_1} < m_{h,A}$.

4.5 Sneutrino branching ratios

In the selectron interpretation, sneutrinos do not directly enter the branching ratios relevant for the $ee\gamma\gamma + \cancel{E}_T$ event, however the mass of the sneutrino $\tilde{\nu}_e$ is necessarily smaller than $m_{\tilde{e}_L}$ due to the sum rule in Eq. (6), and so the sneutrino is certainly relevant in \tilde{e}_L and $\tilde{e}_L + \tilde{e}_R$ models. In Ref. [1] it was shown that the cross section for sneutrino production $p\bar{p} \rightarrow \tilde{\nu}_e \tilde{\nu}_e$ is

comparable to $\tilde{e}_L \tilde{e}_L$ production, and $\tilde{e}_L \tilde{\nu}_e$ production is larger by a factor of 2–3 for a fixed value of $m_{\tilde{e}_L}$. Thus, the viability of the $ee\gamma\gamma + \cancel{E}_T$ event as \tilde{e}_L production (and the ability to distinguish \tilde{e}_L from \tilde{e}_R) depends in part on the phenomenology associated with sneutrinos.

The dominant branching fraction of sneutrinos depends on the size of the \tilde{Z} component of the neutralinos and the gaugino mixings of the chargino, in addition to the mass hierarchy. There are 4×3 kinematic possibilities, where $m_{\tilde{\nu}}$ is lighter or heavier than $m_{\tilde{N}_{2,3,4}}$ and $m_{\tilde{C}_{1,2}}$. In the limit of pure neutralino states $\tilde{N}_1 = \tilde{H}_b$ and $\tilde{N}_2 = \tilde{\gamma}$, the sneutrino has no coupling to the lightest two neutralinos since it does not couple to either pure state. Thus, in the case where $m_{\tilde{\nu}} < m_{\tilde{C}_{1,2}}$, the dominant decay of $\tilde{\nu}$ will be to the kinematically accessible neutralino with the largest \tilde{Z} component. The relative branching fraction into \tilde{N}_1 or \tilde{N}_2 is therefore determined by the size of their \tilde{Z} component *impurity*. The branching ratios are shown in Table 9.

For \tilde{e}_L models, $m_{\tilde{\nu}} > m_{\tilde{C}_1}$, so that decays into the lightest chargino are always possible. The branching ratio for $\tilde{\nu} \rightarrow \tilde{C}_1 l$ is always larger than 53%, while the branching ratio for the $\tilde{\nu} \rightarrow \tilde{C}_2 l$ channel (if open) can reach 26%. The next largest channel is $\tilde{\nu} \rightarrow \tilde{N}_1 \nu$, with a branching ratio up to 36%. The decay $\tilde{\nu} \rightarrow \tilde{N}_2 \nu$ is always open, but with a branching ratio below 6% due to the small \tilde{Z} component in \tilde{N}_2 .

For \tilde{e}_R models $m_{\tilde{\nu}}$ is unconstrained, so the decay $\tilde{\nu} \rightarrow \tilde{N}_1 \nu$ is the only mode that is always open. If decays into \tilde{N}_2 are also allowed, then the dominant decay of $\tilde{\nu}$ can be into either $\tilde{N}_1 \nu$ or $\tilde{N}_2 \nu$. In special cases, we found it is possible for the \tilde{Z} impurity to be larger in \tilde{N}_2 than \tilde{N}_1 , thus the dominant decay could be $\tilde{\nu} \rightarrow \tilde{N}_2 \nu$. This is possible when $m_{\tilde{N}_2} < m_{\tilde{\nu}} < m_{\tilde{C}_1}$, i.e. decays into charginos must be kinematically forbidden (an impossible scenario in \tilde{e}_L models). When a channel into a chargino is sufficiently open, it dominates over decays into the lightest two neutralinos by a factor of more than 10. However, if the sneutrino is heavy $m_{\tilde{\nu}} > m_{\tilde{N}_{3,4}}$, decays into the heavier neutralinos can be moderately large (branching ratio 10–30%), with decays $\tilde{\nu} \rightarrow \tilde{N}_4 \nu$ dominating over $\tilde{\nu} \rightarrow \tilde{N}_3 \nu$ due to the larger \tilde{Z} component in \tilde{N}_4 .

4.6 Selectron branching ratios

We have already discussed \tilde{e}_L branching ratios for \tilde{e}_L models, and \tilde{e}_R branching ratios for \tilde{e}_R models in Sec. 3.3, since they are a fundamental part of the model building. The other slepton (\tilde{e}_R in \tilde{e}_L models, and \tilde{e}_L in \tilde{e}_R models), will have branching ratios similar to \tilde{e}_L (in \tilde{e}_L models), or \tilde{e}_R (in \tilde{e}_R models) if its mass is roughly included in the $ee\gamma\gamma + \cancel{E}_T$ allowed range. In general, \tilde{e}_R , \tilde{e}_L will decay into the kinematically allowed final states with neutralinos, with the largest branching ratio for the channel $\tilde{N}_2 e$, if open. \tilde{e}_L can also decay into $\tilde{C}_{1,2} \nu_e$ if open, with a maximum branching ratio of 27% and 59% respectively.

Final State	Kinematic Condition	Range in \tilde{e}_L models	Range in \tilde{e}_R models
$\tilde{N}_1 \nu_e$	—	→ 36	→ 100
$\tilde{N}_2 \nu_e$	$m_{\tilde{\nu}_e} > m_{\tilde{N}_2}$	→ 5.5	→ 97
$\tilde{N}_3 \nu_e$	$m_{\tilde{\nu}_e} > m_{\tilde{N}_3}$	→ 29	→ 22
$\tilde{C}_1 e$	$m_{\tilde{\nu}_e} > m_{\tilde{C}_1}$	53 → 94	→ 100
$\tilde{C}_2 e$	$m_{\tilde{\nu}_e} > m_{\tilde{C}_2}$	→ 26	→ 48

Table 9: Ranges of selected $\tilde{\nu}_e$ branching ratios (in %), as in Table 5.

4.7 Predictions for LEP

The imminent upgrade of LEP to $\sqrt{s} = 161$ GeV (LEP161) and the forthcoming upgrade to $\sqrt{s} = 190$ GeV (LEP190) provide a potential testing ground for the models constructed. With expected integrated luminosities of 25 pb^{-1} and 500 pb^{-1} (per detector), the one event level is at 40 fb and 2 fb for $\sqrt{s} = 161, 190$ GeV respectively. The first priority is to identify which processes have non-negligible production cross sections, then determine the possible signatures that depend on the branching ratios of the produced sparticles. It is important to emphasize that the following predictions assume the minimum cut $\mathcal{A} = 5 \text{ fb}$ is placed on the $\sigma \times \mathcal{B}^2$ for the $ee\gamma\gamma + \cancel{E}_T$ event. For instance, in some cases we are able to predict a non-negligible minimum number of events with a particular signature must be produced, although we do not necessarily give detector efficiencies. In principle, if one could demonstrate that failure to detect such events implies they do not occur at all, then only two possibilities remain: (1) A supersymmetric explanation of the $ee\gamma\gamma + \cancel{E}_T$ event in our framework must rely on an upward fluctuation from $\sigma \times \mathcal{B}^2$ even lower than 5 fb , or (2) a supersymmetric explanation in our framework is not possible.

Based on Observation 4 in Sec. 2, selectron production is always kinematically forbidden at LEP161 and LEP190 for the selectron that satisfies the kinematics. The other slepton (\tilde{e}_R in \tilde{e}_L models, or \tilde{e}_L in \tilde{e}_R models) can potentially be kinematically accessible at LEP161 or LEP190 by simply requiring its mass be less than the threshold. This is obviously not a requirement (nor a constraint) of the selectron interpretation of the $ee\gamma\gamma + \cancel{E}_T$ event, and so we ignore selectron production at LEP. However, in \tilde{e}_L models it was shown in Eq. (6) that $m_{\tilde{\nu}}$ must be less than $m_{\tilde{e}_L}$, and so sneutrino production could be a visible signal at LEP190 (since $m_{\tilde{\nu}_e} > 81 \text{ GeV}$ for all \tilde{e}_L models), as will be discussed below.

4.7.1 LEP161

In Fig. 11 we present all of the chargino/neutralino production processes that have cross sections above about 10 fb. The cross sections were computed with initial state radiation effects included. In \tilde{e}_L or $\tilde{e}_L + \tilde{e}_R$ models, none of the processes need to have large cross sections, although if it were possible to establish an upper bound on $\sigma(\tilde{N}_1 \tilde{N}_3) \lesssim 600$ fb, then an upper bound on $\sigma \times \mathcal{B}^2$ for the $ee\gamma\gamma + \cancel{E}_T$ event can be established at 7.5 fb, and in \tilde{e}_R models $\sigma \times \mathcal{B}^2 < 5$ fb (i.e. all of our \tilde{e}_R models would be excluded). Given the cut $\mathcal{A} = 5$ fb, then in \tilde{e}_R models one expects a minimum of 22 $\tilde{N}_1 \tilde{N}_3$ pairs to be produced, but no other process (nor any processes in \tilde{e}_L or $\tilde{e}_L + \tilde{e}_R$ models) can have non-negligible minimum rates at LEP161. There are only four processes that could have large rates, which have the following maximum

$$\begin{aligned} e^+ e^- \rightarrow & \quad \tilde{N}_1 \tilde{N}_3 \quad (55, 56, 49) \\ & \tilde{N}_2 \tilde{N}_2 \quad (19, 22, 12) \\ & \tilde{N}_2 \tilde{N}_3 \quad (11, 16, 7) \\ & \tilde{C}_1^+ \tilde{C}_1^- \quad (48, 132, 42) \text{ pairs produced} \end{aligned} \quad (21)$$

for $(\tilde{e}_L, \tilde{e}_R, \tilde{e}_L + \tilde{e}_R)$ models. Notice that the maximum pair production rates are always largest for \tilde{e}_R models, then \tilde{e}_L models, then $\tilde{e}_L + \tilde{e}_R$ models. The rate for $\tilde{N}_1 \tilde{N}_3$ is roughly the same in all models since the cross section is dominated by Z exchange. For the other processes, differing interference contributions between the Z exchange and light slepton exchange cause the differences in the production cross sections (see Table 2). In addition, stop pairs could be produced at LEP161 (see Table 11).

The character of the signal from $\tilde{N}_1 \tilde{N}_3$ production is completely dependent on the decay of \tilde{N}_3 which was described in Sec. 4.3 (see also Table 6). The dominant decay possibilities are $\tilde{N}_3 \rightarrow \tilde{N}_1 "Z"$, $\tilde{N}_3 \rightarrow \tilde{N}_1 A(h)$ (if $m_A(m_h) < 60$ GeV), $\tilde{N}_3 \rightarrow \tilde{l}_R l$ in \tilde{e}_L models (if $m_{\tilde{l}_R} < m_{\tilde{N}_3}$), and $\tilde{N}_3 \rightarrow \tilde{\nu} \nu$ in \tilde{e}_R models (if $m_{\tilde{\nu}} < m_{\tilde{N}_3}$). The general signature is therefore " Z " + \cancel{E} . Extra $b\bar{b} + \cancel{E}$ occurs if the mass difference $m_{\tilde{N}_3} - m_{\tilde{N}_1}$ is larger than m_h or m_A . Some other signatures are possible in special cases: In \tilde{e}_L models one could have excess $l^+ l^- + \cancel{E}$ (if $m_{\tilde{l}_R} < m_{\tilde{N}_2}$), or $\gamma l^+ l^- + \cancel{E}$ (if $m_{\tilde{l}_R} < m_{\tilde{N}_3}$). In \tilde{e}_R models the decay $\tilde{N}_3 \rightarrow \tilde{\nu} \nu$ becomes the dominant decay if the sneutrino (and necessarily \tilde{l}_L) are light. Thus the dominant signature could be invisible, or $\gamma + \cancel{E}$, or $l^+ l^- + \cancel{E}$, if the mass hierarchy is $m_{\tilde{\nu}} < (m_{\tilde{N}_2}, m_{\tilde{C}_1})$, or $m_{\tilde{N}_2} < m_{\tilde{\nu}} < m_{\tilde{C}_1}$, or $m_{\tilde{C}} < m_{\tilde{\nu}}$ respectively. However, in these cases the cross section for $\tilde{l}_L \tilde{\nu}$ at the Tevatron would be quite large (see below).

The dominant signal of $\tilde{N}_2 \tilde{N}_2$ production is $\gamma\gamma + \cancel{E}$ in all models. Note that the process $\sigma(\tilde{N}_2 \tilde{N}_2)$ is always accompanied by $\sigma(\tilde{N}_1 \tilde{N}_3)$ at a comparable rate (when kinematically allowed), which has the same signatures as $\tilde{N}_1 \tilde{N}_3$ production (as above) plus one photon.

$\tilde{C}_1^+ \tilde{C}_1^-$ production can be present with a large rate, the decay signature of \tilde{C}_1 being the usual " W " + \cancel{E} in all models (see Table 7). The exception is if $m_{\tilde{\nu}}$ (and possibly $m_{\tilde{l}_L}$) is lighter than $m_{\tilde{C}_1}$, which can happen only in \tilde{e}_R models. In this special \tilde{e}_R model scenario, if

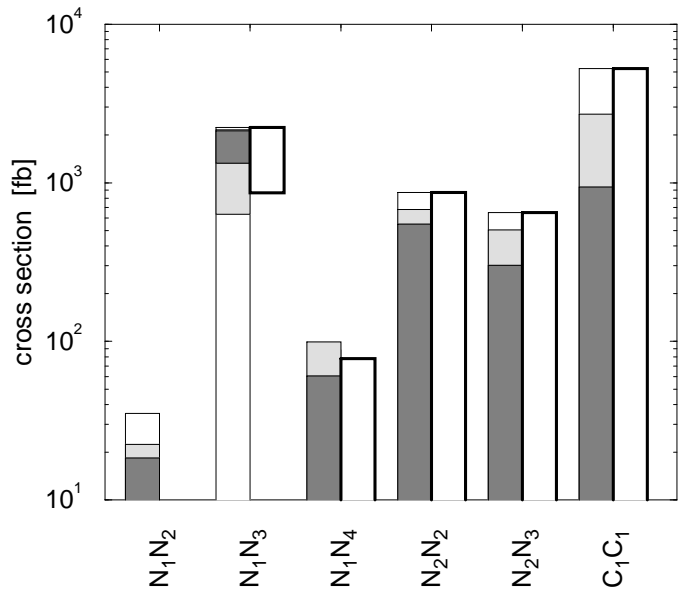


Figure 11: The range of the non-negligible cross sections at LEP161, for all models (shaded bar on left) and only \tilde{e}_R models (thick solid line on right). Each bar represents a particular production cross section, where the maximum and minimum height of the bar (or thick solid line) is the maximum and minimum cross section respectively. The shading on the left bars indicates the range of cross section for all models passing the cut $\mathcal{A} = 5, 7.5, 10$ fb. Bars that touch the x-axis correspond to cross sections that can be smaller than 1 fb.

$m_{\tilde{\nu}} < m_{\tilde{C}_1}$, then the decay signature is likely invisible. However, if the decay $\tilde{\nu} \rightarrow \tilde{N}_2 \nu$ is large, then the signature is $\gamma\gamma + \cancel{E}$. If $m_{\tilde{l}_L} < m_{\tilde{C}_1}$, then additional possible signatures are $l^+l^- + \cancel{E}$ (if $m_{\tilde{l}_L} < m_{\tilde{N}_2}$), or $l^+l^-\gamma\gamma + \cancel{E}$ (if $m_{\tilde{l}_L} > m_{\tilde{N}_2}$). Notice that the latter could be an additional source of $ee\gamma\gamma$ events (see Appendix A). These remarks assume the stop is heavier than \tilde{C}_1 .

As an aside, we find that a maximum of (14, 13, 12) $\tilde{N}_1 \tilde{N}_1$ pairs can be produced, which can be observed as a $\gamma + \cancel{E}$ signal once visible initial state radiation is attached. Although the SM background is severe, there are other possibly important contributions from e.g. $\gamma\tilde{N}_1\tilde{N}_3 (\rightarrow \nu\bar{\nu}\tilde{N}_1)$.

In Fig. 12 we present the ranges of the inclusive production of particular signals at LEP161 for \tilde{e}_L and \tilde{e}_R models. These signatures were generated by searching all possible decay paths. No efficiencies resulting from detector geometry or lepton/photon energy cuts are included. If the signals are the result of decays with moderate mass splittings, then presumably some of the events could be detected after applying reasonable cuts. A lepton l can be either e , μ or τ , with either charge ± 1 . In particular, when referring to a “ $2l$ ” signal, we sum over all family and charge possibilities (including, e.g., like-sign dileptons). X can be any combination of leptons, photons, jets, or nothing. In addition, all the signals implicitly include missing energy in their signature. We only include chargino/neutralino production processes in the inclusive sum, since \tilde{e}_L in \tilde{e}_L models and \tilde{e}_R in \tilde{e}_R models is too heavy to be produced. If the other slepton (\tilde{e}_R in \tilde{e}_L models, \tilde{e}_L in \tilde{e}_R models) is light, then the maximum cross section for particular signatures can be higher.

Jet production is also an important signal. If $\tilde{N}_1\tilde{N}_3$ production is kinematically allowed and if only 3-body decays of \tilde{N}_3 occur, then the rate into the $jj + X + \cancel{E}$ signal is between roughly 400–1800 fb for both \tilde{e}_L and \tilde{e}_R models. If chargino production is open then the rate can be larger. But, if 2-body decays into sleptons are open for \tilde{N}_3 , then the rate can be near zero.

Notice that in \tilde{e}_R models only the $2l + X(+\cancel{E})$ must be produced, the rate being between ~ 2 to 20 events in 25 pb^{-1} of integrated luminosity. The reason that the $2l$ rate always has a non-negligible minimum is due to a combination of effects: \tilde{e}_R models have a minimum $\sigma(\tilde{N}_1\tilde{N}_3) \gtrsim 850 \text{ fb}$, and decays of $\tilde{N}_3 \rightarrow \tilde{N}_1 l^+l^-$ are always non-zero, even if 2-body decays operate. If only 3-body decays occur, then $\tilde{N}_3 \rightarrow \tilde{N}_1 “Z” (\rightarrow l^+l^-)$ occur, with a rate of nearly 10% (summed over families). Alternatively, if $\tilde{N}_3 \rightarrow \tilde{\nu}\nu$ is open, then $\tilde{\nu} \rightarrow l\tilde{C} (\rightarrow l\nu)$ is the decay pattern. If $m_{\tilde{\nu}} < m_{\tilde{C}}$, then it turns out that $m_{\tilde{l}_L} < m_{\tilde{N}_3}$, and so decays $\tilde{N}_3 \rightarrow l\tilde{l}_L (\rightarrow l\tilde{N}_{1,2})$ are non-zero, giving an appreciable $2l$ signal. All of the other inclusive signals could have rates smaller than the one event level. If one of these signatures were found (and deduced to be above background), then looking in the other channels might serve to confirm the signal.

One promising signal is $\gamma\gamma + \cancel{E}$ without any other event activity, which primarily originates from $\tilde{N}_2\tilde{N}_2$ production in the selectron interpretation. (This is part of the inclusive signal $\gamma\gamma + X + \cancel{E}$ described above.) In a scenario with a gravitino LSP, we found that the standard

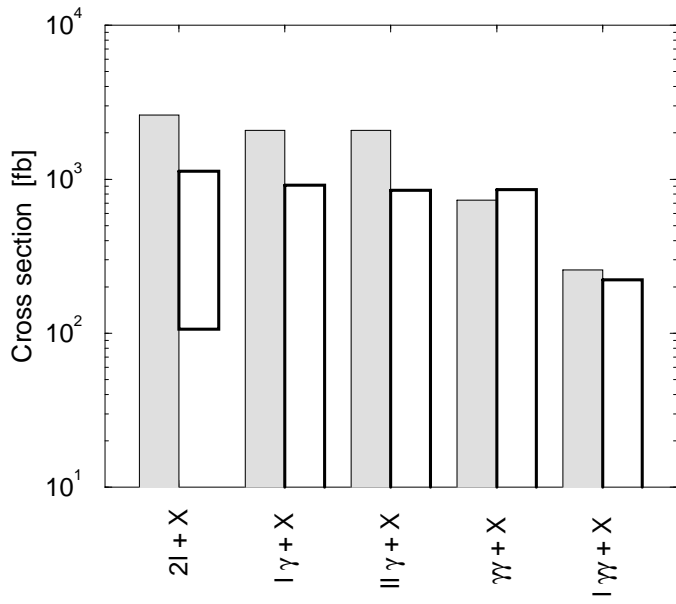


Figure 12: Range of inclusive cross sections for selected signatures at LEP161 without detection efficiencies; all signatures necessarily have missing energy in addition to that above. The shaded bar on the left corresponds to \tilde{e}_L models and the thick solid outline on the right corresponds to \tilde{e}_R models. Here, X = leptons, photons, jets, or nothing, and $l = e, \mu$, or τ summed over both charges and all three families. See the text for details.

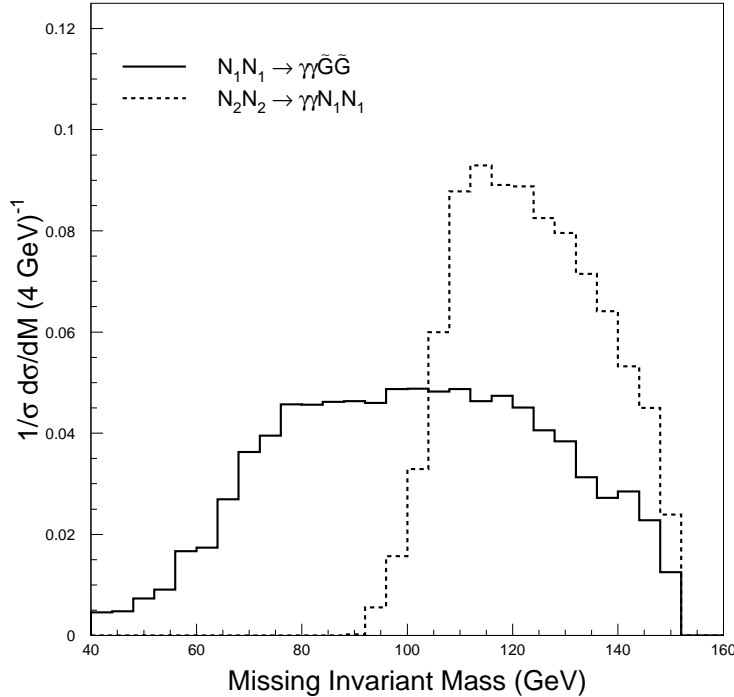


Figure 13: Comparison of the missing invariant mass distribution in the $\gamma\gamma + \cancel{E}$ signal at LEP161 from two different selectron interpretation models, (a) a sample \tilde{N}_1 =LSP model with $m_{\tilde{N}_{1,2}} = 37, 65$ GeV (dashed line), and (b) a model with a gravitino LSP and $m_{\tilde{N}_1} = 65$ GeV (solid line).

model background for $\gamma\gamma + \cancel{E}$ is distinguishable from the gravitino signal $e^+e^- \rightarrow \tilde{N}_1\tilde{N}_1 \rightarrow \gamma\gamma\tilde{G}\tilde{G}$ using the missing invariant mass distribution [4]. Here, we point out that a selectron interpretation with a neutralino LSP can be distinguished from one with a gravitino LSP using the missing invariant mass distribution, assuming the SM background is small (see Ref. [4] for a discussion of the background). In Fig. 13 we show the missing invariant mass distribution $M_{\text{inv}}^2 = (p_{e^+} + p_{e^-} - p_{\gamma_1} - p_{\gamma_2})^2$ at LEP161 for two different models: (a) The \tilde{e}_L sample model in Appendix B with $m_{\tilde{N}_{1,2}} = 37, 65$ GeV, and as usual $\tilde{N}_1 \simeq \tilde{H}_b$, $\tilde{N}_2 \simeq \tilde{\gamma}$. (b) A model with a (very light) gravitino LSP with $m_{\tilde{N}_1} = 65$ GeV, and $\tilde{N}_1 \simeq \tilde{\gamma}$. The difference in the missing invariant mass distribution illustrates how the scenarios might be distinguished using the $\gamma\gamma + \cancel{E}$ signal. It should be noted the general character of the missing invariant mass distribution for the gravitino LSP model in Fig. 13 is not particularly sensitive to $m_{\tilde{N}_1}$, but simply that $m_{\tilde{G}}$ is very small compared to the neutralino or selectron masses.

4.7.2 LEP190

In Fig. 14, we present all the chargino/neutralino production processes with cross sections

possibly larger than about 1 fb for LEP with $\sqrt{s} = 190$ GeV. As above, the cross sections were computed with initial state radiation effects included. Now, $\tilde{N}_1\tilde{N}_3$ production must be large in all models, and many other processes can easily give large rates. The processes with large rates include all of the ones at LEP161, and also $\tilde{N}_1\tilde{N}_2$, $\tilde{N}_1\tilde{N}_4$, $\tilde{N}_2\tilde{N}_4$, $\tilde{C}_1^\pm\tilde{C}_2^\mp$. The maximum rates are as follows:

$$\begin{aligned}
e^+e^- \rightarrow & \quad \tilde{N}_1\tilde{N}_2 \quad (20, 6, 24) \\
& \tilde{N}_1\tilde{N}_3 \quad (785, 780, 780) \\
& \tilde{N}_1\tilde{N}_4 \quad (82, 79, 78) \\
& \tilde{N}_2\tilde{N}_2 \quad (505, 560, 346) \\
& \tilde{N}_2\tilde{N}_3 \quad (335, 416, 230) \\
& \tilde{N}_2\tilde{N}_4 \quad (73, 64, 34) \\
& \tilde{C}_1^+\tilde{C}_1^- \quad (965, 2120, 1195) \\
& \tilde{C}_1^\pm\tilde{C}_2^\mp \quad (409, 695, 350) \text{ pairs produced,}
\end{aligned} \tag{22}$$

for $(\tilde{e}_L, \tilde{e}_R, \tilde{e}_L + \tilde{e}_R)$ models. For $\tilde{N}_1\tilde{N}_3$ production, the minimum number of pairs produced is (400, 475, 320) for $(\tilde{e}_L, \tilde{e}_R, \tilde{e}_L + \tilde{e}_R)$ models given the minimum threshold $\mathcal{A} = 5$ fb. For \tilde{e}_R models only, a minimum of 5 $\tilde{N}_1\tilde{N}_4$ pairs, 25 $\tilde{N}_2\tilde{N}_2$ pairs, 40 $\tilde{N}_2\tilde{N}_3$ pairs, and 250 $\tilde{C}_1^+\tilde{C}_1^-$ pairs must be produced given the minimum threshold $\mathcal{A} = 5$ fb. As for $\tilde{N}_1\tilde{N}_1$ pair production we found a maximum of (177, 164, 152) pairs can be produced.

The detection signatures for the chargino/neutralino pairs common to LEP161 are the same as above. Here we discuss the processes that are different. First, the process $\tilde{N}_1\tilde{N}_2$ gives a $\gamma + \cancel{E}$ signature. The signatures for $\tilde{N}_1\tilde{N}_4$ and $\tilde{N}_2\tilde{N}_4$ are entirely dependent on the \tilde{N}_4 branching ratio; \tilde{N}_4 can decay in a variety of ways outlined in Sec. 4.3. Perhaps the most striking signature is when $\tilde{N}_4 \rightarrow \tilde{N}_1 h(A)$, giving a $b\bar{b} + \cancel{E}$ signature for $\tilde{N}_1\tilde{N}_4$ production and $b\bar{b}\gamma + \cancel{E}$ signature for $\tilde{N}_2\tilde{N}_4$ production. The signature of the process $\tilde{C}_1^\pm\tilde{C}_2^\mp$ also depends crucially on the branching ratio of \tilde{C}_2 , but one lepton with perhaps one photon plus missing energy is typical (assuming the stop is heavier than \tilde{C}_1). Thus, a reasonable expectation for $\tilde{C}_1^\pm\tilde{C}_2^\mp$ production is $l^+l^- (+\gamma) + \cancel{E}$. It is also possible that only 3-body decays of \tilde{C}_2 are open, in which case no photon would appear in the final state. The final states from \tilde{C}_2 decay are summarized in Table 8.

In addition, sneutrino pair production (if open) is another process that is relevant for \tilde{e}_L models. To have $\tilde{\nu}_e\tilde{\nu}_e$ production kinematically accessible with $m_{\tilde{\nu}_e} < 95$ GeV, then the sum rule in Eq. (6) implies $\tan\beta \gtrsim 1.2$ is required for $m_{\tilde{e}_L} > 100$ GeV (as needed by the kinematics of the $ee\gamma\gamma + \cancel{E}_T$ event), and for $m_{\tilde{e}_L} = 107(118)$ GeV, then $\tan\beta > 1.5(2.8)$. Hence sneutrino production in \tilde{e}_L models never occurs at LEP190 if $m_{\tilde{e}_L} > 118$ GeV. The signature of $\tilde{\nu}_e\tilde{\nu}_e$ production depends on the sneutrino branching ratio, but it was already established in Sec. 4.5 that $\tilde{\nu}_e \rightarrow e\tilde{C}_1 (\rightarrow \tilde{N}_1 "W")$ is the dominant decay pattern. Thus the signature is $ee "W" "W" + \cancel{E}$, which is indeed quite prominent.

In Fig. 15 we present the ranges of the inclusive production of particular signals at LEP190 for \tilde{e}_L and \tilde{e}_R models. As in Fig. 12, no detection efficiencies are included. Notice that while only

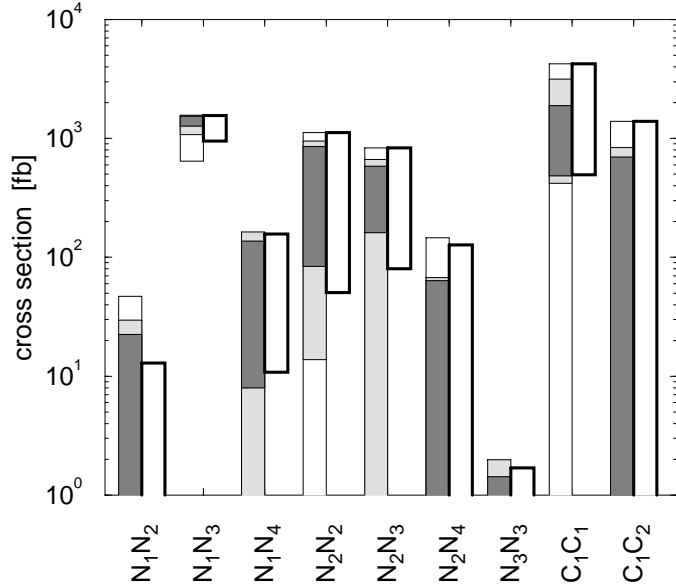


Figure 14: As in Fig. 11, for LEP190.

$\tilde{N}_1\tilde{N}_3$ production had a non-negligible minimum rate (see Fig. 14), both the signals $2l + X + \cancel{E}$ and $\gamma\gamma + X + \cancel{E}$ (which rarely comes from $\tilde{N}_1\tilde{N}_3$ production) are always larger than one event. Further, inclusive production of $l\gamma + X + \cancel{E}$ and $ll\gamma + X + \cancel{E}$ are always larger than the 10 event level for \tilde{e}_R models only. All of the other inclusive signals could have rates smaller than the one event level. As in LEP161, if one of these signatures were found (and deduced to be above background), then looking in the other channels might serve to confirm the signal. Another important search strategy would be inclusive signatures with jets (+ photon(s)) that can have significantly larger rates than the lepton(s) (+ photon(s)) signatures.

4.8 Predictions for Tevatron

The assumption underlying the selectron interpretation is that the Tevatron has already observed a candidate selectron pair production event. Because many more states of the underlying supersymmetric model are accessible at a hadron collider, we here focus on the associated signals that should be observed in the present data set (100 pb^{-1} per detector) or in the next scheduled upgrade ($1\text{--}2 \text{ fb}^{-1}$ per detector). As in Sec. 4.7, we identify the processes that have non-negligible production cross sections, then determine the possible signatures that depend on the branching ratios. Again, it is important to emphasize that the following predictions assume the minimum cut $\mathcal{A} = 5 \text{ fb}$ is placed on the $\sigma \times \mathcal{B}^2$ for the $ee\gamma\gamma + \cancel{E}_T$ event.

In Fig. 16 we present all of the chargino/neutralino production processes that can have cross

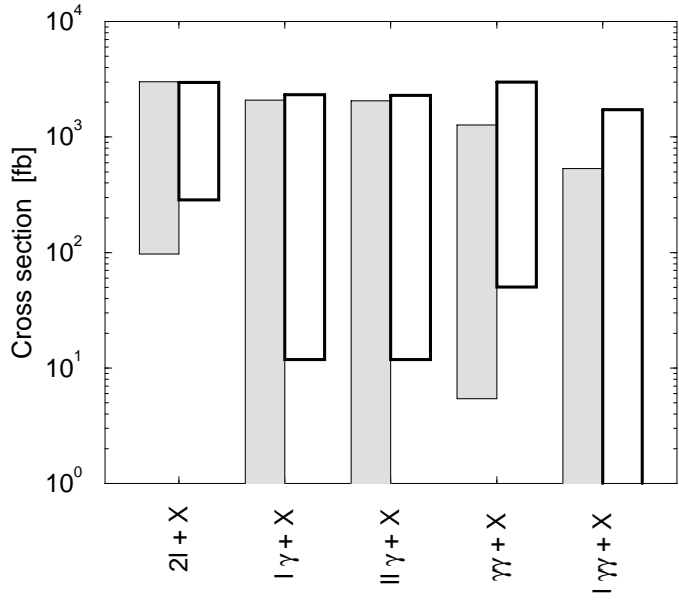


Figure 15: Range of inclusive cross sections for selected signatures without detection efficiencies, as in Fig. 12, but for LEP190.

sections above about 50 fb. We use leading order CTEQ3L [25] structure functions evaluated at $Q^2 = \hat{s}$. At the Tevatron the cross sections do have a contribution from t -channel squark exchange (see Table 2), but the dependence on the squark mass is usually weak for the squark masses in our models. If only \tilde{e}_R is light, then these are the only necessary associated processes to the $ee\gamma\gamma$ event. If \tilde{e}_L is light, however, then there must also be $\tilde{e}_L\tilde{\nu}_e$ and $\tilde{\nu}_e\tilde{\nu}_e$ production. In Ref. [1] we found $\sigma(\tilde{\nu}_e\tilde{\nu}_e) \sim \sigma(\tilde{e}_L\tilde{e}_L)$ and $\sigma(\tilde{e}_L\tilde{\nu}_e) \sim (2 \rightarrow 3)\sigma(\tilde{e}_L\tilde{e}_L)$ for the same $m_{\tilde{e}_L}$, i.e. the cross sections are typically tens of fb. It is also possible that both \tilde{e}_L and \tilde{e}_R can be light; in particular, the other slepton (\tilde{e}_R in \tilde{e}_L models, \tilde{e}_L in \tilde{e}_R models) can be lighter than the one giving the $ee\gamma\gamma + \cancel{E}_T$ event, which can dramatically affect the signatures. The pair production processes that have the largest cross sections and also have a non-negligible minimum cross section are given in Table 10, where the full range from the minimum to the maximum number of pairs produced for an integrated luminosity of 100 pb^{-1} are shown.

The signatures for $\tilde{N}_1\tilde{N}_3$ and $\tilde{C}_1^+\tilde{C}_1^-$ are the same as for LEP (described in Sec. 4.7.1) and the decays of \tilde{C}_2 were also discussed in Sec. 4.7.2. For completeness we list the possible signatures of all of these processes here: $\tilde{N}_1\tilde{N}_3$ will mainly give “Z” + \cancel{E}_T , or $b\bar{b} + \cancel{E}_T$ if $m_A < 60 \text{ GeV}$. If 2-body slepton decays are allowed, then in \tilde{e}_L models one can have $l^+l^- + \cancel{E}_T$, or in \tilde{e}_R models one of invisible, $\gamma + \cancel{E}_T$, or $l^+l^- + \cancel{E}_T$. $\tilde{C}_1^+\tilde{C}_1^-$ production gives typically $l^+l^- + \cancel{E}_T$, or if 2-body decays into $\tilde{l}_L, \tilde{\nu}$ occur (in \tilde{e}_R models only), then depending on the mass hierarchy one can have $\gamma\gamma + \cancel{E}_T$, or $l^+l^- + \cancel{E}_T$, or $l^+l^- \gamma\gamma + \cancel{E}_T$. $\tilde{C}_2^+\tilde{C}_2^-$ production gives similar signatures as $\tilde{C}_1^+\tilde{C}_1^-$ production, given $m_{\tilde{C}_1} \rightarrow m_{\tilde{C}_2}$ and allowing for the possibility of 2-body decays in

Process	Range in \tilde{e}_L models		Range in \tilde{e}_R models		Range in $\tilde{e}_L + \tilde{e}_R$ models	
$\tilde{N}_1 \tilde{N}_3$	31	→	129	43	→	145
$\tilde{C}_1^+ \tilde{C}_1^-$	40	→	285	56	→	264
$\tilde{C}_2^+ \tilde{C}_2^-$	8	→	85	28	→	79
$\tilde{C}_1^\pm \tilde{N}_1$	75	→	638	132	→	540
$\tilde{C}_1^\pm \tilde{N}_2$	2	→	75	3	→	80
$\tilde{C}_1^\pm \tilde{N}_3$	32	→	98	36	→	103
$\tilde{C}_2^\pm \tilde{N}_2$	2	→	76	15	→	69
$\tilde{C}_2^\pm \tilde{N}_4$	3	→	51	17	→	54
						29 → 128
						29 → 258
						15 → 77
						54 → 552
						1 → 75
						28 → 96
						5 → 74
						8 → 55

Table 10: The range of the number of chargino/neutralino pairs produced at the Tevatron assuming an integrated luminosity of 100 pb^{-1} . The processes displayed here include those that have both a large production rate *and* a non-negligible minimum production rate.

the context of both \tilde{e}_L and \tilde{e}_R models as above.

The processes $\tilde{C}_i^\pm \tilde{N}_j$ are unique to the Tevatron, with $\tilde{C}_1^\pm \tilde{N}_1$, $\tilde{C}_1^\pm \tilde{N}_2$, $\tilde{C}_1^\pm \tilde{N}_3$, $\tilde{C}_2^\pm \tilde{N}_2$ and $\tilde{C}_2^\pm \tilde{N}_4$ giving the largest rates. As described above, the chargino typically gives $jj + \cancel{E}_T$ and $l^\pm + \cancel{E}_T$, although possible 2-body decays into sleptons can give $\gamma + \cancel{E}_T$, or $l^\pm + \cancel{E}_T$, or $l^\pm \gamma + \cancel{E}_T$. Thus the signature of $\tilde{C}_1^\pm \tilde{N}_1$ production is one of the above signatures for a single chargino. The signatures of $\tilde{C}_1^\pm \tilde{N}_2$ and $\tilde{C}_2^\pm \tilde{N}_2$ are as above plus one photon. Finally, the decays $\tilde{C}_1^\pm \tilde{N}_3$ and $\tilde{C}_2^\pm \tilde{N}_4$ are one of the above signatures coupled with \tilde{N}_3 or \tilde{N}_4 decay. Here again we can utilize Secs. 4.3, 4.7, to obtain the possible decay signatures. For \tilde{N}_3 , the decay signature is “ Z ” + \cancel{E}_T , $b\bar{b} + \cancel{E}_T$ (if $m_A < 60 \text{ GeV}$), and if 2-body decays to sleptons are open then for \tilde{e}_L models the signature could be $l^+ l^- + \cancel{E}_T$ or $\gamma l^+ l^- + \cancel{E}_T$, while for \tilde{e}_R models the signature could be invisible, or $\gamma + \cancel{E}_T$, or $l^+ l^- + \cancel{E}_T$. Thus, if only 3-body decays were open for charginos and neutralinos the signature of $\tilde{C}_1^\pm \tilde{N}_3$ and $\tilde{C}_2^\pm \tilde{N}_4$ would be “ W ” “ Z ” + \cancel{E}_T , which gives the well-studied trilepton signal [26]. If 2-body decays of the charginos or heavier neutralinos are present, then one or more photons could be present in the final state, with possibly fewer leptons.

In Fig. 17 we present the cross section for many promising signatures at the Tevatron. As in Figs. 12 and 15, no detection efficiencies have been included. We include chargino/neutralino processes in the sum, as well as $\tilde{e}_R \tilde{e}_R$ production in \tilde{e}_R models, and $\tilde{e}_L \tilde{e}_L$, $\tilde{\nu}_e \tilde{\nu}_e$, $\tilde{e}_L \tilde{\nu}_e$ production in \tilde{e}_L models. We see that all six inclusive signatures involving leptons or photons are expected to have minimum rates of roughly 2 to 30 events, regardless of the type of model (\tilde{e}_L or \tilde{e}_R). The $\gamma\gamma + X$, $l\gamma + X$ and $l\gamma\gamma + X$ signatures can be much larger in \tilde{e}_R models, but this only happens in the particular kinematic scenario with $m_{\tilde{N}_2} < m_{\tilde{l}_L}$, $m_{\tilde{\nu}} < m_{\tilde{C}_1} (< m_{\tilde{e}_R})$. In this case, charginos always decay through the 2-body channels $\tilde{C} \rightarrow \tilde{l}_L \nu$ and $\tilde{C} \rightarrow \tilde{\nu} l$, with $\tilde{l}_L, \tilde{\nu} \rightarrow \tilde{N}_2 (\rightarrow \tilde{N}_1 \gamma)$. Thus, processes with intrinsically large cross sections such as $\tilde{C}_1 \tilde{N}_1$ production can lead to a

large $l\gamma + \cancel{E}_T$ signal, and similarly for other processes involving charginos.

The $l\gamma + \cancel{E}_T$ (and $jj\gamma + \cancel{E}_T$) signals are important [16] and can arise from: $\tilde{C}_1\tilde{N}_2$ and $\tilde{C}_2\tilde{N}_2$ production in models with $\tilde{C} \rightarrow l\nu\tilde{N}_1$; $\tilde{C}_i\tilde{N}_1$ production in models with $\tilde{C}_i \rightarrow \nu\tilde{l}_L (\rightarrow l\tilde{N}_2 (\rightarrow \tilde{N}_1\gamma))$ or $\tilde{C}_i \rightarrow l\tilde{\nu} (\rightarrow \nu\tilde{N}_2 (\rightarrow \tilde{N}_1\gamma))$; and $\tilde{l}_L\tilde{\nu}$ production with $\tilde{l}_L \rightarrow l\tilde{N}_2 (\rightarrow \tilde{N}_1\gamma)$. The chargino decays assume $m_{\tilde{t}_1} > m_{\tilde{C}}$. For just $\tilde{C}_i\tilde{N}_2$ production there are roughly 10–130 pairs produced in the present CDF and D0 samples (each) with the probable signatures $\gamma + "W" + \cancel{E}$ (before cuts); “ W ” decays to jj or $l^\pm\nu$ as usual. For “ W ” $\rightarrow jj$, these events have no parton-level SM background.

Many of these signatures should be detectable, since the mass differences between superpartners is often constrained to be small but non-zero, as in Fig. 8. For example, in decays such as $\tilde{N}_3 \rightarrow \tilde{N}_1 "Z"$ and $\tilde{C}_{1,2} \rightarrow \tilde{N}_1 "W"$, the invariant mass of the virtual “ Z ” or “ W ” can be large. In particular, the invariant mass of the “ Z ” from \tilde{N}_3 decay is between 0 to 40–60 GeV, thus an excess in pairs of leptons (or jets) that reconstruct to an invariant mass $m_{l^+l^-} \lesssim 60$ GeV accompanied by a large missing energy is a distinctive signature of $\tilde{N}_1\tilde{N}_3$ production in our models.

In addition to classifying the most promising signatures, we have also performed a number of event level simulations for a limited subset of our \tilde{e}_L and \tilde{e}_R models, with the other slepton heavy. The purpose is to get a feeling for the efficiency of detecting multi-lepton and/or photon signatures. First, we address the issue of efficiencies for the $ee\gamma\gamma + \cancel{E}_T$ event, since this is important for interpreting the threshold \mathcal{A} in the $ee\gamma\gamma$ rate. An efficiency represents the probability that a certain class of events passes a particular set of cuts defined before the data is analyzed. We chose a set of cuts such that: (1) the event would be triggered on and analyzed, and (2) the event would not suffer from obvious detector backgrounds like jets faking leptons or photons. To show the dependence of our efficiencies on the particular set of cuts, we choose a loose set with $|\eta^e| < 2$, $|\eta^\gamma| < 1$, $(p_T^{(e,\gamma)}, \cancel{E}_T) > E_T^{\min} = 10$ GeV and a tight set identical to the loose set except $E_T^{\min} = 20$ GeV. The efficiencies we found range from 0.02–0.23 for the loose cuts, and from 0.01–0.12 for the tight cuts, but efficiencies outside these ranges (from models not covered in the subset) are possible. If E_T^{\min} is increased to 25 GeV, the mean efficiency is 0.04. The loose cuts are sufficient for CDF to have triggered on the $ee\gamma\gamma$ event.

We have also studied $l\gamma$, ll , and $ll\gamma$ signatures using a similar set of cuts ($\cancel{E}_T > 20$ GeV and $p_T^{(l,\gamma)} > E_T^{\min}$), where for the purposes of detection l is summed over e and μ only. Typically, when $E_T^{\min} = 10$ GeV one expects between 1–5 (2–12) $l\gamma + \cancel{E}_T$ events in 100 pb^{-1} for \tilde{e}_R models (\tilde{e}_L models) from chargino/neutralino production alone. An additional 1–2 events are expected from $\tilde{e}_L\tilde{\nu}_e$ production in \tilde{e}_L models. This result is essentially unchanged for the simulation subset of models if $E_T^{\min} = 20$ GeV. This is expected at least for the photons since the kinematics enforce hard photons in the final state from slepton decay. The SM background from $W\gamma$ production yields 105 and 37 events for each set of cuts respectively. With tighter cuts, it is possible to achieve a signal to background ratio near one for some models. The expected ll

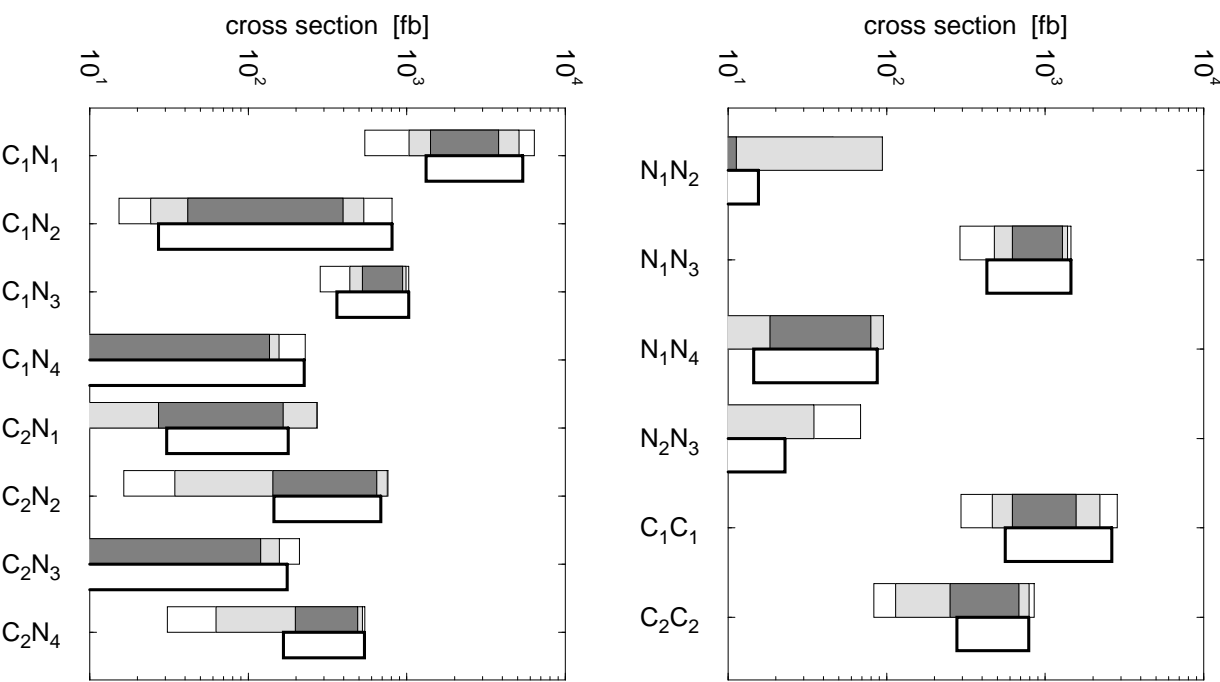


Figure 16: As in Fig. 11, for Tevatron $\sqrt{s} = 1.8$ TeV with all $\tilde{C}_i^\pm \tilde{C}_j^\mp$, $\tilde{N}_i \tilde{N}_j$, $\tilde{C}_i^\pm \tilde{N}_j$ processes shown that can have cross sections larger than about 50 fb.

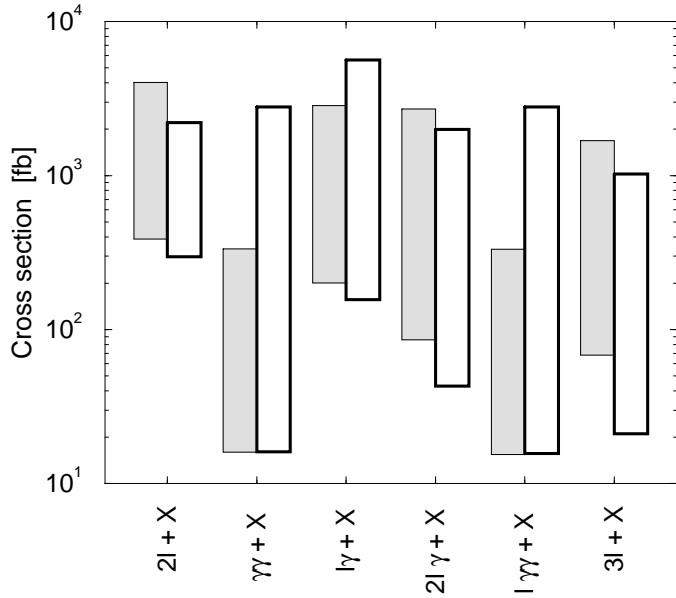


Figure 17: Range of inclusive cross sections for selected signatures without detection efficiencies, as in Fig. 12, but for Tevatron.

signature, resulting mainly from $\tilde{C}_i \tilde{C}_j$ production, is between 0–6 events for $E_T^{\min} = 10$ GeV, and 0–2 for $E_T^{\min} = 20$ GeV. Similarly, the expected $ll\gamma$ signature is between 0–5 events for $E_T^{\min} = 10$ GeV, and 0–2 events for $E_T^{\min} = 20$ GeV. Other signatures, such as $\gamma\gamma$, $l\gamma\gamma$ and $3l$, produce at most 1 or 2 events for $E_T^{\min} = 10$ or 20 GeV. Therefore, it would appear that the $l\gamma$ channel is the most promising for confirming the supersymmetric interpretation of the $ee\gamma\gamma + \cancel{E}_T$ event (assuming $m_{\tilde{t}_1} > m_{\tilde{C}}$), though other signals with limited backgrounds are clearly possible.

4.9 Alternative interpretation

Throughout this section we have described the constraints and predictions in the selectron interpretation. However, in Sec. 2 we described an alternative interpretation involving chargino production that could explain the $ee\gamma\gamma + \cancel{E}_T$ event. Those readers interested in the model building associated with the chargino interpretation are referred to Appendix A, which provides many details and an example model.

5 Comments on models with a light stop

We have seen that the effect of requiring a large $\sigma \times \mathcal{B}^2$ for the $ee\gamma\gamma + \cancel{E}_T$ event is to strongly constrain the chargino, neutralino and slepton sections. Up to now, we have assumed the squarks are sufficiently heavy so as not to directly interfere with the necessary decay chain. However, it is possible that a light stop \tilde{t}_1 can exist simultaneously with the needed hierarchy in the other sectors. In particular, neutralino decays $\tilde{N} \rightarrow \tilde{t}_1 t$ are absent in our models (with the cut $\mathcal{A} = 5$ fb), since all neutralinos are lighter than the top quark. Therefore, the decay chain in the selectron interpretation need not be disrupted, if the radiative neutralino decay can be large with a light stop.

The chargino interpretation described in Appendix A is a different matter, since charginos would always decay to the light stop $\tilde{C} \rightarrow \tilde{t}_1 b$ if kinematically accessible. This is true regardless of the mixing angle $\theta_{\tilde{t}}$ that determines the $\tilde{W}^\pm - \tilde{t}$ coupling, since the Yukawa coupling $\tilde{H}^\pm - \tilde{t}$ is large. Thus, it would seem that a chargino interpretation of the $ee\gamma\gamma + \cancel{E}_T$ event from $p\bar{p} \rightarrow \tilde{C}_i^\pm \tilde{C}_j^\mp$ is not possible unless $m_{\tilde{t}_1} > m_{\tilde{C}}$. This is basically the scenario described in Appendix A.

To construct models with a large $ee\gamma\gamma + \cancel{E}_T$ event rate and a light stop, one must consider the effects of a small $m_{\tilde{t}_1}$ on the radiative neutralino decay width and on the mass hierarchy. As we have remarked in Sec. 4.2, the dynamical mechanism for a large radiative neutralino branching ratio appears not to be strongly dependent on $m_{\tilde{t}_1}$ [11]. For instance, models can be constructed with $m_{\tilde{t}_1} = 50$ GeV, $m_{\tilde{t}_2} \gtrsim 250$ GeV, and a large radiative neutralino branching ratio arising from the dynamical mechanism. However, some suppression to the radiative neutralino branching ratio from light stops is present, so the $ee\gamma\gamma + \cancel{E}_T$ rate is maximized in the limit of all squark masses large. For example, the largest $ee\gamma\gamma + \cancel{E}_T$ rate in \tilde{e}_L and \tilde{e}_R models with a light stop is 13.8 fb and 6.1 fb respectively. Since $m_{\tilde{N}_1} < m_{\tilde{t}_1}$ must be obeyed so that \tilde{N}_1 =LSP, the upper limit on $m_{\tilde{N}_1}$ can be more restrictive than found above if $m_{\tilde{t}_1} \lesssim 74$ (50) GeV in \tilde{e}_L (\tilde{e}_R) models by Observation 1 in Sec. 2. This induces a rough upper limit on $|\mu|$, which also has implications for the chargino masses.

There is an additional degree of freedom in the value of $\theta_{\tilde{t}}$, which determines the SU(2) couplings of $\tilde{t}_{1,2}$ with the gaugino components of charginos and neutralinos. Maintaining a hierarchy between $m_{\tilde{t}_1} \ll m_{\tilde{t}_2}$ ($\simeq m_{\tilde{q}}$) would seem difficult without giving a large $\delta\rho$ [27], but this can be avoided if $\tilde{t}_1 \simeq t_R$ (or $\theta_{\tilde{t}} \simeq \pi/2$ by our definition). However, requiring $m_{\tilde{t}_1} \simeq 50$ GeV, $\theta_{\tilde{t}} \simeq \pi/2$ implies $m_{\tilde{t}_2}$ must be large (perhaps of order 1 TeV or more) if the light Higgs h is to have a mass that is not excluded by LEP. In general this implies that m_h will lie within the region accessible to LEP, though further analysis is needed to be precise; $\sin^2(\beta - \alpha)$ can be below one, and m_h can be near its present lower limit from LEP1. Note also $\theta_{\tilde{t}}$ slightly affects the radiative neutralino decay [11].

Another constraint on models with a light stop comes about if $m_{\tilde{t}_1} + m_b < m_t$. Then top quarks must decay into stops with a branching fraction of about 1/2 if $m_{\tilde{t}_1} \sim 50$ GeV. It was observed in Ref. [16] that a branching ratio of $t \rightarrow \tilde{t}_1 b$ of 50% is not excluded by Tevatron data, if gluinos and squarks with masses of roughly $\mathcal{O}(250)$ GeV exist, giving additional top production to supplement the SM contribution while half the top quarks decay into the lightest stop. For our purposes we note that if the masses of non-stop squarks are greater than roughly 250 GeV, then they are not crucial in maintaining a large radiative neutralino branching fraction.

The simultaneous existence of a light right stop, a heavy left stop, other squarks (except b_L) and the gluino with masses $\mathcal{O}(250)$ GeV, and a large $ee\gamma\gamma + \cancel{E}_T$ rate is therefore an interesting possibility. We explicitly constructed nearly 200 models, mostly of the \tilde{e}_L class due to their larger cross section. We did not find significant differences in the models' distribution in M_1 – M_2 plane, nor in the μ – $\tan\beta$ plane. However, regions in these planes that were populated by heavy stop models with $\sigma \times \mathcal{B}^2$ near the $\mathcal{A} = 5$ fb cut are no longer allowed. For instance, no light stop models approached the gaugino mass unification ($M_2 = 2M_1$) line, and $|\mu|$ was restricted to be less than 62 GeV. Hence, there are a number of phenomenological consequences of assuming a light stop ($m_{\tilde{t}_1} = 50$ GeV). First, as noted above, the branching ratio of $\tilde{C}_i^\pm \rightarrow \tilde{t}_1 b$ is virtually 100% (when kinematically accessible), followed by the one loop decay $\tilde{t}_1 \rightarrow c\tilde{N}_1$ if $m_{\tilde{t}_1} < m_{\tilde{C}}$. Thus all the signatures as noted in Secs. 4.7 and 4.8 arising from charginos become $bc + \cancel{E}_T$. For example, while the dilepton signal from $\tilde{N}_1 \tilde{N}_3$ is unchanged, the dilepton signal from $\tilde{C}_i^\pm \tilde{C}_j^\mp$ becomes $b\bar{b}c\bar{c} + \cancel{E}_T$. Also, the restriction $m_{\tilde{N}_1} < m_{\tilde{t}_1} (= 50$ GeV) results in somewhat tighter restrictions on the upper bounds of the other chargino and neutralino masses. In particular, $m_{\tilde{C}_1} \lesssim 90$ GeV and $m_{\tilde{N}_3} \lesssim 100$ GeV in our light stop models, and the sum $(m_{\tilde{N}_1} + m_{\tilde{N}_3}) \lesssim 150$ GeV. One consequence is that $\tilde{N}_1 \tilde{N}_3$ production is always kinematically allowed at LEP161, with a cross section in the range $1.1 < \sigma(\tilde{N}_1 \tilde{N}_3) < 2.1$ pb.

Stop production at LEP161 may be directly visible with the expected integrated luminosity if $2m_{\tilde{t}_1}$ is below threshold [28]. In Table 11 we present the cross section for stop production at LEP161 and LEP190 for a selection of light stop masses. At LEP161 one would expect roughly 20 (5) stop pairs produced per detector, for $m_{\tilde{t}_1} = 50$ (70) GeV. At LEP190 one would expect roughly 380 (95) stop pairs produced per detector, for $m_{\tilde{t}_1} = 50$ (80) GeV. All of the cross sections were calculated with approximate final state QCD corrections and QED initial state radiation effects included, and assuming $\tilde{t}_1 = \tilde{t}_R$. Also, $\tilde{t}_1 \tilde{t}_1^*$ bound state effects can be important close to the threshold.

It has been noted [16] that when there is a light stop (so that $\tilde{C}_i^\pm \rightarrow \tilde{t}_1 b$ and $t \rightarrow \tilde{t}_1 \tilde{N}_i$), there is a large set of events predicted at the Tevatron by supersymmetry that has no parton-level SM background. Even after all branching ratios and detection efficiencies are included, tens of events remain in the present 100 pb $^{-1}$ at Tevatron. These events arise from three sources, (i) $\tilde{C}_i^\pm (\rightarrow \tilde{t}_1 b) \tilde{N}_2$, see Table 10; (ii) $t (\rightarrow Wb) \bar{t} (\rightarrow \tilde{t}_1 \tilde{N}_2)$; (iii) $\tilde{q} (\rightarrow q \tilde{N}_2) \tilde{q} (\rightarrow q \tilde{g} (\rightarrow t (\rightarrow Wb) \tilde{t}_1))$. In all cases, $\tilde{N}_2 \rightarrow \tilde{N}_1 \gamma$, $\tilde{t}_1 \rightarrow c\tilde{N}_1$, and typically $W \rightarrow jj$. After branching ratios and cuts there should be approximately 35–100 events with the signature $b\gamma + \cancel{E} + \text{jets}$. ‘Jets’ means

$m_{\tilde{t}_1=\tilde{t}_R}$ (GeV)	Cross section (in pb)	
	LEP161	LEP190
50	0.85	0.76
60	0.50	0.56
70	0.20	0.37
80	—	0.19

Table 11: Cross sections for light stop \tilde{t}_1 ($= \tilde{t}_R$) production at LEP161 and LEP190 with approximate final state QCD corrections and QED initial state radiation effects included. Close to the threshold the cross section values may receive large corrections due to $\tilde{t}_1\tilde{t}_1^*$ bound state effects.

1–5 parton level jets, including 1–2 charm jets (an average of 1.5/event). This prediction could lead to a sample that allowed a robust (rather than one event level) detection of superpartners in the present CDF and D0 data. When $W \rightarrow l\nu$ for these events, additional good signatures arise and one expects an excess of “ W ” bc events that would appear in the top sample, and $l^\pm\gamma + \cancel{E}_T + \text{jets}$ events.

The simultaneous existence of a light stop and a light chargino (as necessarily arises in $ee\gamma\gamma + \cancel{E}_T$ models) can give rise to a shift in R_b [29]. We have analyzed models with $m_{\tilde{t}_1} = 50$ GeV, $\tilde{t}_1 = \tilde{t}_R$ and find that the maximum shift in R_b is $\delta R_b^{\max} \lesssim 0.003$ from chargino-stop loops only. Charged Higgs-top loops can also be significant, with a shift $\delta R_b \lesssim -0.0005$ depending on m_A . In all cases $\tan\beta$ must be near 1 for a maximal shift in R_b . For example, $\tan\beta = 1.1, 1.5, 2.0$ can all give a large $ee\gamma\gamma + \cancel{E}_T$ rate, while the shift in R_b is at best 0.0028, 0.0021, 0.0018 for chargino-stop loops only. Further, R_b is sensitive more to the parameter $\tan\beta$ than $m_{\tilde{C}_1}$, as is clear since the chargino mass is inversely related to $\tan\beta$; in the above three cases $m_{\tilde{C}_1}$ is roughly 83, 80, 70 GeV. We note that these calculations have been done assuming $m_{\tilde{t}_1} = 50$ GeV, $\theta_{\tilde{t}} = \pi/2$, which is nearly optimal since the maximum shift in R_b decreases as either the stop mass is increased, or $\theta_{\tilde{t}}$ is taken far from $\pi/2$.

As has been emphasized, getting a significant shift in R_b requires a chargino that has a large Higgsino component, and the related result that μ is small and negative. It is interesting that the value of μ and the chargino properties coming from the analysis of the $ee\gamma\gamma + \cancel{E}_T$ event have the properties needed to give such an effect. Finally, we note that a shift in R_b necessarily implies a shift in α_s extracted from the LEP Z lineshape, through the relation $\delta\alpha_s(M_Z) \sim -4\delta R_b$ [30]. This limits the maximum shift in R_b to about 0.0025, consistent with the above numbers and giving $R_b \lesssim 0.2182$. It is worth emphasizing that a significant shift in R_b (and α_s) is only possible simultaneously with a supersymmetric interpretation of the $ee\gamma\gamma + \cancel{E}_T$ event if \tilde{N}_1 is the LSP [4].

6 Concluding remarks

We have seen that supersymmetry with \tilde{N}_1 =LSP is a viable explanation of the CDF $ee\gamma\gamma + \cancel{E}_T$ event. The primary constraints are the kinematics of the $ee\gamma\gamma + \cancel{E}_T$ event, the radiative neutralino branching ratio $\tilde{N}_2 \rightarrow \tilde{N}_1\gamma$, the selectron decay $\tilde{e} \rightarrow e\tilde{N}_2$ and LEP1–LEP130 data. Given a minimum threshold on the cross section times branching ratio of $p\bar{p} \rightarrow \tilde{e}^+\tilde{e}^- \rightarrow e^+e^-\tilde{N}_2\tilde{N}_2 \rightarrow e^+e^-\gamma\gamma\tilde{N}_1\tilde{N}_1$ at the Tevatron, a selectron interpretation requires M_1 , M_2 , μ , $\tan\beta$, $m_{\tilde{e}}$ in tight ranges (see Table 4 and Figs. 7, 8). The corresponding chargino and neutralino masses and the cross sections at LEP and Tevatron are similarly constrained. This is the origin of the predictions made for both LEP and Tevatron based solely on the $ee\gamma\gamma + \cancel{E}_T$ event, where many signals can be large, and some must be produced. These signals are deduced from the cross sections and branching ratios without efficiencies, although in many cases the mass differences between sparticles cannot be arbitrarily small, and so presumably the signals are detectable. For example, $\tilde{N}_1\tilde{N}_3$ production must occur at LEP190 with the mass difference $40 < m_{\tilde{N}_3} - m_{\tilde{N}_1} < 60$ GeV in all models, which implies a pair of leptons or jets from the decay $\tilde{N}_3 \rightarrow \tilde{N}_1 f\bar{f}$ would have an invariant mass up to roughly 60 GeV. The inclusive signals that must be produced at LEP190 with an integrated luminosity of 500 pb^{-1} are $\sigma(2l + X + \cancel{E}) \gtrsim 50$ events, and $\sigma(\gamma\gamma + X + \cancel{E}) \gtrsim 3$ events. At the Tevatron, the inclusive signals that should have been produced (with an integrated luminosity of 100 pb^{-1}) are $\sigma(2l + X + \cancel{E}_T) \gtrsim 30$ events, $\sigma(\gamma\gamma + X + \cancel{E}_T) \gtrsim 2$ events, $\sigma(l\gamma + X + \cancel{E}_T) \gtrsim 15$ events, $\sigma(2l\gamma + X + \cancel{E}_T) \gtrsim 4$ events, $\sigma(l\gamma\gamma + X + \cancel{E}_T) \gtrsim 2$ events, and $\sigma(3l + X + \cancel{E}_T) \gtrsim 2$ events. All of these signals assume $X = \text{anything}$ (leptons, photons, jets), and are valid for \tilde{e}_L or \tilde{e}_R models. For \tilde{e}_R models only, the inclusive signal that must be produced at LEP161 with an integrated luminosity of 25 pb^{-1} is $\sigma(2l + X + \cancel{E}) \gtrsim 2$ events. Also for \tilde{e}_R models only, the inclusive signals that must be produced at LEP190 (in addition to the ones above) are $\sigma(l\gamma + X + \cancel{E}) \gtrsim 5$ events, and $\sigma(2l\gamma + X + \cancel{E}) \gtrsim 5$ events. We have examined many inclusive signals with leptons and photons, but of course inclusive signals with jets (+ photons) are also important and in some cases can be larger.

The selectron interpretation can be made with the selectron \tilde{e} being either \tilde{e}_L , \tilde{e}_R , or a sum over \tilde{e}_L and \tilde{e}_R contributions. The difference between \tilde{e}_L and \tilde{e}_R is in the $SU(2)_L$ couplings of \tilde{e}_L , causing for example the cross section at the Tevatron $\sigma(p\bar{p} \rightarrow \tilde{e}_L\tilde{e}_L) \approx 2.2\sigma(p\bar{p} \rightarrow \tilde{e}_R\tilde{e}_R)$ (in the mass range of interest), and the presence of \tilde{e}_L couplings to charginos. Thus one way to distinguish \tilde{e}_L (and $\tilde{e}_L + \tilde{e}_R$) models from \tilde{e}_R models is with the associated charged current channel $p\bar{p} \rightarrow \tilde{e}_L\tilde{\nu}_e$ that gives at least $l\gamma + \cancel{E}_T$, with possibly more leptons or photons depending on the decay of $\tilde{\nu}_e$. Studies of such signals are relevant for $l = e, \mu, \tau$. A further source of $l^\pm\gamma + X + \cancel{E}_T$ events comes from $\tilde{C}_{1,2}(\rightarrow \tilde{N}_1 l\nu)\tilde{N}_2(\rightarrow \tilde{N}_1\gamma)$, as well as $\tilde{C}_i^\pm\tilde{C}_j^\mp$ with $\tilde{C} \rightarrow \tilde{e}_L\nu_e$ or $\tilde{C} \rightarrow \tilde{\nu}_e e$ if $m_{\tilde{e}_L}$ or $m_{\tilde{\nu}_e}$ is lighter than the chargino. Thus if no excess of associated events can be attributed to the absence of $\tilde{e}_L\tilde{\nu}_e$ production, then it becomes less likely that the original selectron was \tilde{e}_L , though it cannot be definitive until a clean result is published. In addition,

particular signals must be produced at LEP161/190 for \tilde{e}_R models that are not necessarily present for \tilde{e}_L models, and thus if these associated events were not found, then it becomes less likely that the original selectron was \tilde{e}_R , with the same caveat as above. At LEP it is necessary to study the relative rates of different channels to distinguish \tilde{e}_L from \tilde{e}_R , unless selectron pair production is actually observed there. In fact, if \tilde{e}_L or \tilde{e}_R production is observed (and the LSP can be established to be \tilde{N}_1), then we immediately know which charged slepton is *not* responsible for the $ee\gamma\gamma + \cancel{E}_T$ event, since as we have shown in this paper the slepton giving the $ee\gamma\gamma + \cancel{E}_T$ is kinematically forbidden at LEP161 and LEP190. Thus there is no unique signal to discriminate \tilde{e}_L from \tilde{e}_R (from $\tilde{e}_L + \tilde{e}_R$) models; only through the pattern of multiple signals can the nature of the selectron be determined.

We have also seen that a chargino interpretation of the $ee\gamma\gamma + \cancel{E}_T$ event is a distinct possibility. In either the selectron or chargino interpretation we expect at least the constraints from radiative neutralino decay to hold, and light sleptons are probably also a shared requirement for either interpretation (see Appendix A). One way to eventually distinguish the selectron interpretation from the chargino interpretation is to compare the rates of $ee\gamma\gamma$, $\mu\mu\gamma\gamma$ and $e\mu\gamma\gamma$. Assuming a mass degeneracy among the sleptons of different families, the selectron interpretation predicts roughly an equal number of $ee\gamma\gamma$ and $\mu\mu\gamma\gamma$ events, with a significantly depleted $e\mu\gamma\gamma$ signal originating only from $\tilde{\tau}^+\tilde{\tau}^-$ production followed by $\tau^+\tau^- \rightarrow e^\pm\mu^\mp + X$. Alternatively, in the chargino interpretation one would expect roughly double the number of $e\mu\gamma\gamma$ events as compared with either $ee\gamma\gamma$ or $\mu\mu\gamma\gamma$ events. Thus comparing the $e\mu\gamma\gamma$ rate with either $ee\gamma\gamma$ or $\mu\mu\gamma\gamma$ would provide a useful means to discriminate between the two interpretations. Notice also that events of the type $l^+l^-\gamma\gamma + \cancel{E}_T$ can be produced only from $\tilde{C}_i^\pm\tilde{C}_j^\pm$ and $\tilde{\tau}^+\tilde{\tau}^-$ production.

It is important to remark that the $ee\gamma\gamma + \cancel{E}_T$ event phenomenology could be connected with other phenomena. If the LSP = \tilde{N}_1 is stable, then it could provide a cosmologically significant relic density even if it is mostly a Higgsino [7] (as required by the $ee\gamma\gamma + \cancel{E}_T$ event). For a given value of Ωh^2 the mass of \tilde{N}_1 is correlated with $\tan\beta$, and so gives a subset of the models constructed here. The predictions for associated phenomenology are tighter; and generally the signals can be larger. Also, we have described in detail the effect of assuming a light stop in addition to the $ee\gamma\gamma + \cancel{E}_T$ event, in particular its connection to R_b [29] (and α_s [30]). A light stop has many other consequences [16], that we will not go into detail about here.

However, it is perhaps useful to remark on how can we learn if there is a light stop. The easiest way would be to observe it at LEP. The cross section ranges from about 0.2–0.8 pb over the range $50 < m_{\tilde{t}_1} < 70$ (80) GeV of most interest for LEP161 (LEP190). LEP190 with tens of pb⁻¹ will be definitive. For such light stops and even for somewhat heavier ones up to $m_t - m_{\tilde{N}_1}$ ($\lesssim 100$ GeV in models considered here) searches in $t(\rightarrow \tilde{t}_1\tilde{N}_1)\bar{t}(\rightarrow Wb)$ or stop pair production can be definitive. Indirect evidence for a light stop before there is definitive collider data could come from a convincing R_b excess, from slepton pair production at the Tevatron without associated leptons, and photons from chargino channels because $\tilde{C}_i^\pm \rightarrow \tilde{t}_1b$,

from anomalous behavior of top properties [16], and from the $\gamma+b+$ jets events [16] commented on in Sec. 5. Note that \tilde{t}_1 could be near \tilde{N}_1 in mass, and therefore give very soft fermions plus large missing energy.

We have stated that certain signals must be produced at LEP and Tevatron, and some signals might be produced if kinematically accessible. For example, at LEP161 three neutralino and one chargino pair cross sections are large enough to give a signal if about 25 pb^{-1} is collected. The signatures are described in Sec. 4.7.1 and can sometimes be somewhat unusual. At LEP190 many more processes can be open, which can all give signals with possibly unusual signatures (see Sec. 4.7.2). It is important to emphasize that the predictions assume the minimum cut $\mathcal{A} = 5 \text{ fb}$ is placed on the $\sigma \times \mathcal{B}^2$ for the $ee\gamma\gamma + \cancel{E}_T$ event. In principle, if one could demonstrate that failure to detect the signals implies they do not occur at all, then only two possibilities remain: (1) A supersymmetric explanation of the $ee\gamma\gamma + \cancel{E}_T$ event in our framework must rely on an upward fluctuation from $\sigma \times \mathcal{B}^2$ even lower than 5 fb , or (2) a supersymmetric explanation in our framework is not possible. We note that even if the cut $\mathcal{A} = 5 \text{ fb}$ needs to be relaxed, there are still constraints from requiring a moderate branching ratio for $\tilde{N}_2 \rightarrow \tilde{N}_1\gamma$ as demonstrated in Fig. 2.

The $ee\gamma\gamma + \cancel{E}_T$ event has given us a profound example of how low energy supersymmetry could be discovered with one event. It is not obvious that such an event *could* be explained by supersymmetry, and we emphasize here the predictability of the theory once such an explanation is adopted. In particular, we have shown that assuming the $ee\gamma\gamma + \cancel{E}_T$ event *is* due to supersymmetry with a \tilde{N}_1 = LSP imposes strong constraints on the supersymmetric parameters, and predicts much associated phenomenology. Confirmation at LEP or Tevatron from the myriad of associated signals described in this paper is necessary to be definitive. It is remarkable how much can be learned from the Tevatron data, if the signal is confirmed.

Acknowledgments

This work was supported in part by the U.S. Department of Energy. S. A. is supported mainly by an INFN postdoctoral fellowship, Italy.

Appendix A: Models in the chargino interpretation

The chargino interpretation purports to explain the $ee\gamma\gamma + \cancel{E}_T$ event through chargino production and decay, a priori sharing only the requirement of radiative neutralino decay with the selectron interpretation. The possible sources of $ee\gamma\gamma$ in the chargino interpretation are from $p\bar{p} \rightarrow \tilde{C}_i^\pm \tilde{C}_j^\mp$ with $\tilde{C}_{i,j} \rightarrow \tilde{N}_2 e \nu$, followed by $\tilde{N}_2 \rightarrow \tilde{N}_1 \gamma$. The decay $\tilde{C}_{i,j} \rightarrow \tilde{N}_2 e \nu$ can proceed through either on-shell or off-shell W , \tilde{e}_L and $\tilde{\nu}_e$. However, the 2-body decay $\tilde{C}_1 \rightarrow W \tilde{N}_2$

is not possible, since $m_{\tilde{C}_1} - m_{\tilde{N}_2} \lesssim 25$ GeV when the radiative neutralino branching ratio $\mathcal{B}(\tilde{N}_2 \rightarrow \tilde{N}_1 \gamma)$ is required to be large.

A.1 Chargino production and 3-body decays

If $\tilde{e}_L, \tilde{\nu}_e$ are heavy, the branching ratio for the decay $\tilde{C}_i \rightarrow \tilde{N}_2 e \nu_e$ is dominated by W -exchange, with a branching ratio the same as that for the SM decay $W \rightarrow e \nu_e$ equal to 11%. Chargino production with heavy sleptons therefore implies for every $l^+ l^- \gamma \gamma$ event, roughly 20 other events with jet activity (possibly accompanied by one charged lepton) or two different charged leptons (plus two photons). In addition, the channel $\tilde{C}_i \rightarrow \tilde{N}_1 e \nu$ is always open and it is generally favored by phase space, in particular in the case $i = 1$, since the mass difference $m_{\tilde{C}_1} - m_{\tilde{N}_2}$ is never large. Further, it seems difficult to find a region of the parameter space allowed by LEP data, consistent with a large neutralino radiative decay branching ratio and the general kinematical $ee\gamma\gamma$ requirements, where the non-radiative channels into \tilde{N}_1 are dynamically suppressed. This holds for both on- and off-shell W -exchange, and as a result the branching ratio for the decay $\tilde{C}_i \rightarrow \tilde{N}_2 e \nu$ hardly exceeds 6% for $i = 1$ and is even lower for $i = 2$. Hence, to get > 5 fb $ee\gamma\gamma$ signal from $\tilde{C}_i^\pm \tilde{C}_j^\mp$ production and decay $\tilde{C}_{i,j} \rightarrow W^{(*)} (\rightarrow e \nu) \tilde{N}_2 (\rightarrow \tilde{N}_1 \gamma)$ one needs a cross section at least roughly 1.5 pb (even assuming $\mathcal{B}(\tilde{N}_2 \rightarrow \tilde{N}_1 \gamma) = 100\%$), since $\mathcal{B}(\tilde{C}_i^\pm \tilde{C}_j^\pm \rightarrow \tilde{N}_2 \tilde{N}_2 e^+ e^- \nu_e \bar{\nu}_e)$ is well below 1%. This does not seem to be possible with an individual chargino pair production process, given all the other $ee\gamma\gamma$ constraints. However, a small but non-zero signal can always arise from this source in models which are compatible with the selectron interpretation. We have found models with up to ~ 1 fb $ee\gamma\gamma$ total signal from the sum of $\tilde{C}_i^\pm \tilde{C}_j^\mp$ production and 3-body \tilde{C}_i^\pm decay in our selectron interpretation models. (These contributions were not included in the selectron interpretation.)

A.2 Chargino production and 2-body decays

We consider in the following chargino production followed by 2-body decays into sleptons, which allows an enhancement of the total possible branching ratio into the $ee\gamma\gamma$ final state. The regions are somewhat different in the chargino interpretation with $\tilde{C} \rightarrow \tilde{l} \tilde{l}$ than in the selectron interpretation; in particular we found the constraint $m_{\tilde{N}_2} - m_{\tilde{N}_1} \gtrsim 20$ GeV is no longer required. (We have checked that a neutralino mass difference of order 10 GeV can be sufficient in the chargino interpretation.) This may in principle allow the kinematical mechanism for the enhancement of the radiative neutralino decay branching ratio to operate simultaneously with the dynamical mechanism to obtain a large $ee\gamma\gamma$ rate. In Sec. 4.2 we already encountered particular models in the selectron interpretation where the kinematical mechanism plays an important role, and this may be true for the chargino interpretation to an even greater extent. However, a small mass difference $m_{\tilde{N}_2} - m_{\tilde{N}_1}$ seems only to be allowed when $m_{\tilde{N}_2}$ is small, so that it can presumably receive a large boost after the \tilde{e}_L or $\tilde{\nu}_e$ decay and generate a hard

photon. The only way to construct a model with two very light neutralinos and a heavier chargino is to enter the “light gaugino-Higgsino window” (see Sec. 4.2), but even there it seems difficult to build a model which falls in the region suggested by the $ee\gamma\gamma + \cancel{E}_T$ event kinematics with the constraints from the branching ratios. Also, with a neutralino mass difference of order 10 GeV or more the radiative neutralino branching ratio never approaches 100% from only the kinematical enhancement [11]. Hence, as in the selectron interpretation it would appear that the dynamical mechanism for a large radiative neutralino decay is required. This, along with the following argument for the need of a mostly gaugino \tilde{N}_2 , explains why it seems possible to build models with large $ee\gamma\gamma$ rates in the chargino interpretation only in regions of the gaugino-Higgsino parameter space similar to that in the selectron interpretation.

The maximum $\mathcal{B}[\tilde{C}_i^\pm \rightarrow l'\tilde{l}^{(*)}(\rightarrow l\tilde{N}_2)]$ for $\tilde{l} = \tilde{\nu}_e$ is 1/3, and for $\tilde{l} = \tilde{e}_L$ is 1/6 due to the slepton mass degeneracy assumption and $m_{\tilde{\nu}_e} < m_{\tilde{e}_L}$ (assuming the decay into sneutrinos is not strongly suppressed). Also, the slepton decay channels with \tilde{N}_1 in the final state are always open and enhanced by phase space. Thus to maximize the branching ratio into \tilde{N}_2 , one has to minimize the \tilde{N}_2 Higgsino components (which do not couple with sleptons) and maximize the Higgsino component of \tilde{N}_1 . In this way, the branching ratio for $\tilde{e}_L \rightarrow \tilde{N}_2 e$ is enhanced, analogous to the selectron interpretation. Typically, the branching ratio for the combined decay $\tilde{C}_i^\pm \tilde{C}_j^\mp \rightarrow ee\gamma\gamma$ though 2-body decays into sleptons can reach at best $\sim 4\%$, assuming $\mathcal{B}(\tilde{N}_2 \rightarrow \tilde{N}_1\gamma) = 100\%$. In the \tilde{C}_2 case, a further source of suppression can come from the channel $\tilde{\nu}_e \rightarrow \tilde{C}_1 e$ (if open), that always dominates over $\tilde{\nu}_e \rightarrow \tilde{N}_2 \nu_e$ or $\tilde{\nu}_e \rightarrow \tilde{N}_1 \nu_e$. A similar suppression in the \tilde{C}_2 case can also come from $\tilde{e}_L \rightarrow \tilde{C}_1 \nu_e$. Thus, the actual $ee\gamma\gamma$ rate depends strongly also on the mass hierarchy between $m_{\tilde{\nu}_e}$, $m_{\tilde{e}_L}$ and $m_{\tilde{C}_1}$.

Maximizing the Higgsino component of \tilde{N}_1 and minimizing that of \tilde{N}_2 , leads us to the conclusion that \tilde{N}_2 is mostly photino and \tilde{N}_1 is mostly Higgsino, analogous to the selectron interpretation. However, differences do exist between the chargino interpretation and \tilde{e}_L models in the selectron interpretation. For example, one needs $100 \lesssim m_{\tilde{e}_L} \lesssim 137$ GeV in the selectron interpretation, while in the chargino interpretation one only needs at least one of \tilde{e}_L , $\tilde{\nu}_e$ heavier than roughly 60 GeV but lighter than at least one of the charginos. Of course, additional constraints on $m_{\tilde{e}_L}$, $m_{\tilde{\nu}_e}$ are present, due to the particularly complicated decay chain and the large radiative neutralino branching ratio needed. The right selectron enters the 3-body decay $\tilde{N}_2 \rightarrow \tilde{N}_1 e^+ e^-$, but if its mass is moderately large then the decay cannot be enhanced. Squark masses are relatively unconstrained, although lighter squark masses increase the $\tilde{C}_2 \tilde{C}_2$ cross section, but decrease the radiative branching ratio.

The absence of $ee\gamma\gamma + \cancel{E}_T$ event kinematical solutions with chargino masses less than 95 GeV implies that to construct a chargino interpretation that at least possibly satisfies the kinematics one should conservatively choose to search only for models with $m_{\tilde{C}} > 95$ GeV. Restricting to M_2 , μ and $\tan\beta$ values roughly in the allowed ranges singled out in the selectron interpretation, one finds a rough upper limit of 400, 50 and 1200 fb for the cross section of $\tilde{C}_1 \tilde{C}_1$, $\tilde{C}_1 \tilde{C}_2$ and $\tilde{C}_2 \tilde{C}_2$ production respectively. Given at best a useful branching ratio of about

5%, then a $\tilde{C}_1\tilde{C}_2$ interpretation (alone) can be excluded. For $\tilde{C}_1\tilde{C}_1$ and $\tilde{C}_2\tilde{C}_2$ production, the $ee\gamma\gamma$ signal could be up to roughly 20 and 60 fb, therefore the lower bound on the radiative neutralino decay branching ratio is 50% and 30% respectively, to pass $\mathcal{A} = 5$ fb cut used in the selectron interpretation. The $\tilde{C}_1\tilde{C}_1$ cross section drops rapidly as $m_{\tilde{C}_1}$ is increased, and it appears not to give a sizeable $ee\gamma\gamma + \cancel{E}_T$ signal when $m_{\tilde{C}_1} \gtrsim 110$ GeV. Alternatively, the $\tilde{C}_2\tilde{C}_2$ cross section can still be large, and give a sizeable $ee\gamma\gamma$ signal for $m_{\tilde{C}_2} \sim 150$ GeV (if $m_{\tilde{q}} \sim 250$ GeV). In practice, this sets rough upper limits for M_2 and $|\mu|$ which determine the chargino masses. Further, our analysis of the $ee\gamma\gamma + \cancel{E}_T$ event kinematics in the chargino interpretation gives an indication that large mass differences ($\gtrsim 30$ GeV) between \tilde{C}_i and \tilde{N}_2 may be required to reconstruct the $ee\gamma\gamma + \cancel{E}_T$ event. In the $i = 1$ case this is very difficult, if not impossible, given all the other constraints. Thus, we conclude that sizeable $ee\gamma\gamma + \cancel{E}_T$ signals can probably only be achieved from $\tilde{C}_2^+\tilde{C}_2^-$ production, with the decay chain $\tilde{C}_2 \rightarrow \nu_e\tilde{e}_L (\rightarrow e\tilde{N}_2)$ or $\tilde{C}_2 \rightarrow e\tilde{\nu}_e (\rightarrow \nu_e\tilde{N}_2)$, followed by $\tilde{N}_2 \rightarrow \tilde{N}_1\gamma$. This appears to happen only in a region of the parameter space similar to the selectron interpretation.

A few final remarks on model building are in order. The sneutrino always plays a role when the mass hierarchy $m_{\tilde{C}} > m_{\tilde{e}_L} (> m_{\tilde{\nu}_e})$ exists, and as a consequence the $ee\gamma\gamma$ signal is depleted from $\tilde{C} \rightarrow \tilde{\nu}_e e$ since $\tilde{\nu}_e$ tends to have comparable branching ratio into \tilde{N}_1 and \tilde{N}_2 . Further, if $m_{\tilde{\nu}_e} < m_{\tilde{N}_2}$, then a 2-body decay opens for $\tilde{N}_2 \rightarrow \tilde{\nu}_e \nu_e$, which often suppresses the radiative decay branching ratio. Also, a sneutrino mass larger than $m_{\tilde{C}_1}$ implies a possibly large branching ratio for $\tilde{\nu}_e \rightarrow \tilde{C}_1 e$. To ensure sufficient phase space for the decay $\tilde{C}_2 \rightarrow \tilde{e}_L \nu_e$ and to have the masses fall in regions where we found kinematical solutions, the mass difference $m_{\tilde{C}_2} - m_{\tilde{e}_L} \gtrsim \mathcal{O}(10)$ GeV probably should be enforced. The selectron also must be larger than $m_{\tilde{N}_2}$ by at least ~ 20 GeV for analogous reasons, but not larger than $m_{\tilde{C}_1}$ otherwise the branching ratio for \tilde{e}_L will be dominated by $\tilde{e}_L \rightarrow \tilde{C}_1 \nu_e$. It is clear that maintaining such a mass hierarchy between $m_{\tilde{C}_2}$, $m_{\tilde{e}_L}$, $m_{\tilde{\nu}_e}$, $m_{\tilde{N}_2}$, $m_{\tilde{C}_1}$, $m_{\tilde{N}_1}$ is considerably more difficult than in the selectron interpretation, and to some extent a fine-tuning of the masses of the particles involved is always required. Also, the relevant branching ratio is always small and never exceeds a few percent while in the selectron interpretation it can in principle reach 100%. All of these facts seem to render a chargino interpretation problematic (in stark contrast to a scenario with the gravitino as the LSP [4]).

A.3 Chargino interpretation – an example

We searched our model samples compatible with a selectron interpretation of the $ee\gamma\gamma + \cancel{E}_T$ event for cases where $\tilde{C}_2\tilde{C}_2$ production could yield an additional $ee\gamma\gamma$ signal. We found several tens of candidate models: some in the \tilde{e}_R samples, and a few in the \tilde{e}_L sample. However, the general kinematical requirements for a chargino interpretation of the $ee\gamma\gamma + \cancel{E}_T$ event slightly favor the \tilde{e}_L models, which are located roughly in Region 2 (according to the classification of Sec. 4.2). Such models could give rise to a $ee\gamma\gamma$ signal with the kinematical characteristics of

the event, from simultaneously \tilde{e}_L and \tilde{C}_2 pair production, although the \tilde{C}_2 signal is generally below 6 fb. We report one model as an example of the above: $M_1 = 65$ GeV, $M_2 \simeq M_Z$, $\mu = -53$ GeV $\tan \beta = 2$, $m_{\tilde{e}_L} = 110$ GeV, $m_{\tilde{e}_R} = 350$ GeV, $m_{\tilde{\nu}} = 90$ GeV, $m_{\tilde{t}_1} = 150$ GeV, $m_{\tilde{t}_2} \approx m_{\tilde{q}} = 250$ GeV. The neutralino masses $m_{\tilde{N}_{1,2,3,4}} = 65, 70, 96, 137$ GeV, and the chargino masses $m_{\tilde{C}_{1,2}} = 72, 137$ GeV. The $\tilde{C}_2\tilde{C}_2$ production cross section at the Tevatron is 380 fb, while the $\tilde{e}_L\tilde{e}_L$ cross section is 13 fb. The $\mathcal{B}(\tilde{N}_2 \rightarrow \tilde{N}_1\gamma) = 81\%$, the $\mathcal{B}(\tilde{C}_2 \rightarrow \tilde{\nu}_e e) = 17\%$, the $\mathcal{B}(\tilde{C}_2 \rightarrow \tilde{e}_L \nu_e) = 16\%$, the $\mathcal{B}(\tilde{e}_L \rightarrow \tilde{N}_2 e) \sim 100\%$, and $\mathcal{B}(\tilde{\nu}_e \rightarrow \tilde{C}_1 e) = 77\%$. The $ee\gamma\gamma$ rate is roughly 6 fb from only chargino production, and so is slightly above the $\mathcal{A} = 5$ fb cut imposed in the selectron interpretation. It is worthwhile to remark on how sensitive the $ee\gamma\gamma$ rate is to a change in the masses. For example, one can attempt to raise the $ee\gamma\gamma$ rate from chargino production by slightly reducing the \tilde{e}_L mass in such a way to get a sneutrino lighter than the \tilde{C}_1 , and gain the additional signal from \tilde{C}_2 decays into on-shell sneutrinos and sneutrino decays into \tilde{N}_2 . This would require $m_{\tilde{e}_L} \lesssim 96$ GeV, although the modified model would appear to be farther from the region of masses satisfying the $ee\gamma\gamma + \cancel{E}_T$ event kinematics. However, the radiative neutralino decay branching ratio drops quite sensitively when the already light slepton masses are further reduced. Thus, constructing models in the chargino interpretation is somewhat difficult, and it is not obvious how one ought to perturb around any given model to increase the $ee\gamma\gamma$ rate. However, we did find some models with interesting characteristics, as shown above. A more in-depth analysis is necessary to determine if the chargino interpretation is tenable, and if so the ranges of the parameters needed.

Appendix B: Sample Models

Here four sample models from the set used in the selectron interpretation are provided in Tables 12 and 13. Input parameters and calculated masses are given, along with many branching ratios and cross sections. Notice that the four models' input parameters are similar (except for the slepton and stop masses), but the cross sections for both the $ee\gamma\gamma + \cancel{E}_T$ event and associated phenomenology are quite different.

Model parameters	\tilde{e}_L model	\tilde{e}_R model
M_1, M_2	64.7 , 64.3	74.4 , 77.6
$\mu, \tan \beta$	-37.0 , 1.18	-38.3 , 1.11
$m_A, m_{\tilde{q}} = m_{\tilde{t}_2}$	200 , 500	400 , 500
$m_{\tilde{t}_1}, \theta_{\tilde{t}}$	204 , -0.342	487 , -0.123
$m_{\tilde{l}_L}, m_{\tilde{l}_R}, m_{\tilde{\nu}}$	105 , 272 , 99.6	391 , 104 , 390
$m_{\tilde{C}_1}, m_{\tilde{C}_2}$	79.6 , 110	78.9 , 119
$m_{\tilde{N}_1}, m_{\tilde{N}_2}, m_{\tilde{N}_3}, m_{\tilde{N}_4}$	36.6 , 64.6 , 90.5 , 118	38.2 , 75.1 , 88.5 , 127
$\langle \tilde{N}_1 \tilde{H}_b \rangle^2, \langle \tilde{N}_2 \tilde{\gamma} \rangle^2$	0.997 , 1.000	0.999 , 0.999
$m_h, m_H, m_{H^\pm}, \alpha_h$	70.2 , 229 , 216 , -0.825	69.2 , 415 , 408 , -0.765
$\sigma \times \mathcal{B}^2$	13.2	6.6
$\mathcal{B}(\tilde{N}_2 \rightarrow \tilde{N}_1 \gamma)$	0.98	0.94
$\mathcal{B}(\tilde{N}_3 \rightarrow l^+ l^-), \mathcal{B}(\tilde{N}_3 \rightarrow \nu \bar{\nu}), \mathcal{B}(\tilde{N}_3 \rightarrow q \bar{q})$	0.10 , 0.22 , 0.67	0.10 , 0.20 , 0.69
$\mathcal{B}(\tilde{N}_4 \rightarrow \tilde{\nu} \bar{\nu} + \tilde{\nu} \nu), \mathcal{B}(\tilde{N}_4 \rightarrow \tilde{l}_L \bar{l} + \tilde{l}_L l)$	0.83 , 0.13	- , -
$\mathcal{B}(\tilde{N}_4 \rightarrow \tilde{l}_R \bar{l} + \tilde{l}_R l)$	-	0.80
$\mathcal{B}(\tilde{C}_1 \rightarrow \tilde{N}_1 l \nu), \mathcal{B}(\tilde{C}_1 \rightarrow \tilde{N}_1 q \bar{q}')$	0.34 , 0.66	0.33 , 0.67
$\mathcal{B}(\tilde{C}_2 \rightarrow \tilde{\nu} l), \mathcal{B}(\tilde{C}_2 \rightarrow \tilde{l}_L \nu)$	0.66 , 0.28	- , -
$\mathcal{B}(\tilde{C}_2 \rightarrow \tilde{N}_1 l \nu), \mathcal{B}(\tilde{C}_2 \rightarrow \tilde{N}_1 q \bar{q}')$	0.02 , 0.03	0.33 , 0.66
$\mathcal{B}(\tilde{e}_L \rightarrow \tilde{N}_2 e), \mathcal{B}(\tilde{e}_L \rightarrow \tilde{C} \nu_e)$	0.91 , 0.07	0.30 , 0.59
$\mathcal{B}(\tilde{e}_R \rightarrow \tilde{N}_2 e), \mathcal{B}(\tilde{e}_R \rightarrow \tilde{N}_4 e)$	0.81 , 0.14	0.98 , -
$\mathcal{B}(\tilde{\nu}_e \rightarrow \tilde{N}_3 \nu_e), \mathcal{B}(\tilde{\nu}_e \rightarrow \tilde{C} e)$	0.08 , 0.90	0.10 , 0.61
<u>LEP161 cross sections:</u>		
$\sigma(\tilde{N}_1 \tilde{N}_3), \sigma(\tilde{C}_1 \tilde{C}_1)$	2010 , 405	2130 , 1320
$\sigma(\tilde{N}_2 \tilde{N}_2), \sigma(\tilde{N}_2 \tilde{N}_3)$	191 , 123	40 , -
inclusive $\sigma(2l + X), \sigma(\gamma\gamma + X)$	276 , 184	365 , 36
<u>LEP190 cross sections:</u>		
$\sigma(\tilde{N}_1 \tilde{N}_3), \sigma(\tilde{N}_1 \tilde{N}_4)$	1450 , 89	1530 , 49
$\sigma(\tilde{N}_2 \tilde{N}_2), \sigma(\tilde{N}_2 \tilde{N}_3)$	342 , 243	199 , 164
$\sigma(\tilde{C}_1 \tilde{C}_1), \sigma(\tilde{C}_1 \tilde{C}_2)$	1080 , 167	2760 , -
inclusive $\sigma(2l + X), \sigma(\gamma\gamma + X)$	473 , 331	529 , 177
inclusive $\sigma(l\gamma + X), \sigma(l\bar{l}\gamma + X)$	115 , 73	60 , 59
<u>Tevatron cross sections:</u>		
$\sigma(\tilde{e}_L \tilde{e}_L), \sigma(\tilde{e}_R \tilde{e}_R)$	16.5 , -	- , 7.9
$\sigma(\tilde{\nu}_e \tilde{\nu}_e), \sigma(\tilde{e}_L \tilde{\nu}_e)$	18.5 , 45.0	- , -
$\sigma(\tilde{N}_1 \tilde{N}_3), \sigma(\tilde{C}_1 \tilde{C}_1), \sigma(\tilde{C}_2 \tilde{C}_2)$	1180 , 907 , 552	1270 , 887 , 415
$\sigma(\tilde{C}_1 \tilde{N}_1), \sigma(\tilde{C}_1 \tilde{N}_2), \sigma(\tilde{C}_1 \tilde{N}_3)$	2690 , 113 , 840	2710 , 55 , 915
$\sigma(\tilde{C}_2 \tilde{N}_2), \sigma(\tilde{C}_2 \tilde{N}_3), \sigma(\tilde{C}_2 \tilde{N}_4)$	324 , 28 , 332	190 , 8.4 , 241
inclusive $\sigma(2l + X), \sigma(\gamma\gamma + X)$	1700 , 174	631 , 24
inclusive $\sigma(l\gamma + X), \sigma(2l\gamma + X)$	954 , 714	318 , 237
inclusive $\sigma(l\gamma\gamma + X), \sigma(3l + X)$	171 , 892	22 , 101

Table 12: Two sample models in the selectron interpretation. All masses are in GeV, all cross sections are in fb. Only the largest branching ratios and cross sections are displayed. l is summed over e , μ , and τ in the branching ratios and inclusive cross sections (which have no detector efficiencies included). In the branching ratios \tilde{C} refers to a sum over \tilde{C}_1 and \tilde{C}_2 .

Model parameters	$\tilde{e}_L + \tilde{e}_R$ model	\tilde{e}_R model (with light \tilde{t}_1)
M_1, M_2	70.2 , 76.2	76.5 , 77.0
$\mu, \tan \beta$	-48.8 , 1.26	-38.9 , 1.39
$m_A, m_{\tilde{q}} = m_{\tilde{t}_2}$	200 , 500	400 , 2000
$m_{\tilde{t}_1}, \theta_{\tilde{t}}$	488 , 0.263	50 , $\pi/2$
$m_{\tilde{l}_L}, m_{\tilde{l}_B}, m_{\tilde{\nu}}$	119 , 121 , 113	439 , 105 , 437
$m_{\tilde{C}_1}, m_{\tilde{C}_2}$	84.8 , 118	75.2 , 121
$m_{\tilde{N}_1}, m_{\tilde{N}_2}, m_{\tilde{N}_3}, m_{\tilde{N}_4}$	47.8 , 71.5 , 96.8 , 124	37.4 , 76.6 , 88.4 , 128
$\langle N_1 \tilde{H}_b \rangle^2, \langle N_2 \tilde{\gamma} \rangle^2$	0.990 , 0.998	0.988 , 0.999
$m_h, m_H, m_{H^\pm}, \alpha_h$	67.8 , 227 , 216 , -0.792	59.1 , 411 , 408 , -0.651
$\sigma \times \mathcal{B}^2$	10.2	5.1
$\mathcal{B}(\tilde{N}_2 \rightarrow \tilde{N}_1 \gamma)$	0.92	0.86
$\mathcal{B}(\tilde{N}_3 \rightarrow l^+ l^-), \mathcal{B}(\tilde{N}_3 \rightarrow \nu \bar{\nu}), \mathcal{B}(\tilde{N}_3 \rightarrow q \bar{q})$	0.10 , 0.22 , 0.67	0.10 , 0.20 , 0.68
$\mathcal{B}(\tilde{N}_4 \rightarrow \tilde{\nu} \bar{\nu} + \bar{\nu} \nu), \mathcal{B}(\tilde{N}_4 \rightarrow \tilde{l}_L \bar{l} + \bar{l}_L l)$	0.85 , 0.05	- , -
$\mathcal{B}(\tilde{N}_4 \rightarrow \tilde{l}_R \bar{l} + \bar{l}_R l)$	0.01	0.74
$\mathcal{B}(\tilde{C}_1 \rightarrow \tilde{N}_1 l \nu), \mathcal{B}(\tilde{C}_1 \rightarrow \tilde{N}_1 q \bar{q}'), \mathcal{B}(\tilde{C}_1 \rightarrow \tilde{t}_1 b)$	0.34 , 0.66 , -	0.00 , - , 1.00
$\mathcal{B}(\tilde{C}_2 \rightarrow \tilde{\nu} l), \mathcal{B}(\tilde{C}_2 \rightarrow \tilde{t}_1 b)$	0.78 , -	- , 0.98
$\mathcal{B}(\tilde{C}_2 \rightarrow \tilde{N}_1 l \nu), \mathcal{B}(\tilde{C}_2 \rightarrow \tilde{N}_1 q \bar{q}')$	0.06 , 0.11	0.01 , 0.01
$\mathcal{B}(\tilde{e}_L \rightarrow \tilde{N}_2 e), \mathcal{B}(\tilde{e}_L \rightarrow \tilde{C} \nu_e)$	0.94 , 0.03	0.30 , 0.59
$\mathcal{B}(\tilde{e}_R \rightarrow \tilde{N}_2 e), \mathcal{B}(\tilde{e}_R \rightarrow \tilde{N}_4 e)$	0.97 , -	0.96 , -
$\mathcal{B}(\tilde{\nu}_e \rightarrow \tilde{N}_3 \nu_e), \mathcal{B}(\tilde{\nu}_e \rightarrow \tilde{C} e)$	0.10 , 0.86	0.10 , 0.62
<u>LEP161 cross sections:</u>		
$\sigma(\tilde{N}_1 \tilde{N}_3), \sigma(\tilde{C}_1 \tilde{C}_1)$	1500 , -	2100 , 2680
$\sigma(\tilde{N}_2 \tilde{N}_2), \sigma(\tilde{N}_2 \tilde{N}_3), \sigma(\tilde{t}_1 \tilde{t}_1^*)$	120 , - , -	23 , - , 850
inclusive $\sigma(2l + X), \sigma(\gamma \gamma + X)$	157 , 100	215 , 17
<u>LEP190 cross sections:</u>		
$\sigma(\tilde{N}_1 \tilde{N}_3), \sigma(\tilde{N}_1 \tilde{N}_4)$	1360 , 24	1500 , 41
$\sigma(\tilde{N}_2 \tilde{N}_2), \sigma(\tilde{N}_2 \tilde{N}_3)$	355 , 227	169 , 150
$\sigma(\tilde{C}_1 \tilde{C}_1), \sigma(\tilde{C}_1 \tilde{C}_2), \sigma(\tilde{t}_1 \tilde{t}_1^*)$	880 , - , -	3110 , - , 760
inclusive $\sigma(2l + X), \sigma(\gamma \gamma + X)$	302 , 299	254 , 125
inclusive $\sigma(l \gamma + X), \sigma(l l \gamma + X)$	56 , 51	78 , 78
<u>Tevatron cross sections:</u>		
$\sigma(\tilde{e}_L \tilde{e}_L), \sigma(\tilde{e}_R \tilde{e}_R)$	9.4 , 4.0	- , 7.5
$\sigma(\tilde{\nu}_e \tilde{\nu}_e), \sigma(\tilde{e}_L \tilde{\nu}_e)$	10.5 , 24.6	- , -
$\sigma(\tilde{N}_1 \tilde{N}_3), \sigma(\tilde{C}_1 \tilde{C}_1), \sigma(\tilde{C}_2 \tilde{C}_2)$	688 , 681 , 434	1270 , 1140 , 298
$\sigma(\tilde{C}_1 \tilde{N}_1), \sigma(\tilde{C}_1 \tilde{N}_2), \sigma(\tilde{C}_1 \tilde{N}_3)$	1590 , 86 , 575	3430 , 128 , 974
$\sigma(\tilde{C}_2 \tilde{N}_2), \sigma(\tilde{C}_2 \tilde{N}_3), \sigma(\tilde{C}_2 \tilde{N}_4)$	189 , 29 , 259	218 , 43 , 283
inclusive $\sigma(2l + X), \sigma(\gamma \gamma + X)$	1190 , 43	178 , 16
inclusive $\sigma(l \gamma + X), \sigma(2l \gamma + X)$	369 , 279	50 , 48
inclusive $\sigma(l \gamma \gamma + X), \sigma(3l + X)$	39 , 654	16 , 7.5

Table 13: As in Fig. 12, but for an $\tilde{e}_L + \tilde{e}_R$ model, and a model with a light stop. Note that $\sigma \times \mathcal{B}^2$ sums over both \tilde{e}_L and \tilde{e}_R contributions for the $\tilde{e}_L + \tilde{e}_R$ model.

References

- [1] S. Ambrosanio, G. L. Kane, G. D. Kribs, S. P. Martin, and S. Mrenna, Phys. Rev. Lett. **76**, 3498 (1996).
- [2] S. Park, “Search for New Phenomena in CDF”, 10th Topical Workshop on Proton–Antiproton Collider Physics, edited by Rajendran Raja and John Yoh, AIP Conf. Proc. No. 357 (AIP, New York, 1996); L. Nodulman, “New Particle Searches at CDF”, Proceedings of the International Europhysics Conference on High Energy Physics, edited by J. Lemonne et al. Brussels, 1995.
- [3] We make no attempt to connect our results with unification scale physics using a RGE analysis such as in many studies e.g. G. L. Kane, C. Kolda, L. Roszkowski, and J. D. Wells, Phys. Rev. **D49**, 6173 (1994); the primary issues one would have to address is obtaining low $\tan \beta$, small $|\mu|$, M_2 not necessarily equal to $2M_1$, and $m_{\tilde{e}_L}$ not necessarily close to (perhaps a factor of 2–3 different from) $m_{\tilde{e}_R}$.
- [4] S. Ambrosanio, G. L. Kane, G. D. Kribs, S. P. Martin, and S. Mrenna, Phys. Rev. **D54**, 5395 (1996).
- [5] S. Dimopoulos, M. Dine, S. Raby, and S. Thomas, Phys. Rev. Lett. **76**, 3494 (1996).
- [6] S. Dimopoulos, S. Thomas, and J. D. Wells, Phys. Rev. **D54**, 3283 (1996).
- [7] G. L. Kane and J. D. Wells, Phys. Rev. Lett. **76**, 4458 (1996).
- [8] H. Komatsu and J. Kubo, Phys. Lett. **157B**, 90 (1985); Nucl. Phys. **B263**, 265 (1986); H. E. Haber, G. L. Kane, and M. Quirós, Phys. Lett. **160B**, 297 (1985); Nucl. Phys. **B273**, 333 (1986).
- [9] H. E. Haber and D. Wyler, Nucl. Phys. **B323**, 267 (1989).
- [10] S. Ambrosanio and B. Mele, Phys. Rev. **D52**, 3900 (1995); Phys. Rev. **D53**, 2541 (1996).
- [11] S. Ambrosanio and B. Mele, hep-ph/9609212.
- [12] H. E. Haber and G. L. Kane, Phys. Rep. **117**, 75 (1985).
- [13] M. M. El Kheishen, A. A. Shafik, and A. A. Aboshousha, Phys. Rev. **D45**, 4345 (1992).
- [14] V. Barger, M. S. Berger, and P. Ohmann, Phys. Rev. **D49**, 4908 (1994).
- [15] A. Bartl, H. Fraas, and W. Majorotto, Nucl. Phys. **B278**, 1 (1986); A. Bartl, H. Fraas, W. Majorotto, and N. Oshimo, Phys. Rev. **D40**, 1594 (1989).
- [16] G. L. Kane and S. Mrenna, Phys. Rev. Lett. **77**, 3502 (1996).
- [17] S. Dawson, E. Eichten, and C. Quigg, Phys. Rev. **D31**, 1581 (1985).

- [18] H. Baer, C.-h. Chen, F. Paige, and X. Tata, Phys. Rev. **D49**, 3283 (1994).
- [19] See e.g. Y. Okada, M. Yamaguchi, and T. Yanagida, Phys. Lett. B **262**, 54 (1991); M. Drees and M. Nojiri, Phys. Rev. **D45**, 2482 (1992); H. E. Haber and R. Hempfling, Phys. Rev. **D48**, 4280 (1993); M. Carena, J. R. Espinosa, M. Quirós, and C. E. M. Wagner, Phys. Lett. B **355**, 209 (1995); M. Carena, M. Quirós, and C. E. M. Wagner, Nucl. Phys. **B461**, 407 (1996).
- [20] J. Ellis, G. Ridolfi, and F. Zwirner, Phys. Lett. B **262**, 477 (1991).
- [21] L3 Collaboration, Phys. Lett. B **377**, 289 (1996). See also OPAL Collaboration, Phys. Lett. B **377**, 181 (1996).
- [22] L3 Collaboration, Phys. Lett. B **350**, 109 (1995).
- [23] J. L. Feng, N. Polonsky, and S. Thomas, Phys. Lett. B **370**, 95 (1996).
- [24] The method we use here is very similar to what we used previously in Ref. [1]. However, many aspects of the model building have been refined (and some minor corrections made), so the results here should be taken to supersede and complete those of Ref. [1].
- [25] H. L. Lai et al., Phys. Rev. **D51**, 4763 (1995).
- [26] See e.g. S. Mrenna, G. L. Kane, G. D. Kribs, and J. D. Wells, Phys. Rev. **D53**, 1168 (1996), and references therein.
- [27] M. Drees and K. Hagiwara, Phys. Rev. **D42**, 1709 (1990).
- [28] M. Drees and K.-I. Hikasa, Phys. Lett. B **252**, 127 (1990).
- [29] A. Djouadi et al. Nucl. Phys. **B349**, 48 (1991); M. Boulware, D. Finnell, Phys. Rev. **D44**, 2054 (1991); J. D. Wells, C. Kolda, G. L. Kane, Phys. Lett. B **338**, 219 (1994); D. Garcia, J. Sola, Phys. Lett. B **354**, 335 (1995); G. L. Kane, R. G. Stuart, J. D. Wells, Phys. Lett. B **354**, 350 (1995); A. Dabelstein, W. Hollik, W. Mösl, hep-ph/9506251; M. Carena, H. E. Haber, and C. E. M. Wagner, Nucl. Phys. **B472**, 55 (1996). P. H. Chankowski, S. Pokorski, Phys. Lett. B **366**, 188 (1996); J. Ellis, J. Lopez, D. Nanopoulos, Phys. Lett. B **372**, 95 (1996); J. D. Wells, G. L. Kane, Phys. Rev. Lett. **76**, 869 (1996); E. H. Simmons, Y. Su, Phys. Rev. **D54**, 3580 (1996); P. H. Chankowski, S. Pokorski, Nucl. Phys. **B475**, 3 (1996).
- [30] M. Shifman, Mod. Phys. Lett. **A10** (1995) 605; J. Erler and P. Langacker, Phys. Rev. **D52**, 441 (1995); 5th reference of Ref. [29].
- [31] G. Bhattacharyya and R. N. Mohapatra, Phys. Rev. **D54**, 4204 (1996).
- [32] J. L. Lopez and D. V. Nanopoulos, hep-ph/9607220.
- [33] J. Hisano, K. Tobe, and T. Yanagida, hep-ph/9607234.